Homogeneously catalyzed hydrogenation reactions in inverse micelles with recycling of the catalyst

vorgelegt von
Diplom-Ingenieur
Juan Sebastian Milano Brusco
aus Cumaná – Venezuela

Von der Fakultät II - Mathematik und Naturwissenschaften
der Technischen Universität Berlin
Zur Erlangung des akademischen Grades

Doktor der Ingenieurwissenschaften
Dr. Ing.

genehmigte Dissertation

Promotionsausschuss:

Vorsitzender: Prof. Dr. rer. nat. M. Gradzielski
Berichter: Prof. Dr. rer. nat. R. Schomäcker
Berichter: Prof. Dr. rer. nat. J. Koetz

Tag der wissenschaftlichen Aussprache: 16.11.2009

Berlin 2009
D 83

In the original unity of the first
things lies the secondary cause of
all things, with the germ of their
inevitable annihilation.

Edgar Allan Poe

Abstract

Microemulsion systems were designed and used as solvent systems in catalytic hydrogenation reactions catalyzed by the water soluble catalyst complex Rh–TPPTS in order to achieve reaction rate and selectivity improvement focusing on product isolation and catalyst recycling.

To find intrinsic differences between biphasic systems and microemulsions as reaction medium for catalytic reactions with the water-soluble catalyst complex Rh–TPPTS, the kinetics of the catalytic hydrogenation of dimethyl itaconate (DMI) was studied in a biphasic cyclohexane-water system and in a [Triton X-100/1-pentanol]/cyclohexane/water microemulsion, in both cases using the water-soluble catalyst complex Rh-TPPTS. A typical profile of a zero-order reaction was observed in the case of the biphasic system. Against that the reaction order for DMI changed to 1 in a microemulsion. Based on Osborn-Wilkinson-like kinetics, the irreversible attack of free DMI at the rhodium complex was determined to be the step governing the reaction. The activation energy of the rate determining step is 53 $kJ \cdot mol^{-1}$ and is similar in both systems. Dynamic Light Scattering (DLS) and Small Angle Neutron Scattering (SANS) measurements were used to determine the structural dimensions of the commercial polyoxyethylene-based (Igepal CA-520 and Triton X-100) nonionic microemulsions, showing a linear dependence between the initial hydrogenation rate of DMI and the radius of the micelles. The initial hydrogenation rate of DMI in bulk water was exceeded in both microemulsions. Indications of deformation of the originally spherical Triton X-100 reverse micelles upon addition of the water soluble catalyst complex Rh-TPPTS were found. Microemulsion systems with the nonionic surfactant Triton X-100, the anionic surfactant AOT and the narrow range nonionic surfactant Lutensol XA 50 were also used as reaction medium in the same reaction with the catalyst Rh–TPPTS, accomplishing product isolation and catalyst recycling. An unusual hindering effect of the surfactant on the production of elaidic acid and stearic acid as sunflower oil was hydrogenated in Triton X-100 microemulsion systems with the water-soluble catalyst complex Rh–TPPTS was observed. When the ligand/metal ratio was higher, the reaction was slower but more selective to oleic acid. The Rh–TPPTS catalyst could be recycled up to 3 times after hydrogenation of sunflower oil by extracting the oil phase of a three-phase microemulsion system, observing a continuous deactivation of the catalyst.

Zusammenfassung

Die Verwendung von wasserlöslichen Katalysatoren in zweiphasigen Reaktionsmedien ermöglicht nach der Hydrierung von Substraten wie z.B. Itaconsäuredimethylester (ISDME) eine problemlose Produktabtrennung. Die Reaktionsgeschwindigkeit in diesen Systemen ist jedoch aufgrund des ungünstigen Verteilungskoeffizienten (*P*) oft begrenzt. Deswegen ist die Verwendung von Tensiden, d.h. die Bildung von Mikroemulsionen aus den Reaktionsgemischen eine Möglichkeit, die Limitierung der geringen Wasserlöslichkeit zu umgehen und die Kontaktfläche zwischen Katalysatorphase und Substratphase zu vergrößern und damit die Hydrierung zu beschleunigt. Am Ende der Reaktion kann die Produktabtrennung entweder durch eine temperaturabhängige Phasentrennung stattfinden. Für die Untersuchung wurde ein Katalysatorkomplex verwendet, der aus dem Rhodiumprecursor $Rh_2(COD)_2Cl_2$ und dem wasserlöslichen Liganden TPPTS gebildet wurde. Die Hydrierung von ISDME wurde in zweiphasig Cyclohexan/Wasser System und in Mikroemulsionen durchgeführt. Für das Substrat ISDME ergab sich ein Verteilungskoeffizient von 0.75. Damit liegt eine ausreichende Substratkonzentration für die Reaktion in der Katalysatorphase vor. Die Reaktion verläuft nach einen Kinetik 0. Ordnung. In der Mikroemulsionen hat die Substratkonzentration einen linearen Einfluss auf die Anfangsgeschwindigkeit. Für eine kinetische Auswertung wurde das Modell von Osborn-Wilkinson benutzt und die Aktivierungsenergie der Reaktion in der Triton- Mikroemulsion (53 $KJ \cdot mol^{-1}$) ermittelt. Daraus kann geschlossen werden, dass die Reaktion in dem System ohne Stofftransportlimitierung abläuft. Für das Cyclohexan/Wasser System zeigt der Unterschied zwischen der Aktivierungsenergie im homogenen System (57.9 $KJ \cdot mol^{-1}$) und der effektive Aktivierungsenergie (11.5 $KJ \cdot mol^{-1}$) die Limitierung der Reaktion durch Stofftransport auf. Das molare Verhältnis Wasser/Tensid (ω) und das Verhältnis Pentanol/Triton (δ) sind wichtigen Einfluß der Größe der Mizellen. Bei der Hydrierung von ISDME hat die Größe der Mizellen direkten Einfluss. Die Größe der Mizellen haben wir durch SANS und DLS Messungen gewertet. In der partielle Hydrierung von Sonnenblumenöl hat der Tensidkonzentration direkten Einfluss.

Acknowledgment

Words of acknowledgment are not enough to pay back to those who have done everything within their hands in order to make this piece of work come to reality. First of all to my supervisor Prof. Dr. Reinhard Schomäcker, who portrayed the principal inspiration for this research and gave absolutely everything necessary to allow the harmonious consolidation of this dissertation. Those few minutes of time each day where very important for my learning process at TU Berlin. The freedom and patience given to me was cornerstone for my growth in experimental research.

To Benjamin Frank I owe the assuredness of being and working even better is also possible, “with your help nothing is impossible”. Thanks to Patrick Kurr for being such a flexible person and helping me overcome my limitations. To my friends Mr. Benjamin and Mr. Patrick I would like to say: “Thank you for allowing me to win each time at billiard”, those nights of religious billiard games kept me from throwing the towel. I would like to thank Michael Schwarze for helping me overcome the hard first stage of introduction to the laboratory, “I learned even more from you than you think”. The discussions with Henriette Nowothnick were very important for this dissertation, and “your friendship is even more important”. Gaby Vetter was the first friend I had in the laboratory, and she was fundamental help in my integration to the lab, “I couldn’t imagine a fruitful experimental work in the lab without you”. To the “spirit of the lab” Hary Soerijanto I owe much of my future, “Your recommendations are backbone of much of my decisions”.

To Prof. Dr. Michael Gradzielski and Sylvain Prévost I owe the knowledge I have achieved in our discussions over microemulsions, which I am sure were base for excellent fundamental research, “I thank you for motivating me to always go further in the look for understanding”. Special thanks to Prof. Dr. G.H. Findenegg for being my second supervisor, “It has been an honour for me to learn from our limited discussions and Dersy´s admiration is also shared by me”. My thanks go to Prof. Dr. Reinhard Strey, Dr. Thomas Sottmann and to Dr. Bernhard Gutsche for the wonderful working environment within the AiF project.

Special thanks to the dream-team Jamal Touitou and Verena Strempel for the important discussions, I learned so much by working together in your master thesis and “Hilfskraft”, respectively. To “mis compatriotas” Carlos Carrero and Klaus Friedel many thanks for your special help by not letting me forget my culture. Thanks to Dilek

Akcakayiran for being such an important beacon of hope. Thomas and Tilly Frank, thanks for being my relatives in such a far horizon.

To all my colleagues and friends who have kept me grounded and made it easier for me to go further with my research: Kirsten Langfeld, Xie Xiao, Oliver Schwarz, Jonas Dimroth, Sebastian Arndt, Benjamin Beck, Torsten Otremba, Riny Parapat, Anke Rost, Katja Seifert, Stephane Nai-Im Tholander, Sonia Khennache, Ingo Hoffmann, Claudia Oppel and the incognito-soldier.

Primordial was the decision of my mother to consolidate her dreams with toughness of doing her PhD in Southampton, this decision was the igniting spark that opened many doors of possibilities: “Thanks for never giving up on me and teaching me to fight for happiness”…“I am very proud of being your son”. Thanks to my brother Emir Milano for always believing in me, “I am very sure that if we believe we can, we will succeed”. Special thanks to Hector for being the respectful model dad and for teaching me to work hard for the goals. To Carmelo I would like to thank for bearing with all the brainstorming and I would like to say “Nobody can stop us from realizing our dreams”.

To my very best friend…my everyday dream…the one who never lets go, to Dersy I would like to thank for always being there to guide me and for understanding my crazy ideas. Dersy, “we are one, our decisions are only one”.

I will never forget those days of studying Applied Thermodynamics with my father.

To God almighty for never abandoning me.

"Papa, siempre seguire tus pasos rectificando tus errores y aprendiendo a conocerte, sencillamente entendiendome mi mismo"

Dersy

A mi mama y mi hermano

Table of Content

1 Introduction

Most chemistry industries have adopted catalytic processes in order to achieve process intensification of their installations and since catalytic reactions are preferred nowadays in environmentally friendly green chemistry due to the reduced amount of waste generated, sustainability of catalytic chemical industries is also promoted. Furthermore, catalysts cheapen industrial processes by accelerating reactions and consequently diminishing energy expenses, but they are generally formed by very expensive metal compounds.

In contrast to heterogeneous catalysis, with homogeneous catalysis high reaction rates and selectivities are obtained at relatively low temperatures. But catalyst recyclability is still a paramount challenge and one of the most important ongoing research topics. For this reason almost 80 % of the industrial catalytic processes are heterogeneously catalyzed, and catalytic hydrogenation is no exemption.

An important advantage of homogeneous hydrogenation and which is of great interest for industrial processes, especially those dealing with pharmaceuticals, agrochemicals, fragrances, etc is the introduction of chiral centers to organic substrates via enantioselective hydrogenation for which rhodium and ruthenium complexes are of special importance. These complexes are extremely active, but very expensive and sensitive to oxygen. Since some substrates are thermosensitive and have multiple functional groups, it is an additional advantage that the hydrogenation is carried out under mild conditions and in liquid phase. Process parameters like substrate concentration, stirring velocity, catalyst type and substrate solubility in the catalyst phase should be very well tuned.

The pioneering works of biphasic catalysis and water soluble metal complexes have taken homogeneous catalysis into a promising direction. These contributions have allowed for a cheap way of promoting catalyst recyclability in homogeneous catalysis by heterogenizing the solvent, ergo using a biphasic aqueous/oil system in which the catalyst is dissolved in the aqueous catalyst containing phase. But in this case, the reaction is limited by the solubility of the substrate in the aqueous phase. For this reason surfactants are needed to overcome incompatibility problems between reagents and their partitioning between phases. The applicability of surfactant based microemulsion systems has expanded into numerous industrial

areas and much investigation has been done. The well known advantages of microemulsion systems of increasing mass transfer, dissolving any compound type (polar, nonpolar, organic or inorganic) and the possibility of controlling phase separation by temperature variation are suitable for catalytic reactions. In general, by using microemulsions as reaction media for catalytic reactions, catalyst recycling can be achieved by temperature induced separation of the microemulsion. An important issue is that as a consequence of the high amount of surfactant in such systems, the total separation time is normally rather long and the loss of surfactant by extracting the oil phase is high. By using smaller amounts of surfactant, three phase systems are obtained with non-ionic surfactants and ionic surfactants, and in both cases the duration of complete separation is shorter.

Itaconic acid and its derivatives are important building block monomers used in the plastic industry for the synthesis of acrylic fibers and latex. Itaconic acid is used up to 5 % in styrene butadiene resins and in acrylic latexes for textile, paper, and paint applications. When used as a co-monomer for acrylic fibers, it increases mechanical resistance and affinity to dyes. It also improves the resistance to abrasion and enhances waterproofing of latex in the following applications: paper and card coating; carpet backing, non-woven textiles; adhesives and paints. Enantioselective hydrogenation of dimethyl itaconate allows for the production of pharmaceutically interesting chiral methyl succinates. Since itaconic acid can be produced biochemically by molds (Aspergillus terreus), current studies are focusing in the development of plants to produce itaconic acid using this biochemical route. This may allow replacement of petrochemical products by plant based, thus more sustainable raw material.

An important example and a fundamental aim in oleochemistry hydrogenations is the fat hardening for the production of margarine from vegetable oils by selective hydrogenation of multiply unsaturated fatty compounds to singly unsaturated products. The improvement of the oxidation stability and increment of the melting point of the fat is obtained by decreasing the polyunsaturated fatty acid content in the oil without increasing the content of saturated fatty acid. In concrete, the selective hydrogenation of linoleic acid ($C_{18:2}$) to oleic acid ($C_{18:1}$) without significant formation of stearic acid ($C_{18:0}$) has been studied intensively under homogeneous conditions in organic solvents. Catalyst systems based on platinum/tin, palladium/aluminium, iridium, rhodium, ruthenium, Carbonyl complexes of cobalt, iron and chromium have

been used. However, in all these investigations recycling of the homogeneous catalyst has not been possible.

Many basic investigations have focused on the effect of the reverse micelle structure (size and form) on the microemulsion properties as reaction medium. But none has dealt with a topic of such industrial application as catalytic hydrogenation. Small angle neutron scattering (SANS) and dynamic light scattering (DLS) are well established non-invasive techniques used to characterize microemulsions in much structural detail.

For these reasons a methodology has been developed to study the catalytic hydrogenation of different substrates in different microemulsion systems using the water soluble catalyst complex Rh–TPPTS. A correlation between the size of reverse micelles obtained by SANS and DLS, and the initial hydrogenation rate of dimethyl itaconate (DMI) with the water-soluble catalyst complex Rh–TPPTS using two nonionic microemulsion systems with different water content as dispersive media was obtained.

2 Fundamentals Regarding Catalysis and Microemulsions

The present chapter deals with the fundamentals and state of the literature regarding the topics catalysis, microemulsions and scattering measurements. In order to identify the advantages and disadvantages of homogeneous catalysis, an initial comparison between heterogeneous and homogeneous catalysis is done. Biocatalysis is also discussed. Recently published articles and reviews regarding catalytic systems are brought to debate.

2.1 Catalysis

A catalyst is a substance which increases the rate at which a chemical reaction approaches equilibrium without becoming itself permanently involved. Normally, catalysts tend to change their chemical properties with time, suffering a final process of deactivation. During the catalytic cycle the catalyst may be present in several intermediate forms when a close study of the molecular level is done. The number of times an active catalyst goes through a cycle of states remaining at the end unaltered is called Turn over number (TON). The most optimal catalysts have TON over the millions. The Turn over frequency (TOF) is the TON in a certain period of time **[2.1]**. Many catalysts have specific actions in that they influence only one reaction or a group of definite reactions. When a reaction can proceed by more than one path, a particular catalyst may favour one path more than another and thus lead to a product distribution different from an uncatalyzed reaction affecting the selectivity of a particular reaction **[2.2]**. Different types of selectivity are represented in Figure 2.1.

a. Chemoselectivity, the production of one product type such as alcohols rather than aldehydes.
b. Regioselectivity, the production of a linear ester rather than one with a branching methyl group.
c. Stereoselectivity, the production of one enantiomer of a chiral compound (chiral products are marked with an asterisk in Figure 2.1).

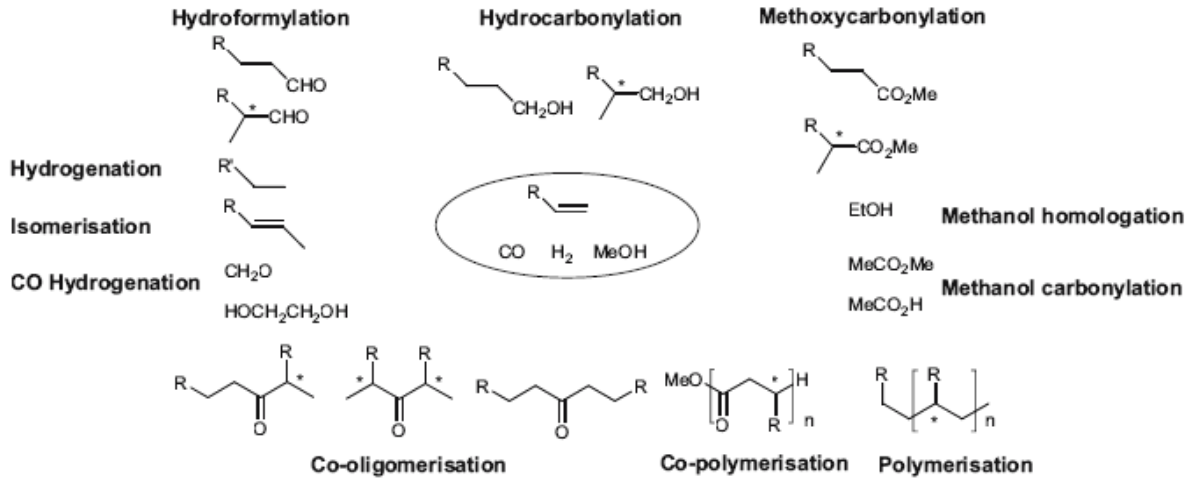

Figure 2.1 Products formed from an alkene, carbon monoxide, hydrogen and methanol. The asterisks represent asymmetric centres in chiral molecules **[2.3]**

2.1.1 Heterogeneous catalysts

Heterogeneous catalysts are insoluble in the medium in which the reaction takes place so that reactions of gaseous or liquid reagents occur at the surface. Heterogeneous catalysts do not show the selectivity shown by chiral homogeneous catalysts, but recent research on surface modifiers has shown that enantioselective reactions, for a restricted range of substrates is becoming possible **[2.4]**. Being insoluble in the reaction medium, heterogeneous catalysts can often be used as fixed beds over which the substrates flow continuously in a liquid or gaseous form. This means that the catalyst can be contained within the reactor at all times. For this reason not only the separation of the products from the catalyst is built into the process, but also, the catalyst is always kept under the same conditions of temperature, pressure, contact with the substrate and products, for which it has been optimised.

2.1.2 Homogeneous catalysts

Homogeneous catalysts are dissolved in the reaction medium and hence all catalytic sites are available for the reaction. For homogeneous catalysts, the separation can be extremely energy intensive and time consuming. Only when the product can be evaporated under the reaction conditions, can homogeneous catalytic reactions be carried out under continuous flow conditions, where the substrates are introduced continuously into the reactor whilst the products are continuously removed by evaporation. More often, commercial processes are carried out in semi-batch

reactors. Part of the liquid catalytic solution containing the product(s), unreacted substrates and catalyst is removed continuously from the reactor to a separator, which is usually a distillation system operating at lower pressure than the reactor. The products and unreacted substrates are then separated from the catalyst and lower boiling byproducts by fractional distillation before the fraction containing the catalyst is returned to the reactor **[2.3]**.

Table 2.1 lists the major disadvantages of homogeneous catalysis in industrial application: the immense difficulty of catalyst recycling, which is responsible for the fact that about 80% of catalytic reactions still employ heterogeneous catalysts and only 20% involve homogeneous catalysts. This is because it is inherently difficult to separate the molecularly dissolved homogeneous catalyst from the reaction products and any unconverted reactants in which the catalyst is dissolved at a molecular level.

Table 2.1 Comparison of homogeneous and heterogeneous catalysis **[2.3, 2.5]**

	Homogeneous Catalysis	Heterogeneous Catalysis
Activity (relative to metal content)	High	Variable
Selectivity	High	Variable
Reaction conditions	Mild	Harsh
Service life of catalysts	Variable	Long
Sensitivity toward catalyst poisons	Low	High
Diffusion problems	None	May be important
Recyclability	Expensive	High
Mode of use	Dissolved in reaction medium	Fixed bed or slurry
Mechanistic understanding	Plausible under defined conditions	Only accessible with sophisticated methods

For this reason, thermal processes are generally used to achieve product isolation and catalyst reuse. An important drawback observed particularly when using homogeneous organometallic catalysts, is that while being worked-up, e.g., by using distillation or chemical techniques, these catalysts suffer from thermal or chemical stress. Most homogeneous catalysts are thermally sensitive, usually decomposing above 150 °C and other conventional processes such as chromatography or extraction also lead to catalyst loss **[2.6]**. Table 2.2 shows this and in detail in a comparison between homogeneous and two versions of heterogeneous catalyses.

Table 2.2 Catalyst removal in homogeneous and heterogeneous catalysis **[2.5]**

	Homogeneous catalysis	Heterogeneous catalysis	
		Suspension	Fixed bed
Separation	Filtration after chemical decomposition Distillation Extraction	Filtration	No separation problems
Additional equipment required	Yes	Little	No
Catalyst recycling	Possible	Easy	Not necessary
Cost of catalyst losses	High	Minimal	Minimal
Catalyst concentration in product	Low	High	–

This comparison again shows the reasons why heterogeneous catalysts are usually preferred over homogeneous catalysts in industry application.

2.1.3 Biocatalysis

The catalysts that come closest to meeting all the requirements to perform ideally reactions are the enzymes. Additionally, significant pressure to introduce cleaner processing in the chemical and pharmaceutical industries is being made. For this reason interest for enzymes as catalysts is growing.

Biocatalysis has many attractive features in the context of green chemistry: mild reaction conditions (physiological pH and temperature), an environmentally compatible catalyst (an enzyme) and solvent (often water) combined with high activities and chemo-, regio- and stereoselectivities in multifunctional molecules. Furthermore, the use of enzymes generally circumvents the need for functional group activation and avoids protection and deprotection steps required in traditional organic syntheses. This affords processes which are shorter, generate less waste and are, therefore, both environmentally and economically more attractive than conventional routes **[2.7, 2.8]**. Despite widespread research efforts in academia and industry, the number and diversity of biocatalyst applications remain rather modest. This situation may be attributed to several perceived limitations of biocatalysis, including the availability of the biocatalysts, their substrate scope, and their operational stability. Through the advances in genomics and bioinformatics, properties of enzymes may be well understood and important characteristics as: enhanced solvent resistance, increased process stability, change of pH and temperature optima, and enhanced and even reversed enantioselectivity (ee) may be well achieved **[2.9]**.

2.2 Innovative systems for catalytic hydrogenations

Much interest has been focused in the synthesis of catalysts with defined properties in terms of activity and selectivity aiming at certain reactions with defined products. To overcome the separation problems, chemists and engineers are investigating a wide range of strategies other than distillation for recycling catalysts. In order to provide an overview of the thinking, methodology, and progress in this area of research without going into much detail, a comparison of the different approaches, using hydrogenation with rhodium-based catalysts as centre point is made. Since a large part of today's knowledge on homogeneous catalysis has been derived from the early studies on hydrogenation **[2.1]**, it is considered as the workhorse of catalytic organic synthesis and most separation strategies have been used for this reaction. The strategies under investigation can be grouped into two types. In the first, the catalyst is anchored to a soluble or insoluble support, and the separation is carried out by a filtration technique. This type of process is often referred to as heterogenizing homogeneous catalysts. The other type involves designing the catalyst so that it is solubilized in a solvent that, under some conditions, is immiscible with the reaction product or the phase it is dissolved in. These reactions involve two phases and are often referred to as biphasic catalysis.

2.2.1 Immobilized catalysts

Initial attempts with the immobilisation of asymmetric hydrogenation catalysts were aimed at improving enantioselectivity by altering reaction rates and decreasing metal-metal interactions **[2.10]**. Recent trends have seen immobilisation as a tool for ease of separation of catalyst from substrate and or product. This is mediated mostly through phase differences, with inorganic and organic polymeric supports used widely as solid state supports.

a. Inorganic supports: The immobilization of catalysts using inorganic supports can be achieved via covalent attachment. An example of these catalysts is the silica immobilized chiral Rh catalyst reported by Kinting et al. in 1985 shown in Figure 2.2 **[2.11, 2.12]**. This catalyst is obtained by anchoring the silylated chiral monophosphines to silica and then leaving it to react with $[RhCl(C_2H_4)_2]_2$. Interestingly, the catalytic behaviour of the heterogenized complexes show

greater stability and selectivity for the hydrogenation of 1-acetamidocinnamic acid than the homogeneous analogue, and the length of the spacer or tether (n) impacted on the selectivity (67 % ee when n = 1 and 87 % ee when n = 5). When recycling of the catalyst was pursued, substantial catalyst leaching (90 % of Rh loss when n = 1 and 38 % when n = 5) was present.

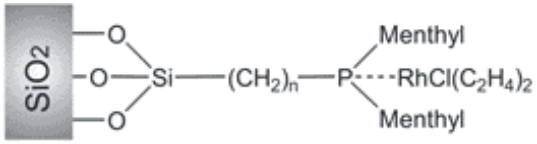

Figure 2.2 Silica immobilized chiral Rhodium catalysts used for hydrogenations

McDonald et al. used a protected BINAP ligand (as phosphine oxide) immobilised in a covalent bidentate manner to silica as the support and subsequently converted to the diphosphine ligand. After complexion of this supported ligand with $[Rh(COD)_2BF_4]$ (see Figure 2.3), the resulted catalyst was used for the asymmetric hydrogenation of (*Z*)-α-acetamidocinnamic acid and α-acetamido acrylic acid showing enantioselectivity levels (84 % ee for the first and 67 % ee for the second run) comparable to the parent homogeneous catalysts. The immobilised catalysts were recycled by filtration, showing decomposition of the catalyst **[2.13]**.

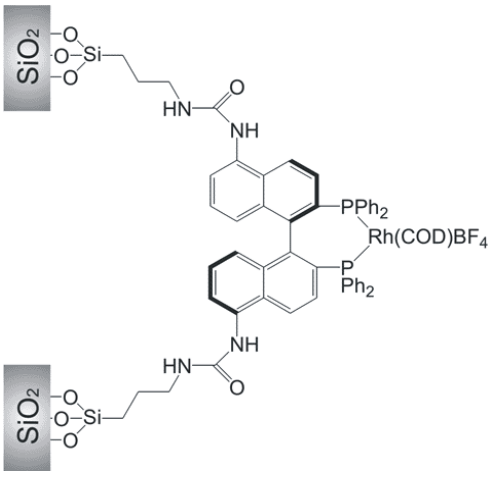

Figure 2.3 BINAP Rhodium complex immobilised covalently to silica

There are other ways of immobilizing catalysts on inorganic supports, for example by taking advantage of the ionic nature of some catalysts. Cationic Rh complex can be fixed on a support containing anionic functional groups

such as a sulfonate. Selke et al. immobilized a carbohydrate-based catalyst by ion-exchange. The cationic Rh chelates of 2,3-bis(*O*-diphenylphosphino)-*β*-D-glucopyranoside were immobilized on silica via ionic interaction, resulting the compound shown in Figure 2.4. When using the catalyst for the hydrogenation of α-acetamido acrylic acid ester, the enantioselectivity obtained was slightly higher (95% ee) than that obtained with homogeneous catalyst (91% ee). Although the silicas were recycled up to 20 times and the enantioselectivity was retained, appreciable amounts of Rh metal leached into the product **[2.11, 2.14]**.

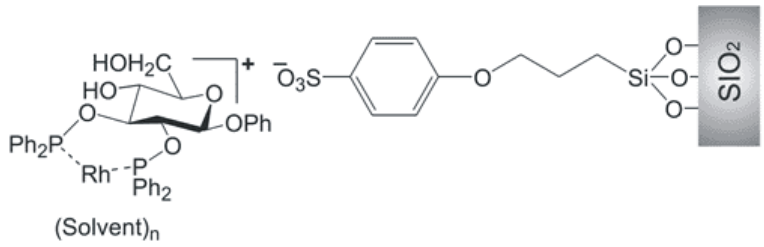

Figure 2.4 Cationic Rh chelate of 2,3-bis(O-diphenylphosphino)-β-D-glucopyranoside immobilized on silica via ionic interaction

b. Organic supports: Organic polymers show solvent-dependent swelling properties that can strongly influence the catalytic performance. MeOPEG-supported (*R*)-BINAP and (3*R*, 4*R*)-Pyrphos ligands have been prepared and shown to be effective in Rh-catalyzed asymmetric hydrogenations. High enantioselectivity was observed (86-96%), and furthermore, this catalyst was found to be easily recyclable with little loss of catalytic activity. A second approach to MeO-PEG immobilized BINAP with MeO-PEG_{5000} was reported by Guerreiro et al. In this case a Ru catalyst was used for the hydrogenation of methyl acetoacetate in methanol at 50 °C, yielding the desired product in 99% ee. This catalyst could be easily recycled for at least four times without any apparent loss of activity **[2.11, 2.15, 2.16]**.

Dendrimer chemistry has been extremely popular in the past decades, and several potential applications of dendrimers, including catalysis have been explored and are very well documented. Dendrimers present well-defined macromolecular structures that enable the construction of precisely controlled catalyst structures. The number of catalysts attached to the support as well as

their location can be regulated, which can be of crucial importance for the catalytic performance of the system **[2.17]**.

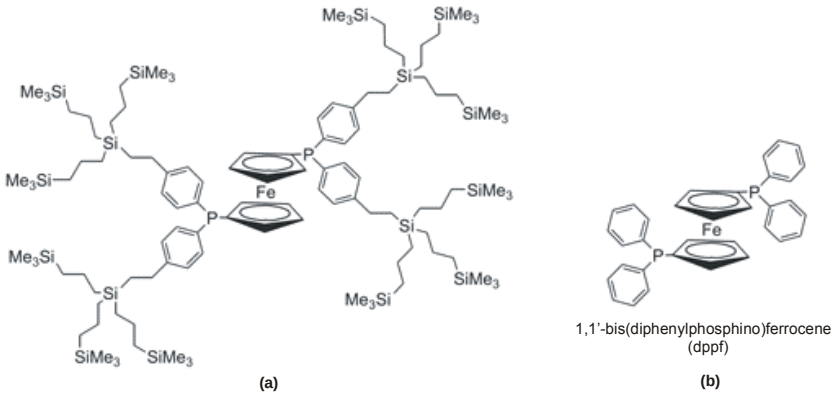

Figure 2.5 Bis(diphenylphosphino)ferrocene complexes (a) Core-functionalized dendrimer and (b) 1,1' bis(diphenylphosphino)ferrocene

Oosterom et al. used a rhodium complex of dendritic ligand (see Figure 2.5) and compared it with dppf (1,1`-bis(diphenylphosphino)ferrocene) for the hydrogenation of dimethyl Itaconate in a membrane reactor. As observed in Figure 2.6, a lower maximum conversion using dppf was obtained and attributed to a combination of 10% lower activity of the catalyst and leaching of active complex. Rh retention of 97% for the dppf complex and 99.8% for the dendritic catalyst were obtained, based on ICP-AES analyses **[2.18]**. Due to the size of the dendrimers, catalyst recycling can be achieved by nanofiltration or even precipitation **[2.16, 2.19]**.

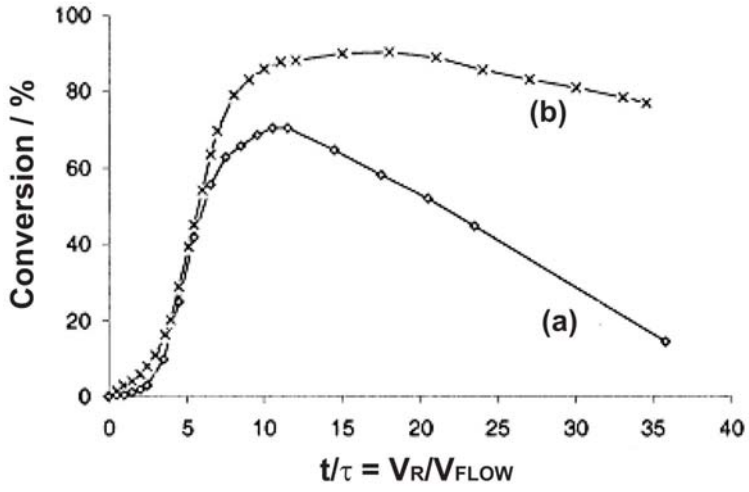

Figure 2.6 Conversion (in %) versus time (expressed in reactor volumes pumped through the reactor which was three per hour) of the continuous hydrogenation of dimethyl itaconate using (a) the dendrimeric ligand and (b) dppf

After going through a large number of innovative supported catalysts, we observe that in general the immobilization of catalysts generates a loss of activity of the catalyst. Catalysts supported in soluble compounds have managed to overcome this loss of activity. Another strategy to reduce the negative effects of catalyst immobilization on the activity is the use of supercritical fluids such as $scCO_2$.

2.2.2 Supercritical fluids

$ScCO_2$ has solvation properties comparable to higher alkanes, and at the same time the diffusion is much higher because of the low density **[2.20, 2.21]**. Carbon dioxide ($scCO_2$) is the most widely used supercritical fluid. It has mild critical properties (Tc = 31.1 °C, pc = 73.8 bar, dc = 0.437 g·mL^{-1}), is non-toxic, non flammable and can be handled safely on laboratory and industrial scales. Contrary to classical organic solvents, CO_2 is not classified as a “volatile organic chemical” (VOC) and applications of CO_2 have a GRAS (“generally regarded as safe”) status. The economic viability of $scCO_2$ technology has been demonstrated by commercial applications in fields as diverse as natural product extraction **[2.22]**, wafer production and dry cleaning **[2.23]**. A commercial scale multi-purpose plant for heterogeneous catalysis involving $scCO_2$ has recently entered operation **[2.24]**. Examples of organometallic catalysis in supercritical fluids are by no means restricted to CO_2 **[2.21, 2.25]**, but only this medium has been used to date in applications focusing on catalyst immobilisation.

Supercritical fluids (SCFs) are substances which have been simultaneously heated above their critical temperature Tc and compressed above their critical pressure pc. At temperatures above Tc, isothermic compression results in a continuous increase in the fluid density, but no condensation to form a liquid occurs. The schematic phase diagram in Figure 2.7 demonstrates this behaviour for carbon dioxide as model SCF. Supercritical fluids fill the entire space available to them like gases, but at the same time can act as solvents for liquids or solids. The solvent properties can be tuned over a wide range by adjustments in the fluid density; this can be achieved by relatively small changes in either temperature or pressure. This unique combination of gas-like and liquid-like tuneable properties offers new approaches for the immobilization of organometallic catalysts **[2.26]**.

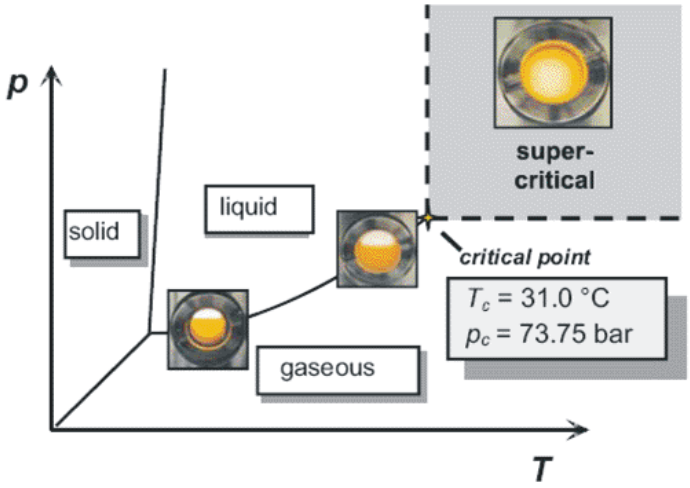

Figure 2.7 Schematic phase diagram of CO_2 with snapshots of the transition from the liquid/gas region to the supercritical region (with a bright orange "CO_2-philic" rhodium complex) **[2.25]**

Three fundamentally different approaches for catalyst immobilization involving SCFs can be distinguished which are depicted in Figure 2.8. First, the tuneable solvent properties of the SCF are used to control the solubility of the organometallic catalyst in the reaction medium with no additional support or solvent (Figure 2.8a). This method is referred to as "catalysis and extraction using supercritical solutions" (CESS). Because of the similarities to the temperature-controlled catalysts in conventional solvents, they are too sometimes referred to as "smart catalysts". An example of this approach is the hydrogenation of isoprene in $scCO_2$ with the ponytail complex Rh(hfacac)($R_2PCH_2CH_2PR_2$) (where R = C_6H_4-*m*-$(CH_2)_2(CF_2)_5CF_3$) (see Scheme 2.1). In this case, due to the decomposition of the catalysts under reaction conditions, the reaction was considerably slower than the hydrogenation by the analogous dppp (1,3-*bis*(diphenylphosphino)propane) complex in organic solvents **[2.21]**. The second approach is liquid/supercritical multiphase catalysis (Figure 2.8b), where the biphasic solvent is forming in fact a triphasic system (liquid-liquid-gas) if gaseous reagents are involved. A biphasic system constituted by PEG 900 and CO_2 was used as reaction media for the hydrogenation of styrene (see Scheme 2.2), with Wilkinson's complex [$(PPh_3)_3RhCl$] as the catalyst. Batch-wise recycling was successfully achieved by extraction of the ethylbenzene product with the $scCO_2$ phase. During this process the catalyst remained stable in the PEG phase and could be recycled four times without noticeable loss of activity. Rhodium contamination in the product was below the detection limit (less than one part per million), but measurable amounts of PEG 900 were detected among the extracted products **[2.27]**.

Finally, the organometallic catalyst can be anchored to a solid organic or inorganic support which is then contacted with the supercritical reaction medium (Figure 2.8c) **[2.26]**. This approach has been widely used in the hydroformylation of 1-octene and styrene using inorganic and organic supported Rh catalysts complexes **[2.28]**.

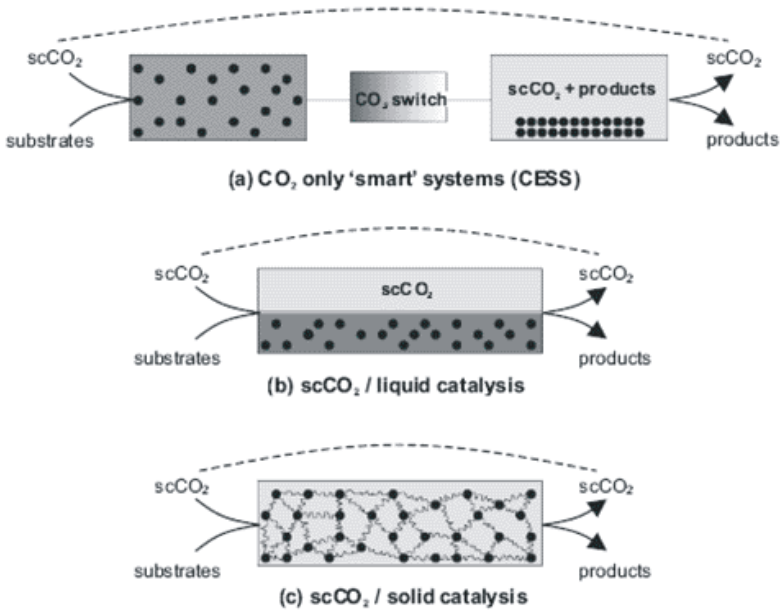

Figure 2.8 Schematic representation of the three approaches possible for immobilizing catalyst using SCFs **[2.26]**

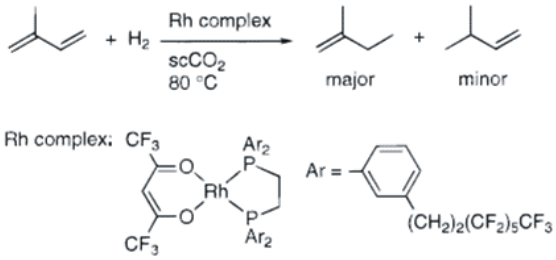

Scheme 2.1 Ponytail complex Rh(hfacac)($R_2PCH_2CH_2PR_2$) (where R = C_6H_4-m-$(CH_2)_2(CF_2)_5CF_3$) used for the hydrogenation of isoprene **[2.21]**

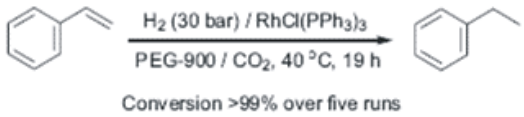

Scheme 2.2 Rhodium-catalysed hydrogenation in the biphasic system PEG/scCO2 **[2.27]**

Most metal-containing complexes, particularly rhodium-based hydrogenation catalysts containing aryl–phosphine ligands, are virtually insoluble in apolar $scCO_2$.

Solubility can be enhanced by the incorporation of the perfluoroalkyl groups characteristic of fluorous chemistry.

2.2.3 Perfluoroalkyl-substituted catalysts

The perfluorinated groups $F(CF_2)_6^-$ $(CH_2)_2$ (H_2F_6) **[2.29]**, can act as solubilizers for aryl phosphines making the corresponding metal complexes sufficiently "CO_2-philic" for catalysis in many cases **[2.30]**. By modifying the well established and highly efficient ligand BINAPHOS, which contains PAr_2 donor groups, with the perfluoroalkyl (H_2F_6) group, the rhodium (*R*,*S*)-3-H_2F_6-BINAPHOS (see Figure 2.9) is readily adjusted to the nonconventional solvent $scCO_2$.The hydrogenation of 2-acetamido methyl acrylate and dimethyl itaconate gives high enantioselectivities (> 96 % ee) **[2.31]**.

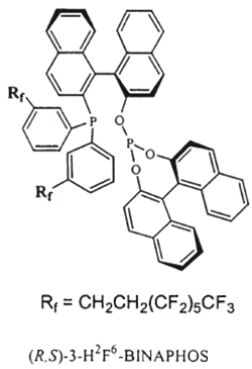

Figure 2.9 Rhodium (R,S)-3-H_2F_6-BINAPHOS used for the hydrogenation of 2-acetamido methyl acrylate and dimethyl itaconate **[2.31]**

Another idea based on fluorous chemistry but focused on catalyst recycling, is the use of flourous biphasic catalysis. Fluorous compounds differ markedly from the corresponding hydrocarbon molecules and are, consequently, immiscible with many common organic solvents at ambient temperature although they can become miscible at elevated temperatures. Hence, this provides a basis for performing biphasic catalysis or, alternatively, monophasic catalysis at elevated temperatures with biphasic product/catalyst separation at lower temperatures. A number of fluorous solvents are commercially available, albeit rather expensive compared with common organic solvents **[2.32]**. In order to perform fluorous biphasic catalysis the (organometallic) catalyst needs to be solubilized in the fluorous phase by deploying "fluorophilic" ligands, analogous to the hydrophilic ligands used in aqueous biphasic catalysis. This is accomplished by incorporating so-called "fluorous ponytails" **[2.33]**.

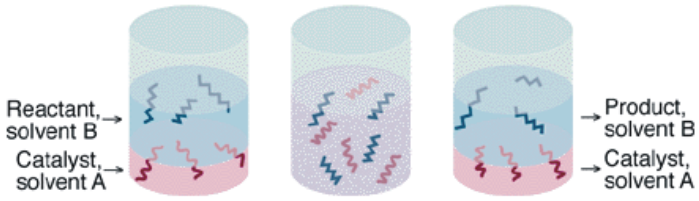

Figure 2.10 (**Left**) A homogeneous catalyst is tailored to dissolve in solvent A, while the reactant is dissolved in solvent B. (**Middle**) At the reaction temperature, catalyst, reactant, and solvents A and B form a single phase in which the reaction takes place. (**Right**) After the reaction is completed, the system is cooled down, resulting in phase separation. The catalyst and product are in separate phases, facilitating separation **[2.33]**

The range of homogeneous reactions that has been transferred into $scCO_2$ or perfluorinated solvents is probably less wide than into ionic liquids (ILs) due to the great versatility of ILs **[2.34]**.

2.2.4 Ionic liquids

Ionic liquids are characterised by the following three definition criteria. They consist entirely out of ions, they have melting points below 100 °C and they exhibit no detectable vapour pressure below the temperature of their thermal decomposition. For these reasons room temperature ionic liquids are attractive media for performing green catalytic reactions and as a consequence of these properties most ions forming ionic liquids display low charge densities resulting in low intermolecular interaction.

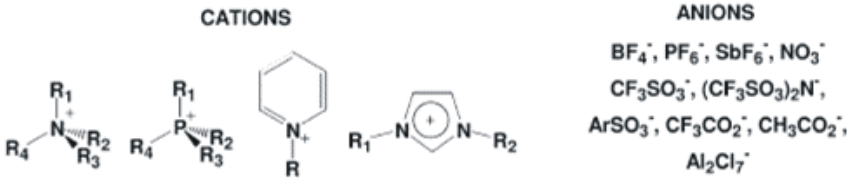

Figure 2.11 Structures of ionic liquids **[2.7]**

As an important example: the asymmetric hydrogenation of (Z)-α-acetamidocinnamic acid and methyl-(Z)-α-acetamidocinnamate by [Rh(COD)(DIPAMP)][BF_4] catalyst (see Figure 2.12) was studied in ionic liquid/isopropanol two-phase catalytic system. In this system 97-100% conversion was achieved and the ee values were over 90%. Application of 1-*n*-butyl-3-

methylimidazolium tetrafluoroborate ([bmim][BF_4]) ionic liquid (see Figure 2.12) made it possible to recycle the catalyst in consecutive cycles. After four cycles, neither significant conversion nor enantioselectivity decrease was observed **[2.35]**.

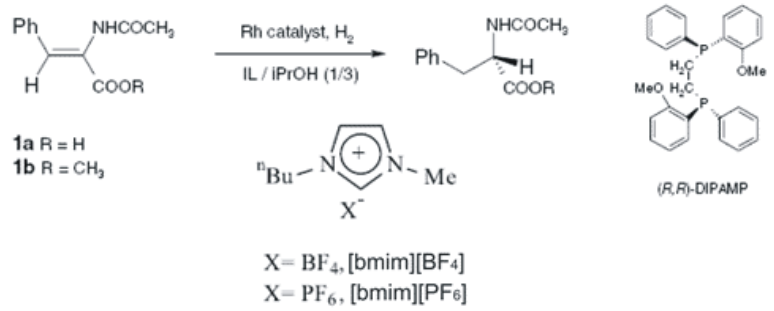

Figure 2.12 Asymmetric catalytic hydrogenation of (Z)-α-acetamidocinnamic acid and methyl-(Z)-α-acetamidocinnamate in ionic liquid/isopropanol biphasic system and the chiral phospine ligand of the Rh catalyst **[2.35, 2.36]**

An important drawback of using ionic liquids as hydrogenation media is the low solubility of hydrogen in these solvents. Where as the solubility under 1 bar of hydrogen in [bmim][BF_4] (0.9 x 10^{-3} M) is similar to that in water (0.8 x 10–3 M), by increasing the pressure to 10 bar the solubility in the ionic liquid (3.0 x 10–3 M) increases to a similar value as that of cyclohexane (3.7 x 10–3 M) **[2.37]**. But when comparing with another ionic liquid, the molecular hydrogen is almost four times more soluble in the ionic liquid 1-*n*-butyl-3-methylimidazolium tetrafluoroborate [bmim][BF4] than in its hexafluorophosphate [bmim][PF6] analogue at the same pressure (50 bar) **[2.36]**.

Rh catalysed asymmetric hydrogenations can be transferred to liquid–liquid two-phase systems using imidazolium based ionic liquids as the mobile phase, but the concept of biphasic catalysis has its origins in the application of water soluble catalysts.

2.2.5 Biphasic catalysis

In the recent years the organometallic chemistry in water is gaining increasing attention particularly with water as the polar phase in multiphase systems, as can be seen in the appearance of an increasing number of original articles and several review articles on this field **[2.38, 2.39, 2.40]**. Water as a solvent offers new opportunities as compared to organic solvents. It favors ionic reactions because of its high dielectric constant (ε25° = 78.5) and the ability to solvate cations as well as

anions. Beyond that, water is the ideal solvent for radical reactions since the strong O–H bonds (enthalpy 436 $kJ \cdot mol^{-1}$) are not easily attacked **[2.41]**. Furthermore water displays particularly high enthalpy changes during the solid-liquid (ΔH_F = 6.003 $kJ \cdot mol^{-1}$) and particularly the liquid-gaseous (ΔH_V = 40.656 $kJ \cdot mol^{-1}$) phase transition, since the phase transitions are associated with the formation or breaking of hydrogen bonds. Additional advantages of water as a solvent are its high heat capacity, its strong pressure dependency of the viscosity, and the high cohesive energy density (c.e.d. = 2.303 $kJ \cdot cm^{-3}$) **[2.38, 2.39, 2.40]**. Although chemical transformations in living systems occur in an aqueous environment, it was only in 1960's that a breakthrough was achieved in the use of water as a solvent, particularly in organometallic catalysis. The main goal in this case was the recycling of the expensive and sometimes toxic catalyst in hydroformylation, a very important industrial application. Nevertheless, this discovery motivated researchers to try to perform many organic reactions in aqueous media, and the development of water-soluble organometallic catalysts has expanded significantly. From an industrial point of view, the use of water as reaction medium allows for waste reduction costs as the catalyst can be recovered via a biphasic process. Furthermore, replacing flammable, carcinogenic, and explosive organic solvents with water leads to a safer working environment.

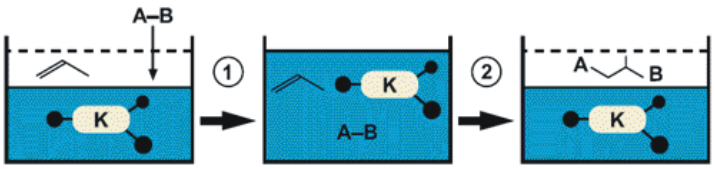

Figure 2.13 Principle of the biphasic catalysis in water: Using a water soluble catalyst complex K diluted in water, a substrate (propylene and CO/H_2) can be converted to product, which is finally concentrated in an exchangeable second phase **[2.42]**

In an ideal phase-separable or biphasic catalysis system (see Figure 2.13), the catalyst and associated ligands would be dissolved in one phase (water soluble catalysts for aqueous biphasic systems) and the reactants and products would be completely soluble in a second phase, which can be removed after reaction and the catalyst phase recycled for further use. If the substrate is soluble in the catalyst phase, it is preferable that the product should be soluble in and isolated from the other phase. To capture the attributes of both a biphasic system and a homogeneous single-phase system, the ideal system would allow for excellent mixing, efficient

transfer between phases, or complete miscibility of the phases under the reaction conditions to achieve high reaction rates **[2.33]**.

For aqueous biphasic systems, the water solubilisation of phosphine ligands is usually achieved via introduction of a highly polar functional group such as an amino, carboxylic acid, hydroxide, or sulfonate. The sulfonated derivatives of ligands containing aryl groups have proven most successful, mostly because of the outstanding solubility in water. Since the initial discovery and application of the *meta*-monosulfonated triphenyl phosphine (TPPMS) **[2.43]** (see scheme 2.3) much success in aqueous catalysis has been achieved via the use of the further sulfonated derivatives such as TPPDS **[2.44]** and TPPTS **[2.45]**. Notably, the standard tris(*m*-sulfonatophenyl)phosphine [$P(C_6H_4$-*m*-$SO_3^-\ Na^+)_3$; TPPTS] has a solubility of ca. 1.1 $kg \cdot L^{-1}$ upon which the success of the catalyst system Rh/TPPTS depends in biphasic, aqueous hydroformylation.

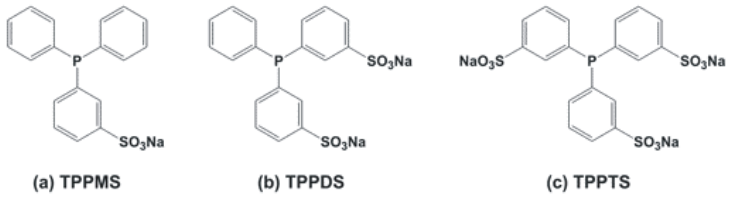

Scheme 2.3 Water-soluble sulfonated phosphines **[2.42]**

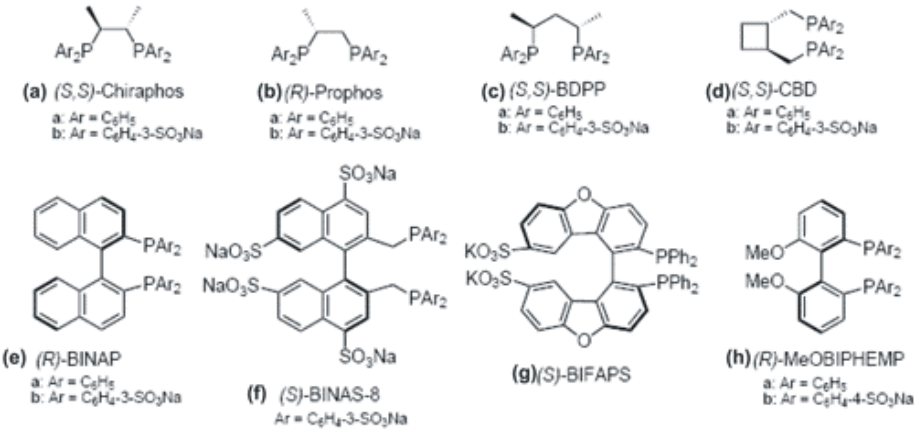

Scheme 2.4 Water-soluble chiral sulfonated diphosphines **[2.39]**

Scheme 2.4 shows a variety of water soluble chiral sulfonated diphosphine ligands. The sulfonation of the ligands does not affect the outcome of the enantio-selectivity for hydrogenation. The water-soluble Rh complex of the ligand (e)-b gave ee up to 70 % in the reduction of acetamidoacrylic acid and its methyl ester **[2.46]**,

quite similar as observed with the unsulfonated complex (e)-a catalyst in ethanol (68-70 %).

It has to be mentioned that water-soluble phosphine complexes of rhodium(I), such as $[RhCl(TPPMS)_3]$, $[RhCl(TPPTS)_3]$, $[RhCl(PTA)_3]$, either preformed, or prepared in situ, catalyze the hydrogenation of unsaturated aldehydes at the C=C bond. **[2.38]** As an example, at 80 °C and 20 bar in 0.3-3 h cinnamaldehyde and crotonaldehyde were hydrogenated to the corresponding saturated aldehydes with 93 % and 90 % conversion, accompanied with 95.7 % and 95 % selectivity, respectively. Using a water/toluene mixture as reaction medium allowed recycling of the catalyst in the aqueous phase with no loss of activity.

A centrifugal partition chromatograph (CPC), shown in figure 2.14 was used as a liquid/liquid continuous catalytic plug flow reactor for the transfer hydrogenation of dimethyl itaconate in a biphasic cyclohexane-water system with the water soluble catalyst complex Rh–TPPTS. In this study the industrial potential of the reactor was not exploited, but it was used under steady-state operations in chemical regime and plug flow mode to allow the discrimination of kinetic models.**[2.47, 2.48]**.

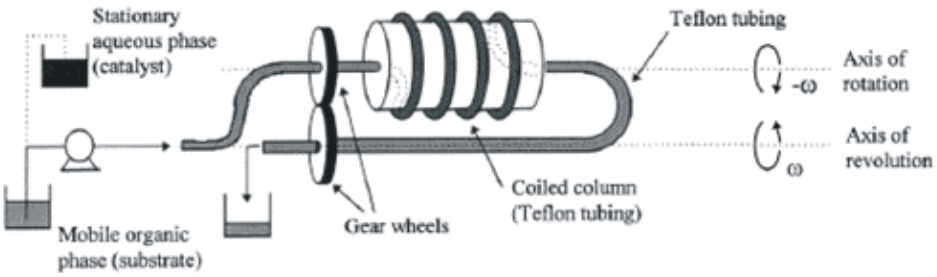

Figure 2.14 Schematic representation of the centrifugal partition chromatograph (CPC) **[2.47]**

With the introduction of water-soluble phosphine ligands and their application in complex catalysts have been possible in biphasic and phase-transfer systems, but the partition coefficient of the substrate to be hydrogenated has an important influence on the reaction rate. For this reason the addition of amphiphiles or surfactants to the reaction media helps to overcome the mass transfer limitations originated by a low solubility in the catalyst containing aqueous phase.

2.2.6 Micellar systems

Micelles are simple spherical supramolecular aggregates, which are formed by amphiphiles in water or media similar to water at concentrations above the critical micelle concentration (CMC). The CMC is the lowest concentration at which micelles form. The formation of micelles is characterized by an often sharp discontinuity in system properties which are intrinsic to reactivity, such as surface tension, self diffusion, and the molality of dissolved compounds. A prerequisite however is sufficient solubility of the amphiphile in water, the medium in which the micelles are formed. The temperature at which the concentration of the amphiphile reaches the CMC is defined as the Krafft point or Krafft temperature, and is generally associated with a sudden increase in solubility. A typical micelle in aqueous solution forms an aggregate with the hydrophilic “head” group of the surfactant in contact with the surrounding solvent, sequestering the hydrophobic “tail” group in the micelle centre. This type of micelle is known as a normal phase micelle. A micellar system appears to be homogeneous since these aggregates are of colloidal size; however, as figure 2.15 shows in reality the absorbed reactants are in a microheterogeneous two-phase system. Micelles can cause an acceleration or inhibition of a given chemical reaction relative to the equivalent reaction in an aqueous medium. In general, the micellar effect is referred to as “micellar catalysis” when it refers to the acceleration of the rate of a reaction; this assignment is however only an approximation for a kinetic analysis. Amphiphiles often eliminate the detrimental effects of water and bring about large increases in both the rate and the enantioselectivity of hydrogenations of prochiral olefins in aqueous solutions.

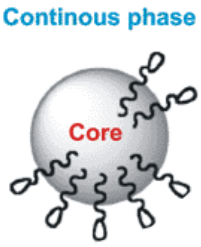

Figure 2.15 Schematic representation of a micelle

An important advantage of using micellar systems as reaction media is the possibility of using any of the many and increasing amount of catalyst complexes in the reactions without the necessity of further procedures to achieve water solubility.

For example with a Rh complex of the ligand BPPM, the hydrogenation of methyl (*Z*)-α-acetamidocinnamate proceeds fast in methanol ($t_{½}$ = 2 min) with 90% e.e. (BPPM = (2*S*,4*S*)-4-diphenylphosphino-2-diphenylphosphinomethylpyrrolidine). In water the same reaction is much slower ($t_{½}$ = 90 min) and markedly less selective (78% ee). Addition of various amphiphiles to the aqueous systems lead to shorter reaction times and enantioselectivities as high as 95% which is even higher than that obtained in methanol **[2.38]**. Additionally, when a 5 wt% sodium dodecyl sulfate (SDS) micellar system is used as reaction media for the hydrogenation of itaconic acid with the Rh–BPPM catalyst complex, 99 % of the catalyst concentrated micelles can be retained by micellar enhanced ultrafiltration (MEUF) and reused without loss in selectivity **[2.49]**.

Micellar systems are known to solubilise only low amounts of some substrates and the required time for ultrafiltration to achieve catalyst recycling is often long. For these reasons microemulsions are in some cases preferred as reaction media.

2.3 Microemulsions

Before going in further details on using microemulsions as reaction media and because microemulsions are central point to this dissertation, some preliminary details and concepts are discussed in the first pages of this section.

A microemulsion is a multicomponent (3 – 4 components) system, e.g., water in hydrocarbon (water/oil) or hydrocarbon in water (oil/water), surfactant, and cosurfactant, and generally it exists only in small concentration ranges. Nevertheless, the capacity for reactants and variability of solubilization properties are high and of practical interest **[2.50]**. A wide range of new amphiphiles (surfactants) have been synthesized in recent decades to keep pace with increasing technical demands. Typical aspects that have been considered include biological degradability and physiological compatibility, cleavability, the ability to form polymers, and the photolytic formation of amphiphiles. Variations were mostly incorporated into the polar head groups. The purity of the surfactants is often uncertain, which casts doubt on the validity of the characterization data, and various techniques aimed at purification have been suggested **[2.51]**.

Microemulsions can be classified into two categories: oil in water microemulsions (O/W) in which the hydrophobic tails of the surfactant is absorbed in

the oil microdroplets while the hydrophilic part is oriented toward the water, and water in oil microemulsions (W/O) with the surfactant dissolved in organic solvents forming spheroidal aggregates called reverse micelles. They can be formed both in the presence and in the absence of water. However if the medium is completely free of water, the aggregates are very small and polydisperse. The presence of water is necessary to form large surfactant aggregates. Water is readily solubilized in polar cores, forming reverse micelles, in which the hydrophilic heads of the surfactant are absorbed in the water microdroplets while the hydrophobic tails are oriented toward the oil.

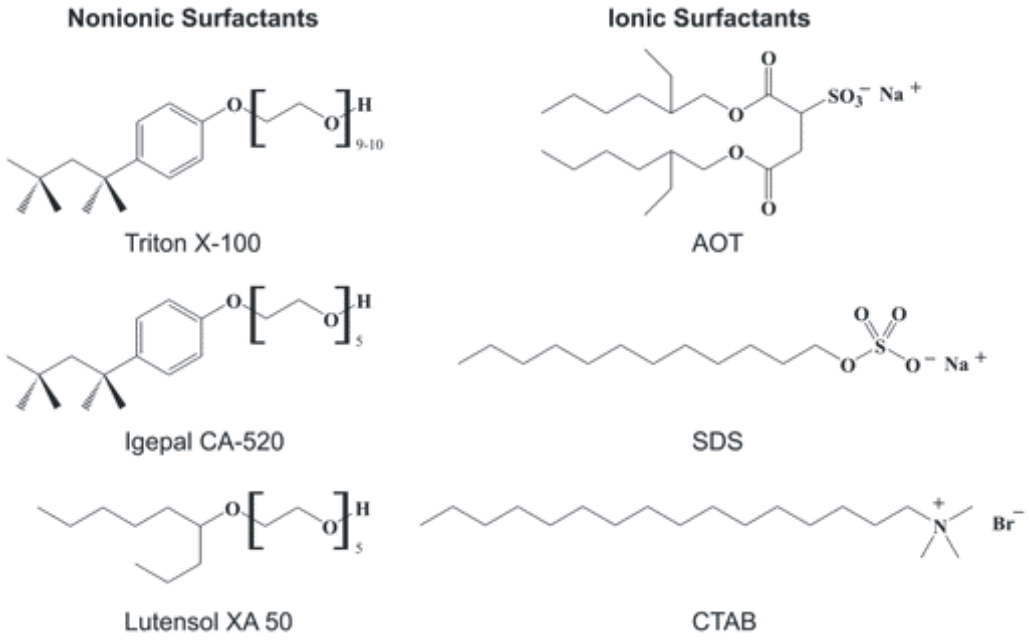

Scheme 2.5 Typical micelle forming nonionic and ionic surfactants

As observed scheme 2.5, the amphiphile surfactant is either not charged (i.e., is nonionic) or consists of an ionic (charged) headgroup **[2.52]**.

When a surfactant is dissolved in a polar solvent, the hydrophobic group of the surfactant responds in some fashion in order to minimize contact between the hydrophobic group and the solvent. In the case of a surfactant dissolved in aqueous medium, the hydrophobic group distorts the structure of the water (by breaking hydrogen bonds between the water molecules and by structuring the water in the vicinity of the hydrophobic group). As a result of this distortion, some of the surfactant molecules are expelled to the interfaces of the system, with their hydrophobic groups oriented so as to minimize contact with the water molecules. The surface of the water becomes covered with a single layer of surfactant molecules with their hydrophobic groups oriented predominantly toward the air. Since air molecules are essentially

nonpolar in nature, as are the hydrophobic groups, this decrease in the dissimilarity of the two phases contacting each other at the surface results in a decrease in the surface tension of the water. On the other hand, the presence of the hydrophilic group prevents the surfactant from being expelled completely from the solvent as a separate phase, since that would require dehydration of the hydrophilic group. The amphiphilic structure of the surfactant therefore causes not only concentration of the surfactant at the surface and reduction of the surface tension of the water, but also orientation of the molecule at the surface with its hydrophilic group in the aqueous phase and its hydrophobic group oriented away from it. In a polar solvent such as water, ionic or highly polar groups may act as hydrophilic groups, whereas in a nonpolar solvent such as heptane they may act as hydrophobic groups. As the temperature and use conditions (e.g., presence of electrolyte or organic additives) vary, modifications in the structure of the hydrophobic and hydrophilic groups may become necessary to maintain surface activity at a suitable level. For nonionic oxyethylene-based surfactant systems, there is a weakened interaction between the oxyethylene groups and the water solvent with increasing temperature. The conformational changes will consequently make the polyoxyethylene chains progressively less polar as the temperature is increased. Becoming less polar, they will interact less favourably with water, leading to reduced hydration, and more favourably among themselves, thus leading to a closer packing of headgroups in the surfactant self-assemblies, as well as to an increased tendency to separate into a more concentrated phase.

Ionic surfactants respond to temperature in the opposite direction to that found with nonionic surfactants, they become more soluble in water as the temperature increases. The dissolution of the ionic surfactant into the constituent solvated ions increases markedly with temperature as seen for simple salts. If this solubility is below the *CMC,* no micelles can form and the total solubility is limited by the (low) monomer solubility. If, on the other hand, the monomer solubility reaches the *CMC,* micelles may form.

The phenomenon of influence of the temperature on the surfactant solubility can be generally denoted as the "Krafft phenomenon", with the temperature for the onset of the strongly increasing solubility being the "Krafft point" or "Krafft temperature". The Krafft point may also vary dramatically with subtle changes in the surfactant chemical structure:

(i) The Krafft point decreases strongly as the alkyl chain length increases. The decrease is not regular but displays an odd-even effect.

(ii) The Krafft point is strongly dependent on the head-group and counterion. Salt addition typically raises the Krafft point, while many other cosolutes decrease it. There are no general trends for the counterion dependence. Thus, for example, for alkali alkanoates the Krafft point increases as the atomic number of the counterion decreases, while the opposite trend is observed for alkali sulfates or sulfonates. For cationics, the Krafft point is typically higher for bromide than for chloride, and still higher for iodide. With divalent counterions, the Krafft point is typically often much higher.

2.3.1 Phase diagrams

Microemulsions are phases in thermodynamic equilibrium with their environment. They are unfortunately only found under certain carefully defined conditions. Formulation of microemulsion phases can be difficult since microemulsions often coexist with other phases such as excess oil and/or water, and are often close to lyotropic liquid crystalline phases. A map of the locations of microemulsion phases in composition space is known as a "phase diagram". Generation of complete phase diagrams for each specific mixture of interest is rather time-consuming, and thus formulators of microemulsions can benefit from an detailed knowledge of how the phase diagrams depend upon the chemical structures of the oil and surfactant, temperature, pressure, and additives such as salt and polymers. Maps of the phase behaviour of three-component mixtures (water, oil and surfactant) are best plotted by constructing the "Gibbs triangle," which describes ternary compositions of oil, water and surfactant in two-dimensional space (Figure 2.16).

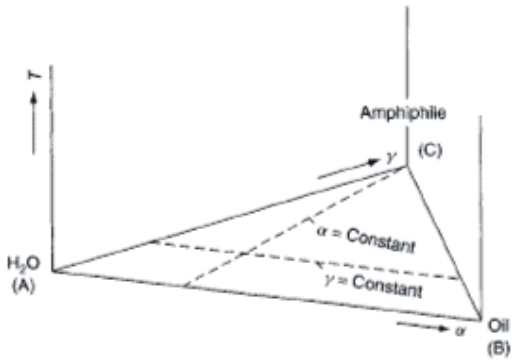

Figure 2.16 Gibbs triangle for water (A), oil (B) and surfactant (C) mixtures, showing lines of constant oil/water ratio (α = constant) and constant surfactant concentration (γ = constant) **[2.53]**

Each of the corners of the triangle represent the three pure components (100 wt %), while the three edges of the triangle map the three binary combinations. The dependence of the ternary Gibbs phase diagram upon changing a variable such as temperature is mapped in three dimensions by vertically stacking the Gibbs triangles into a "prism", with temperature as the vertical ordinate (see Figure 2.17) **[2.54]**. The following common terms are used to describe the compositions of the three-component systems:

$$\alpha = \frac{m_{\text{oil}}}{m_{\text{oil}} + m_{\text{water}}} \qquad \gamma = \frac{m_{\text{surfactant}}}{m_{\text{oil}} + m_{\text{water}} + m_{\text{surfactant}}} \qquad \omega = \frac{n_{\text{water}}}{n_{\text{surfactant}}} \qquad \text{(eq. 2.1)}$$

Visual observations allow determination of phase boundaries in a most precisely and reliably way. Single-phase systems are usually more transparent than mixed multiphase systems which are turbid. Liquid crystalline phases, found at higher surfactant concentrations, are birefringent and easily identified by using crossed polarizers along with a strong light source. Differentiation of 2 and 3 phase regions usually requires waiting for phase separation of the samples. However, since electrical conductivity changes by orders of magnitude as samples change from water-continuous to oil-continuous, conductivity measurements of stirred multi-phase systems may be used to estimate the location of the 3 phase samples central region of the phase diagram (region of intermediate conductivity) **[2.54]**.

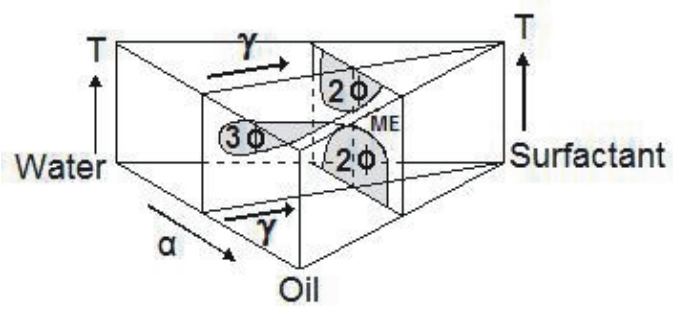

Figure 2.17 Schematic phase prism of a ternary mixture of water-oil-surfactant including two characteristic sections at constant α and constant γ, and which distinctive regions of one phase microemulsion (ME), biphasic (2ϕ) and three-phase system (3ϕ) are observed as a function of the temperature (T)

Schematic phase diagrams of the three binary mixtures of oil/water, surfactant/water and surfactant/oil, which form the three sides of the phase prism, are shown in figure 2.18. First some comments on the binary mixtures:

(i) Oil/Water. Non-polar oils and water remain essentially immiscible over the temperature range of interest.

(ii) Surfactant/Water. The phase diagram for the water-nonionic surfactant (A-C) binary solution is more complex and is characterized by a upper critical solution temperature (UCST) behavior at low temperatures and a closed loop immiscibility island at high temperatures; i.e., it phase separates both upon cooling and upon heating. The closed loop is due to the breaking of hydrogen bonds upon heating and shows up for strong amphiphile surfactants **[2.52]**.

(iii) Surfactant/Oil. As the temperature is increased, ethoxylated alcohols become more miscible with oil. A homogeneous oil-surfactant (B-C) binary mixture phase separates upon cooling.

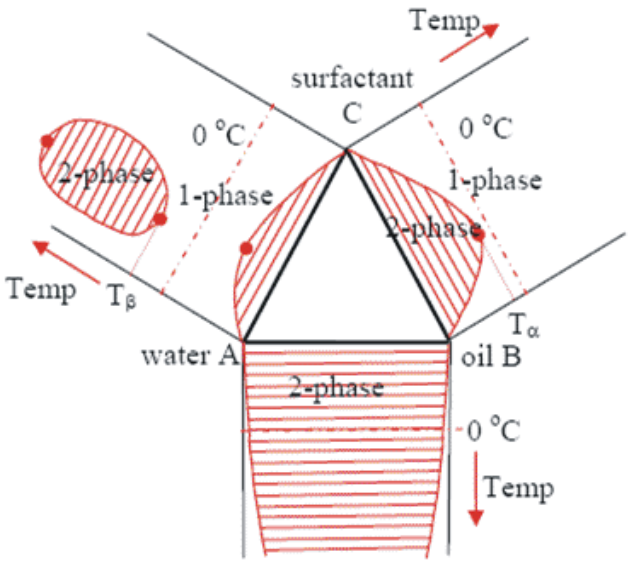

Figure 2.18 Schematic phase diagrams as a function of temperature of the three binary mixtures, oil/water, water/nonionic surfactant and oil/nonionic surfactant, showing tie-lines within the 2 phase regions **[2.55]**

Figure 2.19 shows a "pseudo-binary" section through the phase prism showed in figure 2.17, obtained when the weight fraction of oil to water is fixed at 50/50 (α = 0.5). The phase diagram as a function of temperature (T) and surfactant concentration (γ) takes the shape of a fish: the three-phase region (3ϕ) is the body of

the fish, the tail of the fish is the one-phase region (*1ϕ*), and the body of the fish lies above a *2ϕ* region and below a *2ϕ* region. For nonionic surfactants at low temperatures, this *2ϕ* region located below the body of the fish represents an oil–in–water (o/w) microemulsion coexisting with an excess oil phase (2), this system is also denoted as a Winsor I system. At high temperatures a water–in–oil (w/o) microemulsion coexists with an excess water phase ($\bar{2}$ or Winsor II). The surfactant concentration at the head of the fish, γ_0, is a measure of the "critical microemulsion concentration" *(cμc).* At this surfactant concentration, the middle microemulsion phase forms first. Below the head of the fish (below γ_0), 2ϕ systems are observed where the surfactant is dissolved as monomers in the oil and water phases, and no mixing of oil and water is found. At γ_0, the three-phase region first appears indicating the formation of a middle phase microemulsion phase with an internal interface of surfactant separating oil and water microdomains. At γ_0, the concentration of surfactant in the excess water phase is identical to the critical micelle concentration (γ_{water} = *cmc)*. Thus, the amount of surfactant in the excess oil phase (γ_{oil}) is the overall surfactant concentration minus that dissolved in excess water ($\gamma_0 - \gamma_{water}$) **[2.56]**. Since ethoxylated alcohols dissolve in significant concentrations in the excess oil phase, a knowledge of γ_{oil} is important for the calculation of the amount of surfactant available to cover the internal interfaces within the microemulsion phase **[2.57]**.

As the overall surfactant concentration is increased beyond γ_0 at constant temperature, the amounts of oil and water that are mixed in the microemulsion phase increase, and the volume fraction of the middle phase grows (see the test tubes in Figure 2.19). Eventually, enough surfactant is added to totally transfer oil and water in a one phase microemulsion. Consequently, an important feature of the "fish" phase diagram is that it describes the conditions at which a particular surfactant is most efficient at completely mixing equal amounts of oil and water into a single phase microemulsion. The condition of greatest surfactant efficiency is denoted as $\widetilde{X}$, where the tail (*1ϕ*) and the body of the fish (*3ϕ*) join; $\widetilde{X}$ has the surfactant concentration coordinate $(\tilde{\gamma})$ and the temperature coordinate $(\tilde{T})$.

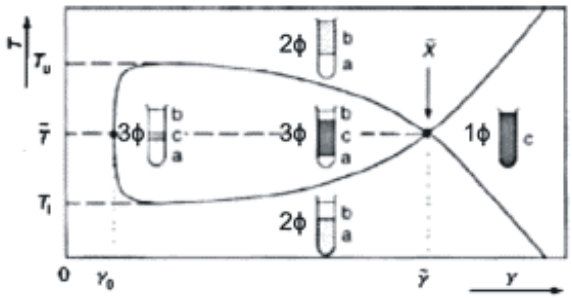

Figure 2.19 Schematic phase diagram of equal amounts of oil and water (α = 0.5) as a function of surfactant concentration (γ) and temperature (T); γ_0 denotes the "critical microemulsion concentration". In addition, T_l and T_U denote the temperature range of the three-phase region, while $\bar{X}$, the point at which the tail and the body of the fish meet, denotes the temperature and surfactant coordinates (T, γ) for the most efficient formation of single microemulsion phases. The test tubes show the types of phase behaviour found in the various regions of the phase diagram **[2.58]**

Another useful pseudo-binary phase diagram is found upon fixing the surfactant concentration *(γ* constant), and varying the ratio of oil to water (vary α) as a function of temperature (see figure 2.20). For surfactant concentrations greater than $\tilde{\gamma}$, a one-phase channel is observed in the phase diagram, which spans all oil to water ratios.

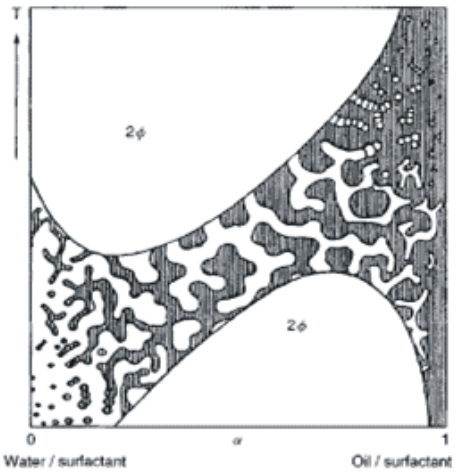

Figure 2.20 Schematic representation of the types of microstructures found within the one-phase channel of the phase diagram at constant surfactant concentration (γ) when the oil/water ratio (α) and temperature (T) are varied.**[2.63]**

Different techniques (SANS **[2.59]**, freeze-fracture electron microscopy **[2.60]**, electrical conductivity **[2.61]**, and self-diffusion measurements using NMR spectroscopy**[2.62]**) along paths of varying oil/water ratios *(α)* and temperature within the one-phase channel (constant surfactant concentration, *γ)* allow the generation of

the schematic diagram of the microstructure of the systems, as shown in Figure 2.20 **[2.50]**. Within the one-phase channel, droplet microemulsions exist at very low *α* values and low temperatures, or at high *α* values and high temperatures. Droplet microemulsions become globular and then bicontinuous as the water/oil ratio *(α)* is changed closer to 50/50.

2.3.2 Reactions in microemulsions

As reaction media, microemulsions are complementary systems to micellar systems. The smaller capacity of micellar systems for dissolving hydrophobic substrates has made them of limited value for applications as reaction media. The microdomains of microemulsions constituted by aqueous core, interface and continuous organic phase allow for the polar and nonpolar, organic and inorganic substrates to be dissolved and distributed. It is well understood that the effect of micelles on the acceleration of reactions is due to the reactant compartmentalization and accumulation. Additionally, water in the core of reverse micelles using ionic surfactants experience deviating electrophilic and nucleophilic properties in comparison to free “bulk water”, due to hydrogen bonds between the head groups of the surfactant and the counterion. Thus, the effect on reactions is often dependent on the water/surfactant (w) ratio. For this reason an accelerating effect for hydrolysis reactions is observed when the size of the micelles decreases **[2.64]**.

Typical reactions studied in reverse micelles include the reduction of ketones with $NaBH_4$. An example is the reduction of a series of phenyl allyl ketones in benzene/hexanol/water microemulsions in the presence of a chiral alkylephedrinium bromide (see figure 2.21) **[2.65]**.

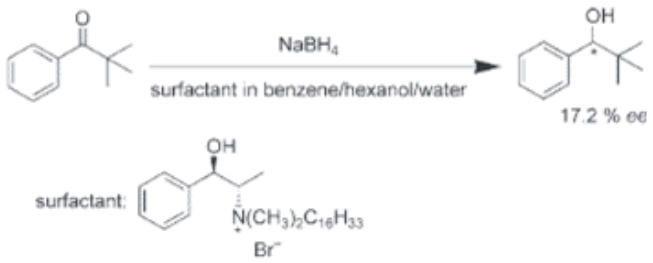

Figure 2.21 Stereoselective ketone reduction in chiral reverse micelles **[2.51]**

An acceleration was observed in the hydrogen-transfer reaction from 1,2-cyclohexanedimethanol to (E)-4-phenyl-3-butene-2-one in toluene catalyzed by [RuCl((S)BINAP)(benzene)]Cl (2 mol%; BINAP) and SDS (6 mol%). The surfactant is essential for the enhancement of catalytic activity and the existence of reverse micelles was proposed **[2.66]**.

The solubilization of reactants in water, and the achievements in rate and selectivity enhancement are sometimes unexpectedly high, but the main problem has been the separation of products, amphiphile, and catalyst after the reaction. Thus, interesting new aspects of using surfactants in aqueous complex catalysis can be found, but at present there is no industrial application and very little literature contributions are focused on catalytic hydrogenations in microemulsions using water soluble catalyst complexes.

As already mentioned earlier in this chapter, a better understanding of the observed effects required a detailed study of the microemulsion structure. Different techniques (SANS **[2.59]**, freeze-fracture electron microscopy **[2.60]**, electrical conductivity **[2.61]**, DLS and self-diffusion measurements using NMR spectroscopy **[2.62]**) allow the study of microemulsions.

2.4 Scattering measurements

The transparency of the microemulsions is a characteristic feature that has rendered them amenable for studies by dynamic light scattering (DLS) **[2.67]**. Such studies are accurate when the samples are highly diluted, enough to safely neglect interactions between aggregates and multiple scattering. This condition is often not satisfied with microemulsions **[2.68]**. Hence experiments and data analysis applying the scattering theories must be performed with special care, and the results must be regarded with a critical mind and be combined with results from other techniques.

2.4.1 Dynamic light scattering (DLS)

According to the semi-classical light scattering theory **[2.69]**, when light impinges on matter, the electric field of the light induces an oscillating polarization of electrons in the molecules. Hence the molecules provide a secondary source of light and subsequently scatter light. The frequency shifts, the angular distribution, the

polarization, and the intensity of the scatter light are determined by the size, shape and molecular interactions in the scattering material. Thanks to this is possible, with the aid of electrodynamics and theory of time dependent statistical mechanics, to get information about the structure and molecular dynamics of the scattering medium through the light scattering characteristics of the system.

In a typical dynamic light scattering (DLS), the autocorrelation function $G^{(2)}(\tau)$ of the intensity scattered by dispersed particles is determined as a function of the delay τ. $G^{(2)}(\tau)$ is related to the modulus of the normalized field autocorrelation function $g_1(\tau)$ by a Siegert relationship

$$G^{(2)}(\tau) = Ag_1^2(\tau) + B \qquad \text{(eq. 2.2)}$$

Here B is a background term often designated as the baseline and A can be considered as another instrumental factor. The time dependence of $g_1(\tau)$ is related to the dynamics of the dispersed particles. For particles in Brownian motion, the time decay of $g_1(\tau)$ is determined by the diffusion coefficient of the dispersed particles. In particular, for monodisperse samples $g_1(\tau)$ is an exponentially decaying function:

$$g_1(\tau) = \exp\left(-\Gamma\tau\right) \qquad \text{(eq. 2.3)}$$

or

$$G^{(2)}(\tau) = A\exp(-2\Gamma\tau) + B \qquad \text{(eq. 2.4)}$$

where the decay rate Γ is linked to the particles' diffusion coefficient D by $\Gamma = DQ^2$, where Q is the modulus of the scattering vector

$$Q = \frac{4\pi m_1}{\lambda_0}\sin(\theta/2) \qquad \text{(eq. 2.5)}$$

m_1 is the refraction index of the solution, λ_0 the wavelength in vacuo of the incident light and θ the scattering angle. At the end the Stokes-Einstein expression for the diffusion coefficient is used to get an average particle radius R_{DLS}

$$D = \frac{kT}{6\pi\eta R_{DLS}} \qquad \text{(eq. 2.6)}$$

where k is Boltzmann's constant, T the absolute temperature, η the viscosity of the dispersion medium and R_{DLS} the particle radius (only valid for non-interacting particles).

The set up is simple. The laser passes through a collimator lens and then hits the cell with the solution. The light is scattered and detected by a photomultiplier that transform a variation of intensity into a variation of voltage.

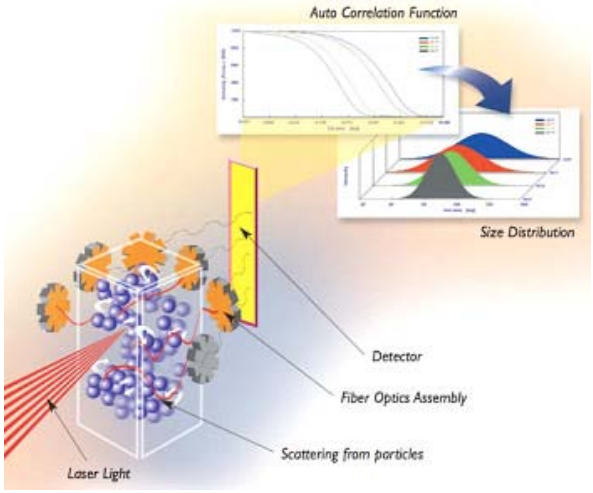

Scheme 2.6 Schematic representation of dynamic light scatterinf (DLS) and the different information extracted from the measurements **[2.70]**

The dynamic information of the particles is derived from an autocorrelation of the intensity trace recorded during the experiment. At short time delays, the correlation is high because the particles do not have a chance to move to a great extent from the initial state that they were in. Two signals are thus essentially unchanged when compared after only a very short time interval. As the time delays become longer, the correlation starts to exponentially decay to zero, meaning that after a long time period has elapsed, there is no correlation between the scattered intensity of the initial and final states. This exponential decay is related to the motion of the particles, specifically to the diffusion coefficient. Finally with help of the Stoke-Einstein relation, a size distribution is determined **[2.69]**.

In contrast to DLS, small angle neutron scattering (SANS) with its higher spatial resolution can be applied to microemulsions to corroborate values obtained for the hydrodynamic radius and add information regarding the core size of the micelles. Small angle neutron scattering (SANS) is a well established technique used to characterize microemulsions in much structural detail **[2.71]**.

2.4.2 Small angle neutron scattering (SANS)

Small-angle neutron scattering (SANS) is a well-established characterization method for microstructure investigations in various materials. It can probe inhomogeneities in the nanometer scale. Since the construction of the first SANS instrument over 35 years ago, this technique has experienced a steady growth. SANS instruments are either reactor-based using monochromated neutron beams or time-of-flight instruments at pulsed neutron sources. SANS has had major impact in many fields of research including polymer science, complex fluids, biology, and materials science. This technique has actually become a "routine" analytic characterization method used even by non-experts.

Neutron interactions with matter are confined to the short-range nuclear and magnetic interactions. Since its interaction probability is small, the neutron usually penetrates well through matter making it a unique probe for investigating bulk condensed matter. Since the neutron can be reflected by some surfaces when incident at glancing angles, it can also be used as a surface probe. Neutrons are scattered by nuclei in samples or by the magnetic moments associated with unpaired electron spins (dipoles) in magnetic samples. Neutrons interactions with hydrogen and deuterium are widely different making the deuterium labelling method an important feature of SANS measurements.

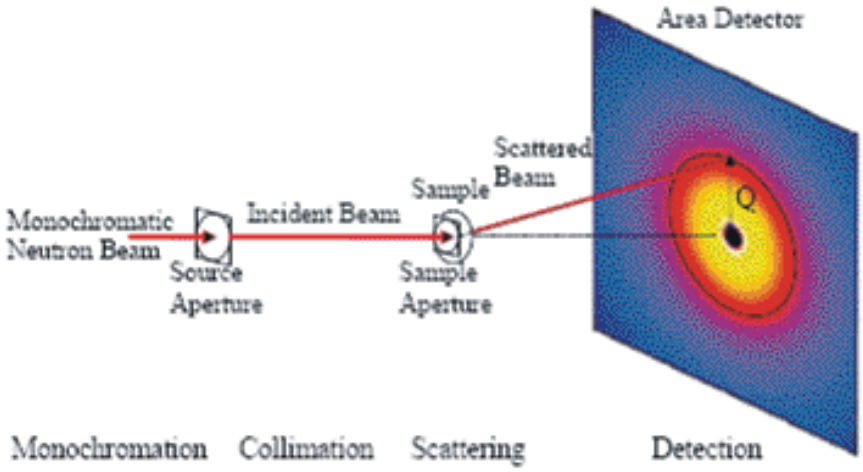

Scheme 2.7 Schematic representation of the SANS technique **[2.52]**

As shown in scheme 2.7, SANS involves the basic four steps used in all scattering techniques: monochromation, collimation, scattering and detection. Monochromation is performed mostly using a velocity selector. Collimation is

performed through the use of two apertures (a source aperture and a sample aperture) placed far (meters) apart. Scattering is performed from either liquid or solid samples. Detection is performed using a neutron area detector inside an evacuated scattering vessel. The large collimation and scattering distances make SANS instruments very large (typically 30 m long) compared to other scattering instruments.

A substantial fraction of SANS research is performed on “complex fluids”. These include micelles, colloids, gels, networks, etc, and could be referred to as “micellar systems”. As mentioned before, on the basis of SANS measurements identification of the shape and size of the micelles is possible. This has allowed the following depiction.

The microemulsion phase region is the focus of most SANS investigations since it is the region of micelle formation and micelles are of nanometer size. The m-phase region is rich in mesophases (with various morphologies). It contains spherical, cylindrical (also called wormlike) and lamellar micelles depending on the temperature range. Structures of these mesophases correspond to cubic (spherical micelles), hexagonal (cylindrical micelles) and lamellar symmetry, respectively. Note also that the “microemulsion” is also called bicontinuous phase. Moreover, oil-in-water micelles are obtained at low temperature and “reverse” (water-in-oil) micelles are obtained at high temperatures.

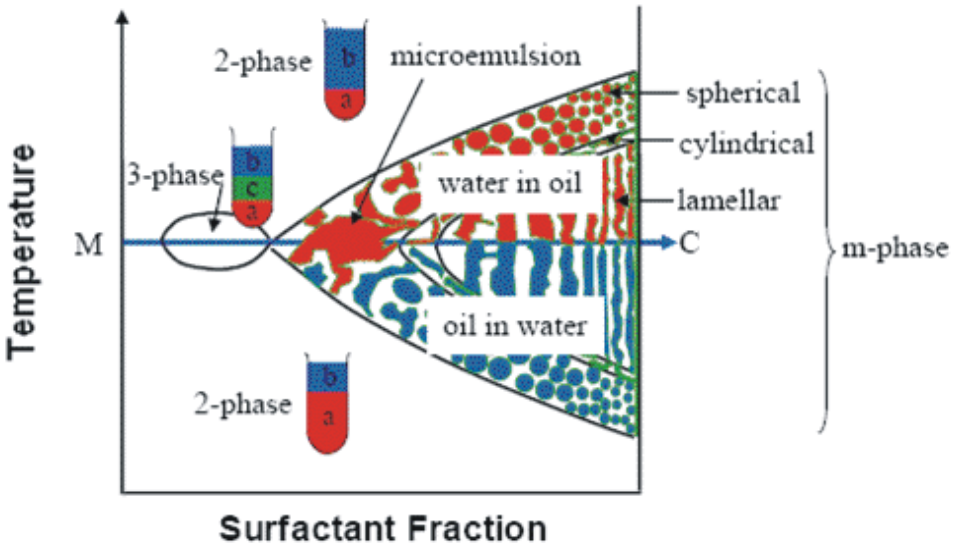

Figure 2.22 Schematic representation of The fish phase diagram determined with SANS measurements **[2.52]**

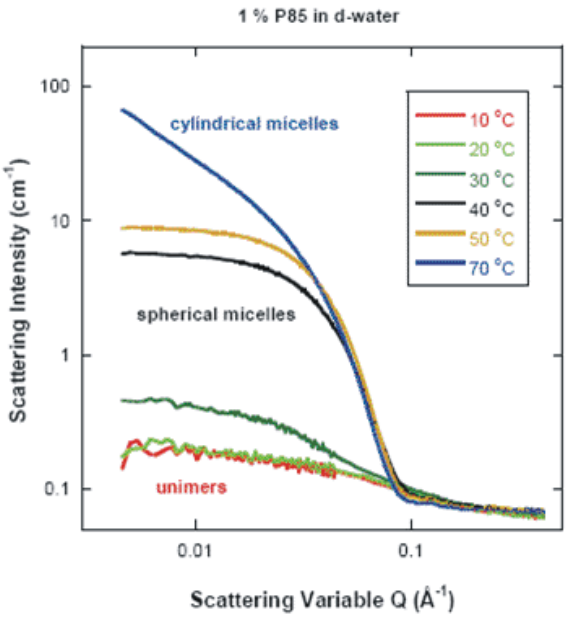

Figure 2.23 Transition from the unimers to the spherical micelles phase to the cylindrical micelles phase regions as temperature is increased for 1 % P85 in d-water **[2.52]**

Figure 2.23 shows an example of the way of differentiating micelle shapes by using SANS measurements. SANS data for a nonionic surfactant (pluronics P85) mixed with d-water are described here. This copolymer solution is equivalent to a surfactant/water mixture. Strictly speaking, this is not a ternary mixture; its phase diagram is different from the surfactant/water/oil mixture but shows some of the same microphases. The pluronics molecule is a triblock copolymer poly(ethylene oxide)-poly(propylene oxide)-poly(ethylene oxide) (PEO-PPO-PEO) which forms micelles above a critical temperature and concentration. PPO is hydrophobic and PEO is hydrophilic. P85 is different from a ternary water/oil/surfactant system, but the overall trends remain the same. Unimers (dissolved macromolecules) are obtained at low temperature and micelles form at high temperature. Varying temperature for a fixed P85 mass fraction shows a transition from a spherical to a cylindrical morphology in the micelle-formation region.

Another example of micelar shape transition can be observed in Figure 2.24 which shows a plot of $I(q)$ vs q for a series of samples containing 1 wt % of poly(oxyethylene) cholesteryl ether ($ChEO_{10}$) and an increasing concentration of poly(oxyethylene)dodecyl ether ($C_{12}EO_3$) (0, 0.05, 0.10, and 0.15 wt %) in D_2O. All of the curves were measured at 20 °C with SANS. With increasing $C_{12}EO_3$ concentration, a transition from a horizontal low q regime to a q^{-1} decay at low q-values occurs, which is a typical signature for a sphere-to-rod transition **[2.72]**.

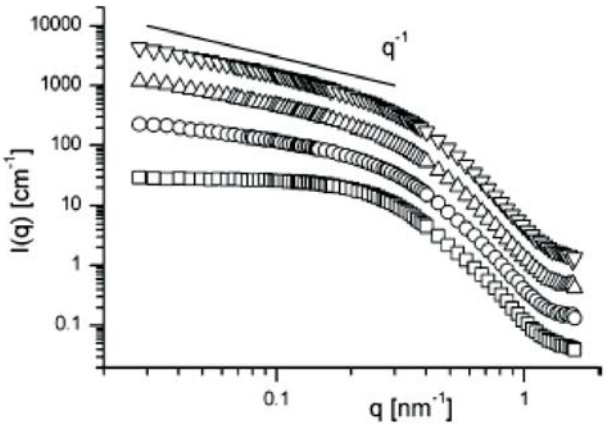

Figure 2.24 Scattered intensity $I(q)$ from SANS experiments on samples containing 1 wt % of $ChEO_{10}$ and an increasing concentration of $C_{12}EO_3$. The fractions of $C_{12}EO_3$ are 0 wt % (squares), 0.05 wt % (circles), 0.10 wt % (upward-pointing triangles), and 0.15 wt % (downward-pointing triangles) **[2.52]**

2.5 References

[2.1] Leeuwen, P.W.N.M.v., *Homogeneous catalysis: understanding the art*. 2004, Dordrecht; London: Springer. p. 400.

[2.2] Perry, R.H., D.W. Green, and J.O. Maloney, *Perry's chemical engineers' handbook.* 1997, New York: McGraw-Hill. p. --.

[2.3] Cole-Hamilton, D.J. and R.P. Tooze, *HOMOGENEOUS CATALYSIS – ADVANTAGES AND PROBLEMS*, in *CATALYST SEPARATION, RECOVERY AND RECYCLING*, D.J. Cole-Hamilton and R.P. Tooze, Editors. 2006, Spinger. p. 1-8.

[2.4] Xia, Q.H., H.Q. Ge, C.P. Ye, Z.M. Liu, and K.X. Su, *Chem. Rev.,* **2005,** *105*, (5), 1603-1662; Burgi, T. and A. Baiker, *Acc. Chem. Res.,* **2004,** *37*, (11), 909-917.

[2.5] Cornils, B. and W.A. Herrmann, *Introduction*, in *Aqueous-Phase Organometallic Catalysis*, B. Cornils and W.A. Herrmann, Editors. 2004, Wiley-VCH. p. 3-24.

[2.6] Cole-Hamilton, D.J., *Science,* **2003,** *299*, (5613), 1702-1706.

[2.7] Sheldon, R., I. Arends, and U. Hanefeld, *Green Chemistry and Catalysis*. 1st ed. 2007, Weinheim: WILEY-VCH Verlag GmbH & Co. KGaA. p. 433.

[2.8] Straathof, A.J.J., S. Panke, and A. Schmid, *Curr. Opin. Biotechnol.,* **2002,** *13*, (6), 548-556; Powell, K.A., et al., *Angew. Chem. Int. Edit.,* **2001,** *40*, (21), 3948-3959.

[2.9] Schoemaker, H.E., D. Mink, and M.G. Wubbolts, *Science,* **2003,** *299*, (5613), 1694-1697.

[2.10] Takaishi, N., H. Imai, C.A. Bertelo, and J.K. Stille, *J. Am. Chem. Soc.,* **1976,** *98*, (17), 5400-5402; Takaishi, N., H. Imai, C.A. Bertelo, and J.K. Stille, *J. Am. Chem. Soc.,* **1978,** *100*, (1), 264-268.

[2.11] Song, C.E. and S.G. Lee, *Chem. Rev.,* **2002,** *102*, (10), 3495-3524.

[2.12] Kinting, A., H. Krause, and M. Capka, *J. Mol. Catal.,* **1985,** *33*, (2), 215-223.

[2.13] McDonald, A.R., C. Muller, D. Vogt, G.P.M. van Klinka, and G. van Koten, *Green Chem.,* **2008,** *10*, (4), 424-432.

[2.14] Selke, R., K. Haupke, and H.W. Krause, *J. Mol. Catal.,* **1989,** *56*, (1-3), 315-328.

[2.15] Dickerson, T.J., N.N. Reed, and K.D. Janda, *Chem. Rev.,* **2002,** *102*, (10), 3325-3343.

[2.16] Fan, Q.H., Y.M. Chen, X.M. Chen, D.Z. Jiang, F. Xi, and A.S.C. Chan, *Chem. Commun.,* **2000**, (9), 789-790.

[2.17] van Heerbeek, R., P.C.J. Kamer, P.W.N.M. van Leeuwen, and J.N.H. Reek, *Chem. Rev.,* **2002,** *102*, (10), 3717-3756.

[2.18] Oosterom, G.E., S. Steffens, J.N.H. Reek, P.C.J. Kamer, and P.W.N.M. van Leeuwen, *Top. Catal.,* **2002,** *19*, (1), 61-73.

[2.19] Kollner, C., B. Pugin, and A. Togni, *J. Am. Chem. Soc.,* **1998,** *120*, (39), 10274-10275.

[2.20] Noyori, R., *Chem. Rev.,* **1999,** *99*, (2), 353-354; Jessop, P.G., T. Ikariya, and R. Noyori, *Chem. Rev.,* **1995,** *95*, (2), 259-272.

[2.21] Jessop, P.G., T. Ikariya, and R. Noyori, *Chem. Rev.,* **1999,** *99*, (2), 475-493.

[2.22] Zosel, K., *Angewandte Chemie-International Edition in English,* **1978,** *17*, (10), 702-709.

[2.23] Wells, S.L. and J. DeSimone, *Angew. Chem. Int. Edit.,* **2001,** *40*, (3), 519-527.

[2.24] Licence, P., J. Ke, M. Sokolova, S.K. Ross, and M. Poliakoff, *Green Chem.,* **2003,** *5*, (2), 99-104.

[2.25] Leitner, W., *Acc. Chem. Res.,* **2002,** *35*, (9), 746-756.

[2.26] Gordon, C. and W. Leitner, *SUPERCRITICAL FLUIDS*, in *CATALYST SEPARATION, RECOVERY AND RECYCLING*, D.J. Cole-Hamilton and R.P. Tooze, Editors. 2006, Spinger. p. 215-236.

[2.27] Heldebrant, D.J. and P.G. Jessop, *J. Am. Chem. Soc.,* **2003,** *125*, (19), 5600-5601.

[2.28] Meehan, N.J., A.J. Sandee, J.N.H. Reek, P.C.J. Kamer, P.W.N.M. van Leeuwen, and M. Poliakoff, *Chem. Commun.,* **2000**, (16), 1497-1498; Shibahara, F., K. Nozaki, and T. Hiyama, *J. Am. Chem. Soc.,* **2003,** *125*, (28), 8555-8560.

[2.29] Kainz, S., D. Koch, W. Baumann, and W. Leitner, *Angewandte Chemie-International Edition in English,* **1997,** *36*, (15), 1628-1630.

[2.30] Lange, S., A. Brinkmann, P. Trautner, K. Woelk, J. Bargon, and W. Leitner, *Chirality,* **2000,** *12*, (5-6), 450-457.

[2.31] Francio, G., K. Wittmann, and W. Leitner, *J. Organomet. Chem.,* **2001,** *621*, (1-2), 130-142.

[2.32] Barthel-Rosa, L.P. and J.A. Gladysz, *Coord. Chem. Rev.,* **1999,** *192*, 587-605.

[2.33] Baker, R.T. and W. Tumas, *Science,* **1999,** *284*, (5419), 1477-1479.

[2.34] Olivier-Bourbigou, H., *Catalysis in Nonaqueous Ionic Liquids*, in *Multiphase Homogeneous Catalysis*, B. Cornils, et al., Editors. 2005, Wiley-VCH: Weinheim. p. 407-603.

[2.35] Frater, T., L. Gubicza, A. Szollosy, and J. Bakos, *Inorg. Chim. Acta,* **2006,** *359*, (9), 2756-2759.

[2.36] Berger, A., R.F. de Souza, M.R. Delgado, and J. Dupont, *Tetrahedron-Asymmetry,* **2001,** *12*, (13), 1825-1828.

[2.37] Dyson, P.J., D.J. Ellis, and T. Welton, *Can. J. Chem.,* **2001,** *79*, (5), 705-708.

[2.38] Joó, F., *Aqueous Organometallic Catalysis*. 1st ed. 2001, Dordrecht: Kluwer. p. 300.

[2.39] Sinou, D., *Adv. Synth. Catal.,* **2002,** *344*, (3-4), 221-237.

[2.40] Amrani, Y., L. Lecomte, D. Sinou, J. Bakos, I. Toth, and B. Heil, *Organomet.,* **1989,** *8*, (2), 542-547.

[2.41] Cornils, B., C. Kohlpaintner, and E. Wiebus, in *Encyclopedia of Chemicals Processing and Design*, J. McKetta and G.E. Weismantel, Editors. 1998, Dekker: New York. p. 273.

[2.42] Auch-Schwelk, B. and C. Kohlpaintner, *Chem. unserer Zeit,* **2001,** *35*, (5), 306-312.

[2.43] Ahrland, S., J. Chatt, N.R. Davies, and A.A. Williams, *J. Chem. Soc.,* **1958**, (JAN), 276-288.

[2.44] Herrmann, W.A. and C. Kohlpaintner, *Inorg. Synth.,* **1998,** *32*, 8-25.

[2.45] Cornils, B. and E.G. Kuntz, *J. Organomet. Chem.,* **1995,** *502*, (1-2), 177-186.

[2.46] Wan, K.T. and M.E. Davis, *J. Chem. Soc. Chem. Comm.,* **1993**, (16), 1262-1264.

[2.47] de Bellefon, C., N. Tanchoux, S. Caravieilhes, and D. Schweich, *Catal. Today,* **1999,** *48*, (1-4), 211-219.

[2.48] Tanchoux, N. and C. de Bellefon, *Eur. J. Inorg. Chem.,* **2000**, (7), 1495-1502.

[2.49] Schwarze, M. and R. Schomäcker, *Chemie Ingenieur Technik,* **2006,** *78*, (7), 931-936; Schwarze, M., *Wässrig-mizellare Lösungen als Reaktionsmedium für Hydrierreaktionen mit homogen gelösten Katalysatoren: Reaktionstechnische Untersuchungen zur Katalysatorrückführung mittels MEUF*, in *Fakultät II - Mathematik und Naturwissenschaften*. 2008, Technical University Berlin: Berlin. p. 153.

[2.50] Schwuger, M.J., K. Stickdorn, and R. Schomäcker, *Chem. Rev.,* **1995,** *95*, (4), 849-864.

[2.51] Dwars, T., E. Paetzold, and G. Oehme, *Angew. Chem. Int. Edit.,* **2005,** *44*, (44), 7174-7199.

[2.52] Hammouda, B., *PROBING NANOSCALE STRUCTURES – THE SANS TOOLBOX (http://www.ncnr.nist.gov/staff/hammouda/the_SANS_toolbox.pdf)*.

[2.53] Kahlweit, M., R. Strey, and G. Busse, *J. Phys. Chem.,* **1990,** *94*, (10), 3881-3894.

[2.54] Wormuth, K., O. Lade, M. Lade, and R. Schomäcker, *Microemulsions*, in *Handbook of Applied Surface and Colloid Chemistry*, K. Holmberg, Editor. 2001, John Wiley & Sons. p. 605-627.

[2.55] Kahlweit, M. and R. Strey, *Angewandte Chemie-International Edition in English,* **1985,** *24*, (8), 654-668.

[2.56] Burauer, S., T. Sachert, T. Sottmann, and R. Strey, *Phys. Chem. Chem. Phys.,* **1999,** *1*, (18), 4299-4306.

[2.57] Kunieda, H., A. Nakano, and M.A. Pes, *Langmuir,* **1995,** *11*, (9), 3302-3306.

[2.58] Kahlweit, M., G. Busse, and B. Faulhaber, *Langmuir,* **1996,** *12*, (4), 861-862.

[2.59] Lichterfeld, F., T. Schmeling, and R. Strey, *J. Phys. Chem.,* **1986,** *90*, (22), 5762-5766.

[2.60] Jahn, W. and R. Strey, *J. Phys. Chem.,* **1988,** *92*, (8), 2294-2301.

[2.61] Kahlweit, M., G. Busse, and J. Winkler, *J. Chem. Phys.,* **1993,** *99*, (7), 5605-5614.

[2.62] Lindman, B., K. Shinoda, U. Olsson, D. Anderson, G. Karlstrom, and H. Wennerstrom, *Colloids Surf.,* **1989,** *38*, (1-3), 205-224.

[2.63] Schomäcker, R., *Nachr. Chem. Tech. Lab.,* **1992,** *40*, (12), 1344-1351.

[2.64] Garcia-Rio, L., J.C. Mejuto, and M. Perez-Lorenzo, *New J. Chem.,* **2004,** *28*, (8), 988-995.

[2.65] Zhang, Y.M. and P.P. Sun, *Tetrahedron-Asymmetry,* **1996,** *7*, (11), 3055-3058.

[2.66] Nozaki, K., M. Yoshida, and H. Takaya, *J. Organomet. Chem.,* **1994,** *473*, (1-2), 253-256.

[2.67] Zhu, D.M., K.I. Feng, and Z.A. Schelly, *J. Phys. Chem.,* **1992,** *96*, (5), 2382-2385; Zhu, D.M., X. Wu, and Z.A. Schelly, *Langmuir,* **1992,** *8*, (6), 1538-1540.

[2.68] Dvolaitzky, M., et al., *J. Chem. Phys.,* **1978,** *69*, (7), 3279-3288.

[2.69] Berne, B. and P. Pecora, *Dynamic Light Scatterring*. 1st ed. 1976, New York: Wiley. p. 371.

[2.70] *http://ujkeb.com/facilities.html*.

[2.71] Chen, S.H., *Annu. Rev. Phys. Chem.,* **1986,** *37*, 351-399; Chen, S.H., J. Rouch, F. Sciortino, and P. Tartaglia, *J. Phy.: Condens. Matter,* **1994,** *6*, 10855-10883; Gradzielski, M., D. Langevin, and B. Farago, *Phys. Rev. E: Stat. Phys., Plasmas, Fluids,,* **1996,** *53*, (4), 3900-3919; Gradzielski, M., D. Langevin, and B. Farago, *Prog. Colloid Polym. Sci.,* **1996,** *100*, 162-169; Abécassis, B., F. Testard, L. Arleth, S. Hansen, I. Grillo, and T. Zemb, *Langmuir,* **2006,** *22*, (19), 8017-8028; Freeman, K.S., N.C.B. Tan, S.F. Trevino, S. Kline, L.B. McGown, and D.J. Kiserow, *Langmuir,* **2001,** *17*, (13), 3912-3916.

[2.72] Moitzi, C., N. Freiberger, and O. Glatter, *J Phys Chem B,* **2005,** *109*, (33), 16161-16168.

3 Experimental Details

3.1 Catalyst preparation

Taking into account that the water-soluble catalyst complex Rh–TPPTS is sensitive to oxygen, it was prepared under nitrogen environment in a 25 mL flask with three necks. The catalyst precursor $[Rh(COD)Cl]_2$ and the ligand TPPTS were weighed alone and introduced into the flask, which was already attached to an open nitrogen line to one of the necks. As observed in Figure 3.1, after introducing the catalyst components into the flask, the other necks were shut with a gummy septum and the last one with a balloon. The balloon is an additional reservoir of nitrogen. After the balloon was filled up, the nitrogen was closed isolating the mixture within the nitrogen environment in the flask. The mixture was mixed with a magnetic stirrer for 24 hours before it was used for the hydrogenations. For a standard reaction, 22 mg of catalyst precursor (0.089 mmol Rh) were mixed under nitrogen with 1240 mg TPPTS 30 % solution (380.4 mg, 0.67 mmol of TPPTS).

Figure 3.1 25 mL flask with three necks used for the preparation of the water-soluble catalyst complex Rh–TPPTS, attached to a nitrogen line and an additional nitrogen reservoir balloon. The mixture is stirred by a magnetic stirrer

3.2 Catalytic hydrogenation runs

3.2.1 Reactor design

A thermostated double wall 200 mL glass reactor equipped with a gas dispersion stirrer was used in this study. As observed in Figure 3.2, the reactor has a bottom drain and is closed with a flat flange lid. Between the lid and the reactor, the seal is

achieved by an o-ring. The lid of the reactor has 5 necks (four GL 14 and one NS 14,5) surrounding a middle neck (NS 29) through which the gas dispersion stirrer is introduced into the reactor. The NS 14,5 – connection is used for the nitrogen inlet. One of the GL 14 – screw-connections is shared between the vacuum pump and the hydrogen inlet. Another GL 14 – screw-connection is attached to a pressure indicator. The other two GL 14 – screw-connections are used when an ultrafiltration module is necessary, which in our case is not necessary consequently they are closed. The reactor has an additional side neck with a GL 14 – screw-connection sealed by a septum, which is used to extract samples to monitor the reaction properties (conversion and selectivity).

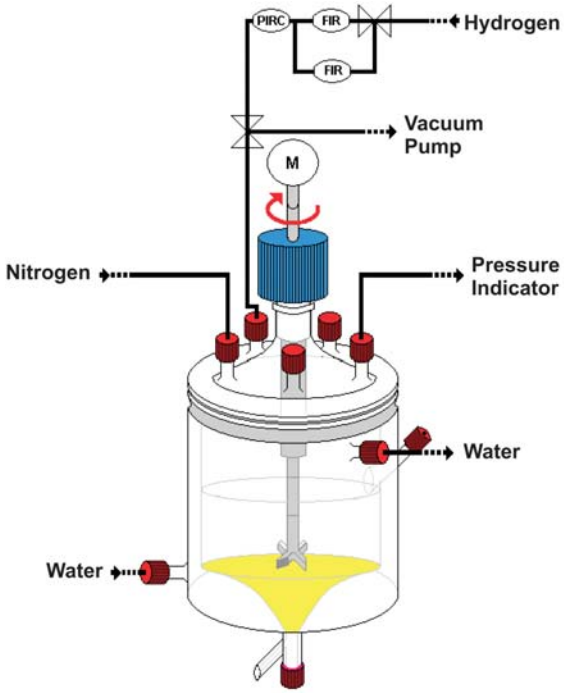

Figure 3.2 Schematic diagram of the glass reactor

3.2.2 Data achievement

The evolution of the hydrogenation is followed through the hydrogen flow being consumed by the reaction. In order to monitor the hydrogenation, two flow regulators and one pressure regulator are attached to the hydrogen line. Depending on the hypothesized reaction rate, one of the two flow regulators (0-5 $mL \cdot min^{-1}$ and 0-8 $mL \cdot min^{-1}$) can be used by allowing the flow through it. This can be achieved by activating a magnetic valve located on the hydrogen line before the flow regulator. Access to another set of two flow regulators (0-20 $mL \cdot min^{-1}$ and 0-50 $mL \cdot min^{-1}$) is possible by turning a two way switch which allows flow through another hydrogen line. The pressure set point is given to the pressure regulator and when some

hydrogen is consumed by the hydrogenation, more hydrogen is replaced into the reactor to keep the pressure constant.

3.2.3 Hydrogenation experiments

Semibatch reactions were performed under a constant pressure of 1.1 bar. The hydrogenations were studied in different reaction mediums: biphasic system without surfactant (cyclohexane – water), one phase microemulsion (ME), biphasic system with surfactant ($\underline{2}$ and $\overline{2}$) and three-phase system (3ϕ). The appearance of the systems is shown in Figure 3.3.

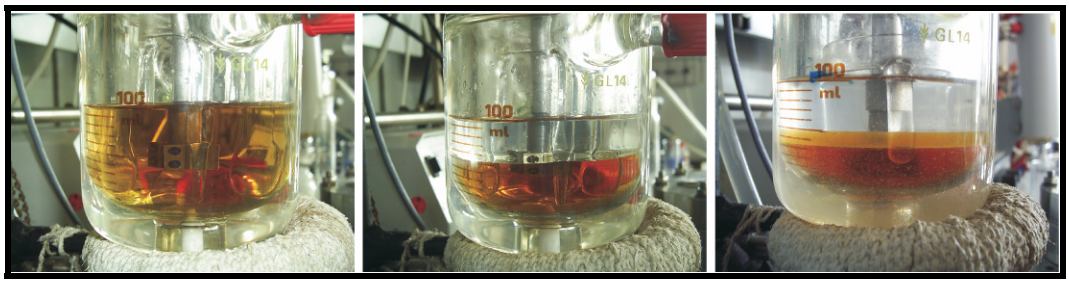

Figure 3.3 Surfactant systems used for the hydrogenations with the water-soluble catalyst complex Rh–TPPTS (0.81 mmol·L^{-1} of Rh and 6.09 mmol·L^{-1} of TPPTS)

For the hydrogenations, the reaction medium was first added to the reactor: the biphasic system without surfactant is directly added to the reactor, whereas the surfactant systems were prepared one day before and agitated with a magnetic stirrer overnight. After closing the reactor by fixing the lit of the reactor and attaching the gas lines (hydrogen and nitrogen), the reactor was evacuated at 150 mbar ($P_{vap}(C_6H_{12})$= 131.7 mbar at 25 °C) and refilled with nitrogen three times after introducing the solvent. The catalyst was extracted from the three-neck flask shown in Figure 3.1 with a syringe and injected into the reactor. The amount of catalyst was controlled by weighing the syringe empty and after injecting it through the side-neck septum into the reactor. The substrate was also injected through the same septum as the catalyst. After injecting the catalyst and the substrate, the reactor was evacuated at 150 mbar and refilled with nitrogen three additional times, respectively. The mixture was stirred with 400 rpm at 40 °C to allow for total mix of the substrate for 30 min and afterwards for 30 min at reaction temperature. The reaction was initiated after evacuating the reactor at 150 mbar, followed by increasing pressure to 1.1 bar

with hydrogen gas and subsequent stirring with 800 rpm. A decreased and finally stopped hydrogen flux indicated the end of the reaction.

3.2.4 Catalyst recycling experiments

Using biphasic systems or three-phase systems as reaction medium, the product concentrated oily upper phase is extracted to isolate the product. Using one phase microemulsions as reaction medium, phase separation is achieved by decreasing or increasing the temperature until the system temperature abandons the one phase system temperature region at the surfactant concentration within the fish diagram (Figure 2.19). After a batch hydrogenation is finished and the temperature induced phase separation is achieved, the extraction is done with a peristaltic pump Ismatec ISM597A with Fluran HCA (F-5500-A) flexible tubes (d = 2.06 mm) that are resistant to cyclohexane and allow maximum flows of 15 mL·min^{-1}. While the reaction temperature is re-established, a new surfactant solution is added with the same pump, which is constituted mostly of cyclohexane. Following the injection of fresh amount of substrate, the reaction is restarted.

4 Catalytic Hydrogenation of Dimethyl Itaconate (DMI) in a Microemulsion in comparison to a Biphasic System

4.1 Introduction

The homogeneous catalytic hydrogenation of dimethyl itaconate (DMI) is generally performed in methanol or tetrahydrofurane, which are suitable solvents for both, the reactant and the catalyst **[4.1, 4.2]**. However, at the end of the hydrogenation, the catalyst and the reaction product are difficult to separate, and consequently, the catalyst cannot be reused without further processing. Thermal operations separating the product from the catalyst such as distillation and rectification normally cause thermal stress on the catalyst at the expense of the catalytic activity **[4.3]**. A solution for this separation problem could be the use of aqueous micellar systems as reaction medium with a consecutive ultrafiltration process after the reaction (micelle-enhanced ultrafiltration) **[4.4, 4.5]**. Furthermore water-soluble catalysts, formed from a catalyst precursor in combination with water-soluble phosphine ligands, can be applied for these reactions **[4.3, 4.6]**. This allows for the use of biphasic systems **[4.7, 4.8, 4.9]**, where the catalyst and small amounts of the substrate are dissolved in the aqueous phase, whereas the major parts of both substrate and reaction product are dissolved in the organic phase. In 1984, Ruhrchemie/Rhône-Poulenc (RCH/RP) launched the first 100 000 tons per year plant in Oberhausen (Germany), which operates with a water-soluble rhodium complex in a two phase system **[4.10]**. Addition of surfactants can enhance the reaction rate by improving mass transfer from organic to aqueous phase **[4.11].** Recently, the application of microemulsions as thermodynamically stable biphasic systems has been used in the synthesis of a variety of fine chemical by catalytic reactions **[4.4]**. When using microemulsions, catalyst recovery can be achieved by ultrafiltration due to different solubilization behavior of catalyst and reaction product within the different fractions of these media. Much research has been done on the synthesis of new catalysts, mostly for asymmetric reactions **[4.2, 4.12]** it has been even recently demonstrated that the commercial-scale manufacture of such catalysts is possible **[4.13]**, and they are actually commercially available. This is not the case for water soluble chiral catalysts, for which solubilization in water is usually achieved via introduction of a highly polar functional group such as sulfonate **[4.14]**. So far this has only been realized on laboratory scale. Limited research has

been done about the kinetic behaviour of water-soluble catalysts in hydrogenations, and even less work has been focused on the effect of surfactants on these reactions.

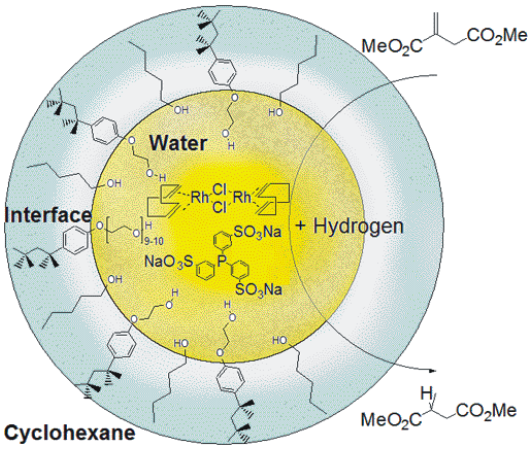

Scheme 4.1 Reverse micelle-reactor concept for the catalytic hydrogenation of dimethyl itaconate using the water-soluble catalyst complex Rh–TPPTS

This chapter serves as experimental model for the use of microemulsion systems in the catalytic hydrogenation of DMI, using the water-soluble catalyst complex Rh–TPPTS (see Scheme 4.1). This medium allows for dissolving sufficient amounts of substrate, and for a large internal interfacial area between substrate and catalyst containing phases. A qualitative kinetic comparison of the catalytic hydrogenation of DMI was made between two systems, (a) a biphasic system (cyclohexane/water), and (b) a microemulsion ([Triton X-100/1-pentanol]/cyclohexane/water). For the description of both a rate law based on the Osborn–Wilkinson kinetics was applied.

4.2 Experimental

4.2.1 Chemicals

The solvents cyclohexane (≥ 99.5%, Roth), decane (≥ 95%, Fluka) and 1-pentanol (≥ 99%, Merck) were degassed and purged under nitrogen and used without further purification. The catalyst precursor $[Rh(cod)Cl]_2$ (98%, Strem) was kept under nitrogen and used as received. The water-soluble ligand TPPTS (30.7 wt % in water, Celanese) and the surfactant Triton X-100 (100%, Sigma-Aldrich) were used as

received. The substrate dimethyl itaconate “DMI” (≥ 97 %, Fluka) was used as received.

4.2.2 Catalyst preparation

For a standard reaction, 22 mg of catalyst precursor (0.089 mmol Rh) were mixed under nitrogen with 1240 mg TPPTS 30% solution (380.4 mg, 0.67 mmol of TPPTS). This mixture was stirred under nitrogen at ambient temperature for 24 h before it was used in the hydrogenation reaction.

4.2.3 Microemulsion preparation

The following common terms are necessary to describe the compositions of the four-component system:

$$\alpha = \frac{m_{\text{oil}}}{m_{\text{oil}} + m_{\text{water}}} \qquad \gamma = \frac{m_{\text{surfactant}} + m_{\text{co-surfactant}}}{m_{\text{oil}} + m_{\text{water}} + m_{\text{surfactant}} + m_{\text{co-surfactant}}} \qquad \text{(eq. 4.1)}$$

Test tubes were prepared with different compositions of water and cyclohexane (α) but fixed weight fractions of Triton X-100 and 1-pentanol (γ). The sequence in which the components were added was (1) cyclohexane, (2) Triton X-100, (3) 1-pentanol, and (4) water. Before and after water addition, the solution was agitated for 5 min, respectively. The test tubes were immersed in a thermostated water bath, and phase distribution was observed after 15 min. This procedure was repeated with increasing temperature in steps of 1 K. The change in phase distribution depending on temperature and composition followed a typical trend behaviour for systems with nonionic surfactants **[4.15]**.

4.2.4 Partition coefficient measurements

Different amounts of DMI (10, 20, 30, 40, 50, 60, 70, 80, 160, 320, 480, 640 mg) were added to a biphasic system of 5 mL of cyclohexane and 5 mL of water, respectively, followed by agitation for 5 min. After thermostating at 40 °C in a water bath for 30 min, the test tubes were again agitated and kept at ambient temperature

for 30 min. The concentration of DMI in the aqueous phase was measured by high pressure liquid chromatography (HPLC) using a Dionex instrument (capillary column: Multospher 120 RP 18-5µ, ca. 250 mm x 4 mm; HPLC pump: P580A, 0.7 mL min^{-1} ACN:water 60:40 v/v; column thermostat: STH585 , 25 °C; UV/Vis detector: 170S, λ = 220 nm). Under these conditions, DMI had a retention time of 4.9 min.

4.2.5 Catalytic hydrogenation runs

A thermostated double wall 200 mL glass reactor equipped with a gas dispersion stirrer was used in this study (see Figure 4.1). Semibatch reactions were performed under a constant pressure of 1.1 bar. The reaction rates were calculated using the monitored hydrogen flow for keeping the pressure at a constant level. The hydrogenation of DMI was studied in two solvent systems: (a) a biphasic system (50 mL of cyclohexane + 50 mL of water) and (b) a microemulsion (100 mL of [Triton X-100/1-pentanol]/cyclohexane/water).

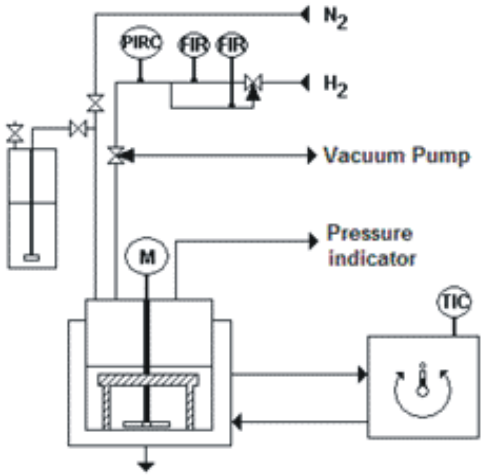

Figure 4.1 Schematic flow sheet of the batch reactor used for the nonasymmetric catalytic hydrogenation of DMI

The biphasic system is directly added to the reactor, whereas the microemulsion was prepared one day before (see section 4.2.3) and agitated overnight. The reactor was evacuated at 150 mbar and refilled with nitrogen three times after introducing the solvent and after injection of the catalyst solution (1.2 mL) and the DMI, respectively. The mixture was stirred with 400 rpm at 40 °C for 30 min and afterwards for 30 min at reaction temperature. The reaction was initiated after

evacuating the reactor at 150 mbar, followed by increasing pressure to 1.1 bar with hydrogen gas and subsequent stirring with 800 rpm. A decreased and finally stopped hydrogen flux indicated the end of the reaction. The complete hydrogenation of DMI to dimethyl methylsuccinate (DMS) was confirmed by gas chromatography (GC) using a HP 5710A instrument (Lipodex E capillary column, ca. 25 m, d = 0.25 mm, 0.6 bar N_2, 90 °C, FID) obtaining a retention time of DMS between 20-21 min. Microemulsion samples were separated into organic and aqueous phases by addition of water. After phase separation the organic phase was analyzed.

4.3 Results and discussion

4.3.1 Phase behaviour diagram of the water-cyclohexane-Triton X-100 microemulsion (*T vs.* α)

The amount of surfactant has an influence on the size of the one-phase region within the phase diagram, as shown in Figure 4.2. The higher the amount of Triton X-100 is, the wider the one-phase region is. The shift to a more suitable temperature range (5 - 45°C) in a large range of water concentrations furthermore allows for higher catalyst concentrations. It is also known that the incorporation of short-chain alkanols stabilizes reverse micelles **[4.16]**. Consequently, 1-pentanol as cosurfactant was added and taken into account in the surfactant concentration (γ).

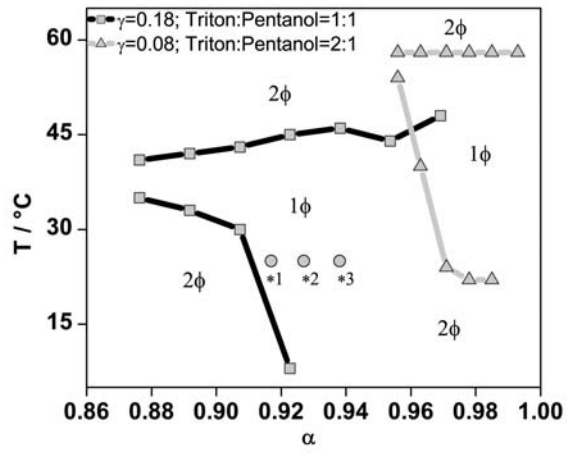

Figure 4.2 Phase prism section of the quaternary system [Triton X-100-1-pentanol]/cyclohexane/water with two constant weight fractions of Triton X-100 and 1-pentanol

4.3.2 Partition coefficient (P_{DMI})

In a biphasic system with a water-soluble catalyst, the reactant must be able to migrate into the aqueous catalyst phase in order to get in contact with the catalyst. The partition coefficient of DMI is described by the relationship:

$$P_{\mathrm{DMI}} = \frac{c_{\mathrm{DMI,org}}}{c_{\mathrm{DMI,aq}}} \qquad \text{(eq. 4.2)}$$

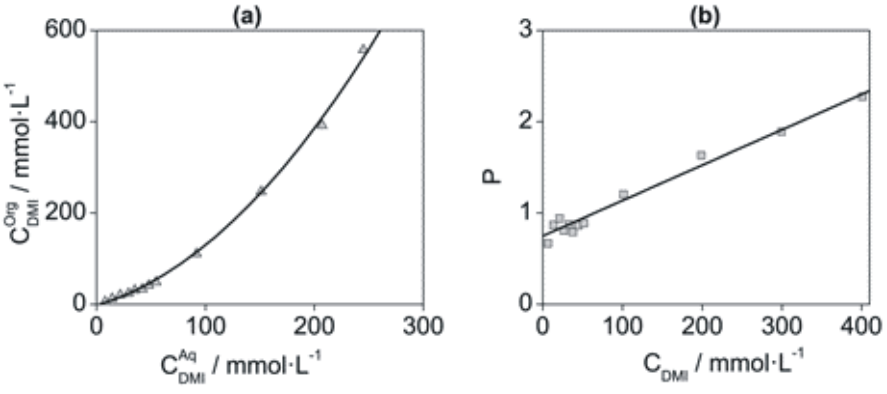

Figure 4.3 (a) Partition isotherm (25 °C) of DMI in a cyclohexane/water (50 vol % water) biphasic system. (b) Influence of DMI concentration on the partition isotherm (25 °C) of DMI in a cyclohexane/water (50 vol % water) biphasic system

As can be seen in Figure 4.3a, the partition coefficient of DMI is constant only at low DMI concentrations (<50 mmol·L^{-1}), by increasing the DMI concentration to higher values (>50 mmol·L^{-1}) more DMI concentrates in the cyclohexane phase. The behaviour of the partition coefficient in a cyclohexane/water (1:1 vol) biphasic system relative to the DMI concentration in the system (Figure 4.3b) can be described by the following linear equation:

$$P_{\mathrm{DMI}} = 0.0039 \times \frac{C_{\mathrm{DMI}}}{\mathrm{mmol \cdot L^{-1}}} + 0.7486 \qquad \text{(eq. 4.3)}$$

4.3.3 Catalytic hydrogenation of dimethyl itaconate (DMI)

The reaction studied in this chapter is the hydrogenation of dimethyl itaconate (DMI) catalyzed by a $[Rh(cod)Cl]_2$–TPPTS complex:

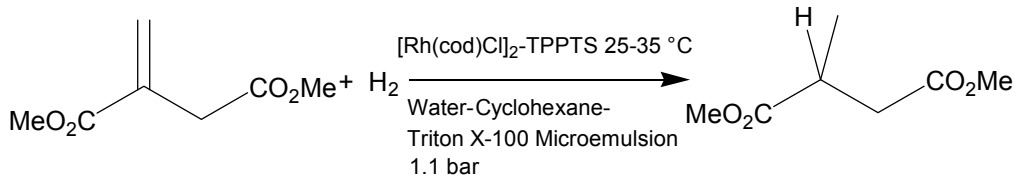

(eq. 4.4)

GC analysis of the organic phase of the biphasic system or of the separated microemulsion shows an almost complete conversion (>98%) of DMI into dimethyl methylsuccinate (DMS). Contrary to other reports **[4.7, 4.17]** no side product was observed.

4.3.4 Influence of the surfactant on the reaction profile (biphasic system)

In a biphasic system the hydrogenation of DMI follows a typical zero order reaction profile, as shown in Figure 4.4a. The reaction rate expressed by the hydrogen consumption flux ($dV \cdot dt^{-1}$, $mL \cdot min^{-1}$) is constant until the end of the hydrogenation. The addition of surfactant accelerates the reaction (Figure 4.4b, c).

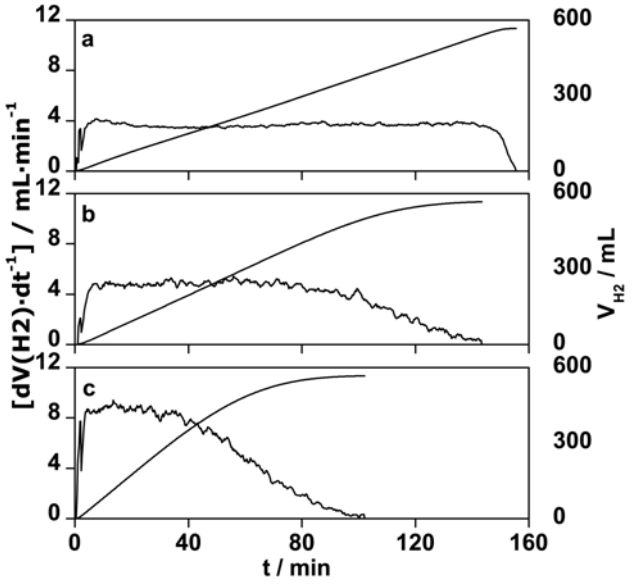

Figure 4.4 Hydrogen flux vs time and consumed hydrogen vs time in the hydrogenation of DMI (4 g of DMI, 50 mL of water, 50 mL of cyclohexane) at 25 °C and 1.1 bar, with 22 mg of $[Rh(cod)Cl]_2$ and 380.4 mg of TPPTS in (a) a biphasic system, (b) a biphasic system with addition of 4 g of Triton X-100 and 4 g of 1-pentanol, and (c) a multiphasic system with addition of 7.43 g of Triton X-100 and 7.43 g of 1-pentanol

The existence of a constant reaction rate at the initial period indicates the multiphasic character of the solvent system (b, two phases; c, three phases). The

higher the concentration of surfactant, the higher is the initial plateau of constant reaction rate. A distinctive change in the profile indicates different barriers for the reaction, i.e., rate limitation by chemical reaction or mass transfer between the phases. In case of the biphasic system without surfactant, the reaction is mainly limited by solubility of the substrate in the aqueous phase. Addition of surfactant results in a higher solubility of the substrate in the aqueous micellar phase containing the catalyst. Thus, the reaction rate is constant until the initial reservoir of substrate inside the micelles or at the interface has reacted; afterwards the rate is governed by the depletion of DMI in the system. A higher surfactant concentration increases the local concentration of the substrate within the micellar aqueous phase and consequently accelerates the reaction.

As can be seen from the extrapolated intercepts (t = 0) of reaction rates depicted in Figure 4.4, the addition of surfactant increases the initial reaction rate. Although the effect is not linear with respect to the surfactant concentration, the reaction rate can be more than doubled by adding defined amounts of surfactant and cosurfactant (7.43 g Triton X-100 + 7.43 g 1-pentanol) to the reaction medium.

4.3.5 Reaction in a microemulsion

In a microemulsion with composition *1 in the “one-phase” region of Figure 4.2, the rate of the catalytic reaction decreases as the substrate is converted, indicated by the total hydrogen uptake of the reactor, as shown in Figure 4.5. The reaction can be considered as first order. In order to test the catalytic activity at the end of the reaction, 4 g DMI were repeatedly added two times. In the second cycle the reaction reinitiated at almost the same initial rate. A slightly lower reaction rate in the third cycle can be referred to the amount of product (DMS) dissolved in the system.

4.3.6 Influence of the substrate concentration

The typical differences between zero- and first-order reactions are observed in the influence of the reactant concentration on the reaction rate in the investigated solvent systems. It is very important to mention that the apparent “reaction orders” are related to mass transport of the substrate into the aqueous phase and thereby to the contact between DMI and catalyst. As can be seen in Figure 4.6 the concentration of

the substrate has no influence on the initial reaction rate in a biphasic system. Against that, a strong influence can be observed in a microemulsion. Both systems provide almost the same initial reaction rate of 4 $mL \cdot min^{-1}$ of hydrogen consumption at 0.127 $mol \cdot L^{-1}$ DMI (2 g DMI in 100 mL solution).

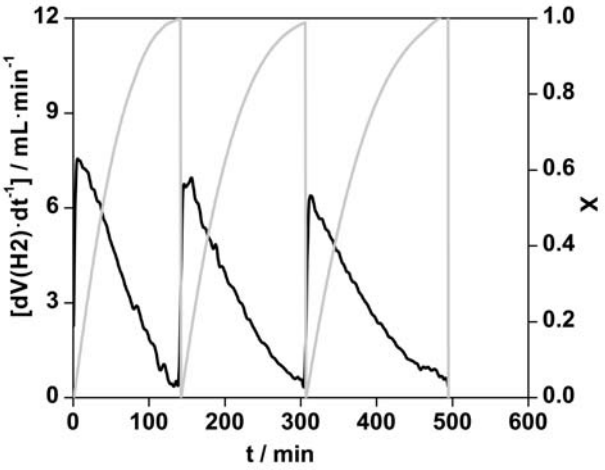

Figure 4.5 Hydrogen flux vs time and consumed hydrogen vs time in the hydrogenation of DMI in a microemulsion system (4 g of DMI, 4.13 mL of water, 79.3 mL of cyclohexane, 7.43 g of Triton X-100, and 7.43 g of 1-pentanol) at 25 °C and 1.1 bar, using 22 mg of [Rh(cod)Cl]2 and 380.4 mg of TPPTS

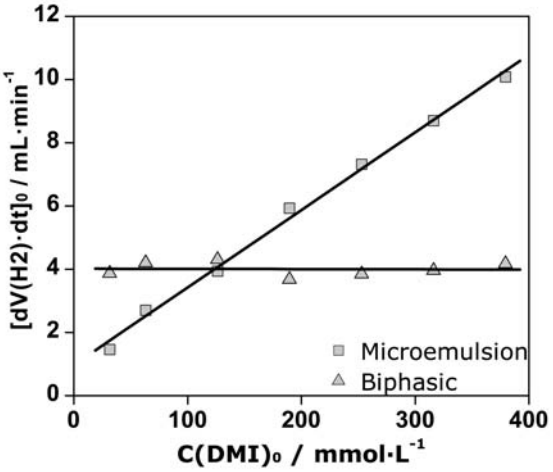

Figure 4.6 Influence of DMI concentration on initial reaction rate of the catalytic hydrogenation of DMI in a biphasic system (50 mL of water, 50 mL of cyclohexane) and in a microemulsion system (4.13 mL of water, 79.3 mL of cyclohexane, 7.43 g of Triton X-100, and 7.43 g of pentanol) at 25 °C and 1.1 bar, using 22 mg of [Rh(cod)Cl]2 and 380.4 mg of TPPTS

4.3.7 Influence of the catalyst concentration

Hydrogenation experiments were carried out with different catalyst concentrations, while maintaining the water concentration and the ligand/metal ratio constant. Figure 4.7 shows a linear dependence of the initial reaction rate with respect to the catalyst concentration. The overloading of the micelles with higher concentrations of catalyst has been reported to result in the formation of inactive metal clusters **[4.18]**. This was avoided by the use of an optimized ligand/metal ratio of 7.5.

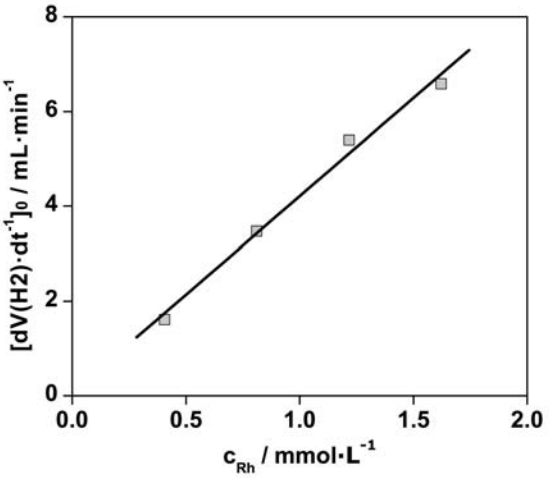

Figure 4.7 Influence of catalyst concentration on initial reaction rate of the catalytic hydrogenation of DMI in a microemulsion system (2 g of DMI, 4.13 mL of water, 79.3 mL of cyclohexane, 7.43 g of Triton X-100, and 7.43 g of 1-pentanol) at 27 °C and 1.1 bar, with molar ratio TPPTS/Rh) 7.5

4.3.8 Influence of the ligand concentration

Hydrogenations with different ligand/metal ratios (n_{Lig}/n_{Met}) were performed, maintaining both, the water and the metal concentrations constant. The influence of the ligand concentration was found to be complex. The same behaviour was also investigated previously in an H-transfer reduction using sodium formate/water in biphasic catalysis **[4.8, 4.19]**. A higher ligand concentration lowers the reaction rate, as shown in Figure 4.8. Interestingly in experiments at ligand/metal ratios below 7, the reaction rate increases to a maximum after staying constant for a certain period of time. At the same time, the system turns from an initially orange colour to black, and at the end of the reaction the catalyst is deactivated. Against that, at ligand/metal ratios above 7, the reaction starts at a maximum reaction rate and the colour of the

system stays the same. The catalyst stays active after hydrogenation is finished (see Figure 4.5).

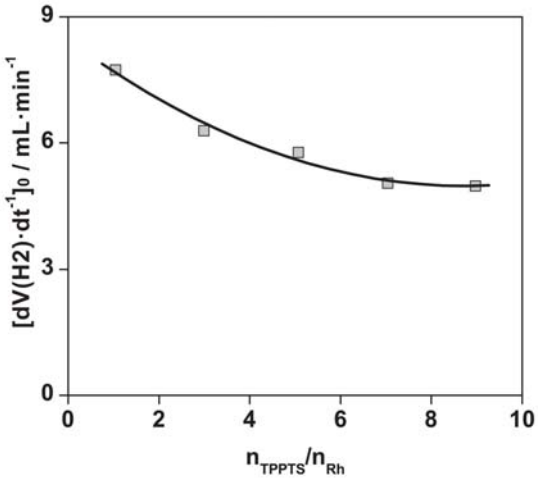

Figure 4.8 Influence of molar ratio TPPTS/catalyst on initial reaction rate of the catalytic hydrogenation of DMI in a microemulsion system (2 g of DMI, 4.13 mL of water, 79.3 mL of cyclohexane, 7.43 g of Triton X-100, and 7.43 g of 1-pentanol) at 27 °C and 1.1 bar, using 30 mg of $[Rh(cod)Cl]_2$

4.3.9 Influence of the cosurfactant concentration

The hydrogenation of DMI was carried out in microemulsions with different amounts of 1-pentanol, keeping the concentrations of water, Triton X-100, and catalyst constant, as well as the ligand/metal ratio. As can be seen in Table 4.1, higher amounts of 1-pentanol diminish the initial rate of the reaction.

Table 4.1 Influence of Cosurfactant (1-Pentanol) Concentration on the Initial Reaction Rate of the Catalytic Hydrogenation of DMI in a Microemulsion (2 g of DMI, 4.13 mL of Water, 79.3 mL of Cyclohexane, and 7.43 g of Triton) at 25 °C and 1.1 bar, Using 22 mg of $[Rh(cod)Cl]_2$ and 380.4 mg of TPPTS

$c_{Pentanol}$ / mol·L^{-1}	$(dV \cdot dt^{-1})_0$ / mL·min^{-1}
0.45	4.53
0.65	4.14
0.85	3.94

One reason may be the size of the reverse micelles. The higher the 1-pentanol concentration, the smaller the micelles are, providing less capability to dissolve substrate and bringing it in contact with the catalyst. This consideration is in agreement with the basic assumption, that the reaction takes place inside the reverse

micelles. Dynamic Light Scattering was used to obtain the size of the reverse micelles, but the results were not satisfying due to high deviation and low reproducibility, because of the very small size of the micelles. Investigation of the micelle size using small angle neutron scattering (SANS) is the main topic of chapter 5.

4.3.10 Influence of the water concentration

The reaction rate of the catalytic hydrogenation of DMI in a microemulsion can be enhanced by adding more water to the system. The same consideration used to explain the influence of the 1-pentanol concentration is useful here: the higher the water concentration, the larger are the reverse micelles and thereby provide increased capability to dissolve substrate molecules. However, further increase of the water concentration from composition *2 to *3 in Figure 4.2 results in a decreased initial reaction rate (see Table 4.2).

Table 4.2 Influence of Water Concentration in the Initial Reaction Rate of the Catalytic Hydrogenation of DMI in a Microemulsion (4 g of DMI, 79.3 mL of Cyclohexane, 7.43 g of Triton, and 7.43 g of Pentanol) at 30 °C and 1.1 bar, Using 22 mg of $[Rh(cod)Cl]_2$ and 380.4 mg of TPPTS

c_{water} / mol·L^{-1}	$(dV \cdot dt^{-1})_0$ / mL·min^{-1}
2.29	6.21
2.73	6.78
3.17	6.71

Since the composition is located near the two-phase region, an explanation of this behaviour can be the existence of a maximum in the optimal size of the micelles, which has already been reported **[4.20]**. As for the impact of cosurfactant, this explanation is discussed on chapter 5.

4.3.11 Kinetics

In case of a microemulsion as reaction medium, there is a strong dependence of the initial reaction rate on the substrate concentration (Figure 4.6). This suggests that the hydrogen insertion step, which does not depend on the substrate concentration, is not the only step relevant for the overall reaction rate. The kinetic model used by Wilkinson et al. **[4.21]** combines the hydrogen insertion and the attack of the

uncomplexed substrate at the dihydrido complex in one step. Due to this combination, that introduces the dependence of the rate on the substrate concentration and directly on the contact between the catalyst and the substrate, is the motivation for using this model. Additionally, the reversible hydrogenation of the catalyst into the dihydrido complex is counted as another important step. Both steps are shown in the Scheme 4.2.

Scheme 4.2 Osborn-Wilkinson Catalytic Cycle [a]

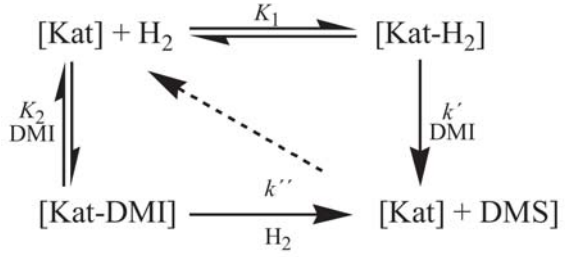

[a] "Kat" = Catalyst

The attack of uncomplexed hydrogen on the substrate-complex, to give a transition state, is assumed to be neglected; for this reason low values of K_2 were expected. For both systems rate laws based on the Osborn–Wilkinson kinetics were used, which describe the influence of the substrate concentration well. For the microemulsion, eq 4.5 was found in a model discrimination to be appropriate for the fit of experimental data.

$$-\frac{\mathrm{d}c(\mathrm{DMI})}{\mathrm{d}t}=\frac{k'K_1c(\mathrm{H_2})c(\mathrm{cat})c(\mathrm{DMI})}{1+K_1\mathrm{c}(\mathrm{H_2})+K_2c(\mathrm{DMI})} \qquad \text{(eq. 4.5)}$$

For the biphasic system, the Osborn-Wilkinson differential equation was used with the difference that the concentration of DMI in the aqueous phase was calculated using the following linear approximation:

$$C_{\mathrm{Aq}}^{\mathrm{DMI}}=\frac{n_{\mathrm{DMI}}}{V_{\mathrm{Aq}}\left(P_{\mathrm{DMI}}\alpha+1\right)} \qquad \text{(eq. 4.6)}$$

and the concentration of the catalyst in the same phase were taken into account, where n_{DMI} is the molar amount of DMI in the whole system, α is the volumetric ratio of organic phase to aqueous phase, P_{DMI} is the partition coefficient of DMI, which was estimated with the linear approximation represented by eq 4.3, and V_{Aq} is the volume of the aqueous phase. The estimation of kinetic parameters was performed by fit of eq 4.5 to experimental data of concentration vs time by means of Berkeley Madonna numerical integration software (see programs 1 & 2 of Appendix A). The experimental results compared to fitted model curves are shown in Figures 4.9 and 4.10.

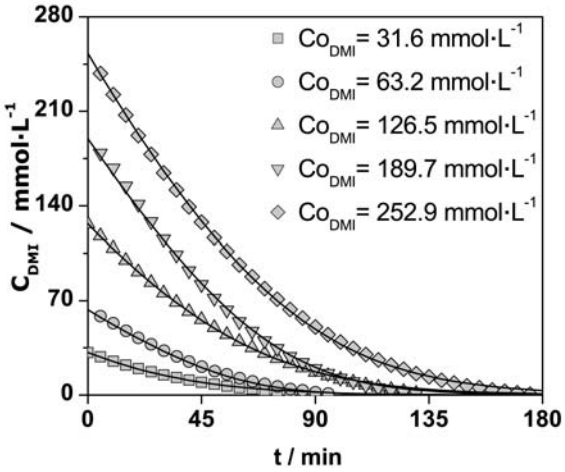

Figure 4.9 Fit of the kinetic model represented by eq 4.5 to experimental concentration vs time profiles of the hydrogenation of DMI in a microemulsion system (4.13 mL of water, 79.3 mL of cyclohexane, 7.43 g of Triton X-100, and 7.43 g of 1-pentanol) at 25 °C and 1.1 bar

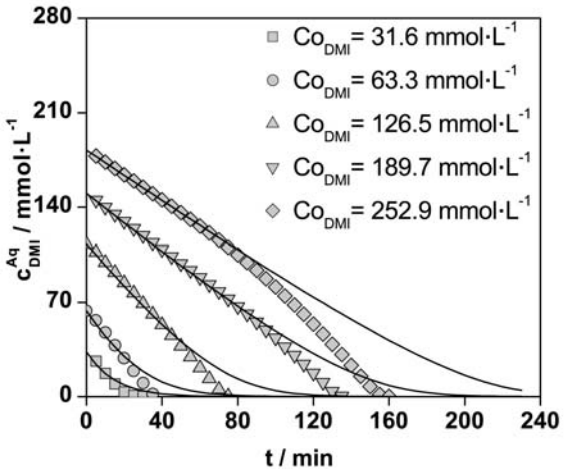

Figure 4.10 Fit of the kinetic model represented by eq 4.5, modified with eq 4.6, to experimental concentration vs time profiles of the hydrogenation of DMI in a two-phase system (50 mL of cyclohexane and 50 mL of water) at 25 °C and 1.1 bar

The Osborn–Wilkinson model could adequately fit only the initial points of the hydrogenations done in cyclohexane/water biphasic systems, because of the variation of the partition coefficient (P_{DMI}) at higher concentrations of DMI (>50 mmol·L^{-1}). The decreasing magnitude of the partition coefficient of DMI with decreasing concentration of DMI in the system allows the even higher availability of substrate in the aqueous phase. Also, the increasing concentration of the product DMS, which as shown by de Bellefon **[4.7]** has an even bigger partition coefficient than DMI, surfeits the cyclohexane phase, extracting the substrate DMI from the organic phase to the water phase, and enabling a better contact with the catalyst. Figure 4.11 shows the rate expressed as hydrogen flux during the hydrogenation of 5 g of DMI (316.1 mmol·L^{-1}) in 100 ml of a biphasic C_6H_{12}/H_2O system. In this Figure, the partition coefficient influence and the extracting effect of the product (DMS) on the hydrogenation are noticeable by a weak acceleration of the reaction between 40 and 60 min.

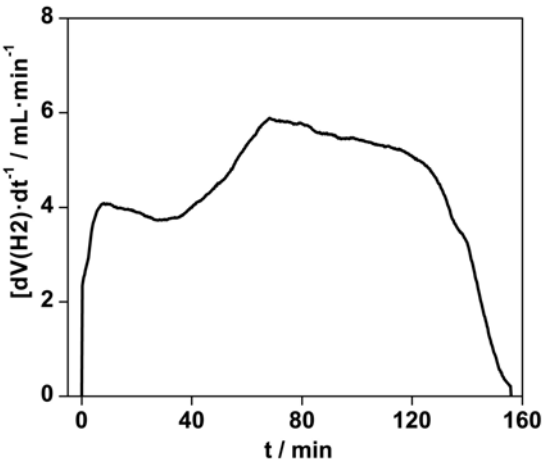

Figure 4.11 Hydrogen flux vs time in the hydrogenation of DMI (5 g of DMI) in a biphasic system (50 mL of water, 50 mL of cyclohexane) at 25 °C and 1.1 bar, with 22 mg of [Rh(cod)Cl]2 and 380.4 mg of TPPTS

As can be seen in Table 4.3, the equilibrium constant K_1 for both systems (biphasic and microemulsion) are similar and are greater than 1, meaning that the formation of the dihydrido complex is favoured and stabilized in the aqueous phase of the biphasic system as well as in the reverse micelles of the microemulsion. This independence of the equilibrium constant K_1 of the system can be explained by the fact that the catalyst is located, in both systems, in the aqueous phase (where the solubility of hydrogen is the only limitation factor).

Table 4.3 also shows that the values of the rate constants *k*' were equal for both systems, remarking the independency of the reaction from the different systems.

Table 4.3 Rate Constants and Activation Energies for the Hydrogenation of DMI in Different Solvent Systems [a]

System	k' / L·mmol^{-1}·min^{-1}	K_1 / L·mmol^{-1}	K_2 / L·mmol^{-1}	$E_{A,k'}$ / kJ·mol^{-1}	$E_{A,eff}$ / kJ·mol^{-1}
Microemulsion [b]	0.07	1.57	0.04	52.89	61.56
Biphasic [c]	0.07	1.46	0.08	57.87	11.45
Biphasic **[4.10]**	—	—	—	71.00	—

[a] k', K_1, and K_2 are given for T = 25 °C; $E_{A,k'}$ and $E_{A,eff}$ are calculated from rate constants between 25 and 35 °C. [b] 4.13 mL of water, 79.3 mL of cyclohexane, 7.43 g of Triton, and 7.43 g of 1-pentanol. [c] 50 mL of cyclohexane, 50 mL of water.

The Arrhenius law only applies to elementary reactions, not to complex systems **[4.22]**. However, it was used to estimate the activation energy of the reaction for both systems, since in the narrow range of investigated temperatures (298–308 K); a change in the rate-determining step is not expected. The temperature dependence of the overall reaction is represented by an effective activation energy $E_{A,eff}$, which was approximated with an Arrhenius plot. Effective rate constants (k_{eff}) were obtained with the help of the temperature-dependent Henry coefficients *He* (eq 4.7), which were determined from solubility data **[4.23]**:

$$V_R \times \frac{dc(P)}{dt} = \frac{dn(H_2)}{dt} = \frac{dV}{dt} \times \frac{p_0}{R\,T_0} = V_R \times k' \times c_0(cat) \times c(H_2) = k_{eff} \times c(H_2)$$

$$k_{eff} = \frac{dV}{dt} \times \frac{p_0}{R\,T_0} \times \frac{1}{He\,\left(p_{tot} - p(H_2O)\right)} \qquad \text{(eq. 4.7)}$$

with

$$He = \frac{p(H_2)}{c(H_2)} = \frac{p_{tot} - p(H_2O)}{c(H_2)}$$

The activation energy of the irreversible hydrogen insertion ($E_{A,k'}$) was also approximated with an Arrhenius plot, using the rate constant of the irreversible step of the reaction (*k'*).

The activation energy for the hydrogen insertion for both, microemulsion and biphasic system (52.89 and 57.97 kJ·mol^{-1}) seem to be according to a kinetic control, and in comparison to the activation energy corresponding to the H-transfer reduction of DMI done by de Bellefon et al. (71 kJ·mol^{-1}) **[4.7, 4.8]**, there is a similar range. The difference between the activation energy of the elemental reaction and the effective

activation energy for the biphasic system (11.47 $kJ \cdot mol^{-1}$) demonstrates the existence of mass transport limitation. On the one hand, the effective rate constant (k_{eff}) takes into reference the observed initial velocity of the reaction, which results from reaction kinetic and mass transport processes, and on the other hand, the rate constant (k') results from merely the kinetics of the reaction.

The enthalpy of the hydrogenation of DMI in both systems (cyclohexane/water and [Triton X-100/1-pentanol]/cyclohexane/water microemulsion) was approximated with a van't Hoff reaction isochor, using the equilibrium constant of the reversible dihydrido complex formation (K_1). Similar enthalpies of 55 ± 5 $kJ \cdot mol^{-1}$ were estimated for both systems.

3.4 References

[4.1] Heller, D., R. Kadyrov, M. Michalik, T. Freier, U. Schmidt, and H.W. Krause, *Tetrahedron-Asymmetry,* **1996,** *7*, (10), 3025-3035; Knowles, W.S., *Acc. Chem. Res.,* **1983,** *16*, (3), 106-112; RajanBabu, T.V., B. Radetich, K.K. You, T.A. Ayers, A.L. Casalnuovo, and J.C. Calabrese, *J. Org. Chem.,* **1999,** *64*, (10), 3429-3447.

[4.2] Berens, U., M.J. Burk, A. Gerlach, and W. Hems, *Angew. Chem. Int. Ed.,* **2000,** *39*, (11), 1981-+.

[4.3] Cornils, B. and E.G. Kuntz, *J. Organomet. Chem.,* **1995,** *502*, (1-2), 177-186.

[4.4] Dwars, T., E. Paetzold, and G. Oehme, *Angew. Chem. Int. Ed.,* **2005,** *44*, (44), 7174-7199.

[4.5] Weitbrecht, N., M. Kratzat, S. Santoso, and R. Schomacker, *Catal. Today,* **2003,** *79*, (1-4), 401-408; Schwarze, M. and R. Schomäcker, *Chem. Ing. Tech.,* **2006,** *78*, (7), 931-936.

[4.6] Herrmann, W.A. and C.W. Kohlpaintner, *Angewandte Chemie-International Edition in English,* **1993,** *32*, (11), 1524-1544.

[4.7] de Bellefon, C., N. Tanchoux, S. Caravieilhes, and D. Schweich, *Catal. Today,* **1999,** *48*, (1-4), 211-219.

[4.8] Tanchoux, N. and C. de Bellefon, *Eur. J. Inorg. Chem.,* **2000**, (7), 1495-1502.

[4.9] Grosselin, J.M., C. Mercier, G. Allmang, and F. Grass, *Organometallics,* **1991,** *10*, (7), 2126-2133.

[4.10] Kuntz, E.G., *(Rhône-Poulenc Ind.). FR Patent 2.230.654, 1983; FR Patent 2.314.910, 1975; FR Patent 2.338.253, 1976; FR Patent 2.349.562, 1976; FR Patent 2.366.237, 1976; FR Patent 2.473.505, 1979; FR Patent 2.478.078, 1980; FR Patent 2.550.202, 1983; FR Patent 2.561.650, 1984.*

[4.11] Ohkubo, K., T. Kawabe, K. Yamashita, and S. Sakaki, *J. Mol. Catal.,* **1984,** *24*, (1), 83-86; Cheprakov, A.V., N.V. Ponomareva, and I.P. Beletskaya, *J. Organomet. Chem.,* **1995,** *486*, (1-2), 297-300.

[4.12] Noyori, R., *Asymmetric Catalysis in Organic Synthesis*. 1st ed. 1994, New York: John Wiley and Sons, Inc. p. 400.

[4.13] Johnson, N.B., I.C. Lennon, P.H. Moran, and J.A. Ramsden, *Acc. Chem. Res.,* **2007,** *40*, (12), 1291-1299.

[4.14] Sinou, D., *Adv. Synth. Catal.,* **2002,** *344*, (3-4), 221-237.

[4.15] Schomäcker, R., *Nachr. Chem. Tech. Lab.,* **1992,** *40*, (12), 1344-1351.

[4.16] Moulik, S.P. and B.K. Paul, *Adv. Colloid Interface Sci.,* **1998,** *78*, (2), 99-195.

[4.17] Hablot, I., J. Jenck, G. Casamatta, and H. Delmas, *Chem. Eng. Sci.,* **1992,** *47*, (9-11), 2689-2694.

[4.18] Haumann, M., H. Koch, and R. Schomacker, *Catal. Today,* **2003,** *79*, (1-4), 43-49.

[4.19] Bényei, A. and F. Joo, *J. Mol. Catal.,* **1990,** *58*, (2), 151-163.

[4.20] Zhu, D.M., X. Wu, and Z.A. Schelly, *Langmuir,* **1992,** *8*, (6), 1538-1540; Zhu, D.M., K.I. Feng, and Z.A. Schelly, *J. Phys. Chem.,* **1992,** *96*, (5), 2382-2385.

[4.21] Osborn, J.A., F.H. Jardine, J.F. Young, and Wilkinso.G, *J. Chem. Soc. A: Inorg. Phys. Theor.,* **1966**, (12), 1711-&.

[4.22] Masel, R., *Chemical Kinetics and Catalysis*. 1st ed. 2001, New York: Wiley/Interscience. p. 968.

[4.23] *Hydrogen and Deuterium*. IUPAC Solubility Data Series, ed. C. Young. Vol. 5/6. 1981, Oxford: Pergamon Press. p. --.

5 Catalytic Hydrogenation of Dimethyl Itaconate in Nonionic Microemulsions: Influence of the Size of Micelle

5.1 Introduction

Micelles are supramolecular assemblies in a colloidal dimension. These assemblies are based on the amphiphilic characteristics of surfactants or amphiphiles, which are molecules with a polar headgroup and a hydrophobic tail. Micelles can be formed in water and in nonpolar solvents (see Scheme 5.1), for which the names of micelles and reverse micelles have been given, respectively. Reverse micelles are formed by association of polar headgroups of amphiphiles with colloidal drops of water in an organic medium once the amphiphiles concentration in the interface is appropriate **[5.1]**.

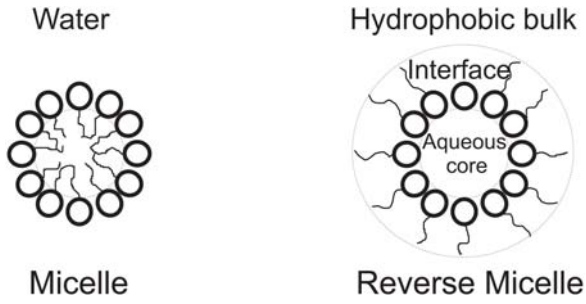

Scheme 5.1 Scheme of a micelle and a reverse micelle

The delimitation of hydrophilic and hydrophobic micro-domains is an important feature of reverse micelles favourable to reactions **[5.2]**. For this reason they are being regarded as microreactors, which capacity for reactants and variability of solubilization properties are high and of practical interest **[5.3]**. Contrary to the case of aqueous micelles, reactions in reverse micelles are possible at high concentrations of hydrophobic substrates, and in regard to homogeneous reaction media they can be divided, as observed in Scheme 5.1, into three spatial domains: the aqueous core, the hydrophilic–hydrophobic interface, and the surrounding hydrophobic medium. Water in the core may display deviating electrophilic and nucleophilic properties relative to “bulk water” because of strong interactions with the head groups of the surfactant, depending on the size of the droplets. Thus, the effect of this medium on reaction rates is often dependent on the water/surfactant (ω) molar ratio **[5.4]**.

We have published a kinetic study that compares the catalytic hydrogenation of dimethyl itaconate in a Triton X-100 microemulsion and in a biphasic system **[5.5]**. In this study an important influence of the microemulsion formulation on the initial rate of the hydrogenation was noticed. The Triton X-100 system used in the earlier study needed the addition of 1-pentanol as cosurfactant, which also had an inhibition effect on the hydrogenation. Cosurfactants are used in order to stabilize the surfactants in the interface. When the amphiphile molecules have large polar groups, as Triton X-100 has **[5.6]**, the interactions between each surfactant molecule destabilizes the micelle. For this reason the addition of short-chain alkanols, which also have amphiphilic properties and position themselves in between the surfactant molecules, cushion the interactions stabilizing the micelles **[5.5, 5.7]**. The cosurfactant has also an important effect on the size of the micelles. Accordingly the determination of the size and the structural characterisation of the microemulsion droplets is an important aspect in understanding catalytic reactions in microemulsions. Due to the small size of the micelles, which diameters are typically in the range of 1—100 nm **[5.8, 5.9]**, microemulsions are usually transparent; this characteristic feature has rendered them amenable for studies by dynamic light scattering (DLS) **[5.9, 5.10]**. Such studies are accurate when the samples are highly diluted, enough to safely neglect interactions between aggregates and multiple scattering. This condition is often not satisfied with microemulsions **[5.11]**. Hence experiments and data analysis applying the scattering theories must be performed with special care, and the results must be regarded with a critical mind and be combined with results from other techniques. In contrast to DLS, small angle neutron scattering (SANS) with its higher spatial resolution can be applied to such systems to corroborate values obtained for the hydrodynamic radius and add information regarding the core size of the micelles. Small angle neutron scattering (SANS) is a well established technique used to characterize microemulsions in much structural detail **[5.12, 5.13]**, and it has been successfully applied to Triton X-100 micellar systems **[5.14]**.

The present chapter reports the correlation between the size of reverse micelles obtained by SANS and DLS, and the initial hydrogenation rate of dimethyl itaconate (DMI) with the water-soluble catalyst complex Rh-TPPTS using two nonionic microemulsion systems with different water content (characterised by ω) as dispersive media. In addition, the influence of the cosurfactant/surfactant mass ratio (δ) as a reaction parameter was studied.

5.2 Experimental

5.2.1 Chemicals

The solvents cyclohexane (≥ 99.5 %, Roth), and 1-pentanol (≥ 99 %, Merck) were degassed and purged under nitrogen and used without further purification. Cyclohexane-d_{12} (99.5 %, Deutero GmbH), deuterium oxide (99.9 %, Deutero GmbH), poly(ethylene glycol) 400 and 1000 (100 %, Fluka), the water-soluble ligand TPPTS (30.7 wt% in water, Celanese), and the surfactants Triton X-100 (100 %, Sigma-Aldrich) and Igepal CA-520 (100 %, Sigma-Aldrich) were used as received. The catalyst precursor $[Rh(cod)Cl]_2$ (98 %, Strem) was kept under nitrogen and used as received.

5.2.2 Microemulsion preparation

The following common terms were used to describe the compositions of the four-component systems; these terms are simplified in case of using a three component system (without cosurfactant):

$$\alpha = \frac{m_{\text{oil}}}{m_{\text{oil}} + m_{\text{water}}} \qquad \gamma = \frac{m_{\text{surfactant}}}{m_{\text{oil}} + m_{\text{water}} + m_{\text{surfactant}}} \qquad \delta = \frac{m_{\text{cosurfactant}}}{m_{\text{surfactant}}}$$

(eq 5.1)

$$\omega = \frac{n_{\text{water}}}{n_{\text{surfactant}}} \qquad \omega_T = \frac{n_{\text{water}}}{n_{\text{surfactant}} + n_{\text{cosurfactant}}}$$

where m indicate a mass and n a number of moles

The surfactants used were the commercially available Triton X-100 and Igepal CA-520, respectively. Both are based on *t*-octylphenoxypolyethoxyethanol (Scheme 5.2) with different number of ethoxyethanol groups. Igepal CA-520 has approximately half the ethoxyethanol groups (n = 5) of Triton X-100 (n = 9-10).

Test tubes were prepared with different compositions of water and cyclohexane (α) but fixed weight fractions of Triton X-100 and 1-pentanol (γ). The sequence in which the components were added was: (1) cyclohexane, (2) Triton X-100, (3) 1-pentanol, and (4) water. Before and after water addition, the solution was agitated for 5 min. The test tubes were immersed in a thermostated water bath, and phase behaviour was observed after 15 min. This procedure was repeated with increasing temperature of 1 K stepwise. The same procedure was used for the Igepal CA-520 system. The change in phase behaviour depending on temperature and composition followed a pattern typical for non-ionic surfactant-based microemulsions.

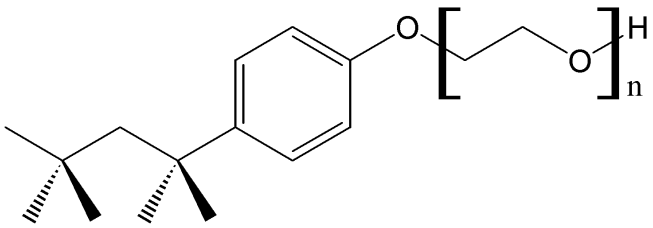

Scheme 5.2 (p-tert-Octylphenoxy)polyethoxyethanol chemical formula

5.2.3 Cosurfactant partition

Many publications dealing with microemulsion quaternary systems take into consideration that the cosurfactant, which in our case is 1-pentanol partitions itself between the interfacial film and the continuous oily phase **[5.11, 5.15]**. It is important to start by analyzing the percentage of pentanol possibly accumulated in the core of the micelles. For this reason, a partition study of 1-pentanol in biphasic systems cyclohexane/water with PEG 400, cyclohexane/water with PEG 1000 and cyclohexane/water alone was made. The compositions for the Triton X-100 systems shown in the Table 5.1 were used to prepare the samples, and instead of adding Triton X-100, the same molar amount of PEG was added. PEG 400 represents a good approximation for the polar group of the Triton X-100 molecules, and the cyclohexane/water systems with and without PEG 1000 allows us to observe the influence of PEG and its ethoxyethanol chain length on the pentanol partition. The pentanol concentration in the cyclohexane phase was analysed by gas chromatography (GC) using a *Shimadzu 2010 GC (DB-5HT column, approx. 30 m, d = 0.32 mm, 0.4 bar N_2, 70 °C, FID*) obtaining a retention time for 1-pentanol of approximately 3 min.

5.2.4 Catalytic hydrogenation runs

The hydrogenation of DMI catalyzed by the water soluble catalyst complex Rh-TPPTS (Scheme 5.3) was selected as a reference for studying the influence of the micelles size on the reaction kinetics. DMI has a partition coefficient smaller than *1* at low DMI concentrations (<50 mmol L^{-1}) in a cyclohexane-water biphasic system, but by increasing the DMI concentration to higher values (>50 mmol L^{-1}) more DMI accumulates in the cyclohexane phase and the partition coefficient becomes higher than *1*. This partition behaviour can be influenced by the presence of surfactants in the solution, changing the apparent order of the reaction from zero in a biphasic system to one in microemulsions **[5.5]**.

Table 5.1 Composition of the different microemulsions for both systems: [Triton X-100/1-pentanol]/cyclohexane/water and Igepal CA-520/cyclohexane/water

Sample	Surfactant [a]	α	γ (%)	ω	ω_T	δ
ME 1	*Triton X-100*	0.94	10	20.0	3.10	0.75
ME 2	*Triton X-100*	0.95	10	15.0	2.31	0.75
ME 3	*Triton X-100*	0.97	10	10.0	1.54	0.75
ME 4	*Triton X-100*	0.94	10	20.0	2.42	1.00
ME 5	*Triton X-100*	0.95	10	15.0	1.80	1.00
ME 6	*Triton X-100*	0.97	10	10.0	1.20	1.00
ME 7	*Triton X-100*	0.94	10	20.0	1.98	1.25
ME 8	*Triton X-100*	0.95	10	15.0	1.47	1.25
ME 9	*Triton X-100*	0.97	10	10.0	0.98	1.25
ME 10	*Triton X-100*	0.94	10	20.0	1.68	1.50
ME 11	*Triton X-100*	0.95	10	15.0	1.25	1.50
ME 12	*Triton X-100*	0.97	10	10.0	0.83	1.50
ME 13	*Igepal CA-520*	0.956	3.36	30.0	–	–
ME 14	*Igepal CA-520*	0.956	3.70	27.5	–	–
ME 15	*Igepal CA-520*	0.956	4.00	25.0	–	–
ME 16	*Igepal CA-520*	0.956	4.40	22.5	–	–
ME 17	*Igepal CA-520*	0.956	5.00	20.0	–	–
ME 18	*Igepal CA-520*	0.956	3.30	30.6	–	–
ME 19	*Igepal CA-520*	0.960	3.30	27.5	–	–
ME 20	*Igepal CA-520*	0.964	3.30	25.0	–	–
ME 21	*Igepal CA-520*	0.968	3.30	22.5	–	–

[a] *For the reactions, all the microemulsions were prepared with cyclohexane and water. For the Triton X-100 system, 1-Pentanol was used as cosurfactant.*

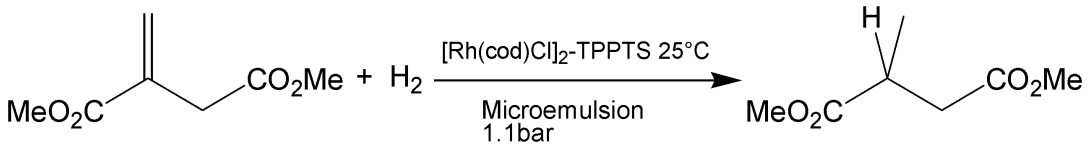

Scheme 5.3 Hydrogenation of dimethyl itaconate formal reaction

First, the catalyst complex was prepared by mixing 22 mg of the catalyst precursor $[Rh(cod)Cl]_2$ (0.089 mmol Rh) with 1240 mg aqueous 30% TPPTS solution (380.4 mg, 0.67 mmol TPPTS) under nitrogen. This mixture was stirred under nitrogen at ambient temperature for 24 h before it was used in the hydrogenation reaction. The high molar ratio TPPTS/Rh (7.5) is used to ensure that the hydrogenation starts at a maximal reaction rate and to avoid the formation of rhodium metal **[5.5]**. A thermostated double wall 200 ml glass reactor equipped with a gas dispersion stirrer was used in this study. Semi-batch reactions were performed under a constant hydrogen pressure of 1.1 bar. The reaction rates were calculated using the monitored hydrogen flow rate for keeping the pressure at a constant level.

The microemulsions were prepared one day before the experiment and agitated overnight. The reactor was evacuated at 150 mbar and refilled with nitrogen 3 times after introducing the solvent and again after injection of the catalyst solution (1.2 g) and 2 g of DMI, respectively. The mixture was stirred at 400 rpm and 40 °C for 30 min and afterwards at reaction temperature for 30 min. The reaction was initiated after evacuating the reactor to 150 mbar, followed by an increase of the pressure to 1.1 bar with hydrogen gas and subsequent stirring at 800 rpm. A decreasing and finally expiring hydrogen flux indicated the end of the reaction. The complete hydrogenation of DMI to dimethyl methylsuccinate (DMS) was confirmed by gas chromatography (GC) using a *HP 5710A instrument (Lipodex E capillary column, ca. 25 m, d = 0.25 mm, 0.6 bar N_2, 90 °C, FID)* obtaining a retention time of DMS of approximately 20 min. Microemulsion samples were separated into organic and aqueous phases by addition of water. After phase separation the organic phase was analyzed. Table 5.1 shows the compositions of the different microemulsions used as media for the hydrogenation experiments.

5.2.5 Dynamic light scattering of nonionic microemulsions

All samples were measured without catalyst. Dynamic Light Scattering (DLS) was employed in order to study the size of the micelles of the Igepal CA-520 systems in terms of the hydrodynamic radius. Correlation functions were recorded at the scattering angle of 90° using a typical ALV goniometer setup with a Nd:YAG-laser as light source (wavelength λ = 532 nm). The constant output power was 150 mW. All measurements were done at 25 °C controlled by a toluene matching bath. The

correlation functions were generated using an ALV-5000/E multiple *τ* digital correlator and finally analyzed by inverse Laplace transformation (CONTIN) **[5.16]**.

5.2.6 Small angle neutron scattering of nonionic microemulsions

SANS spectra were recorded on the instrument V4 at the BER reactor of the Helmholtz Zentrum Berlin, Germany. Data were recorded on a 64 x 64 2-dimensional gas detector (128 x 128 pixels), at a constant wavelength of 6.3 Å (FWHM 18%). Samples were filled into quartz cuvette (QS, Hellma) with neutron path length of 1 mm and thermostated at 25.3 °C +/- 0.4. Three sample-detector distances were used: 1, 4, 12 m, with collimation at 2, 4 and 12 m respectively. Data reduction was performed using the software package BerSANS, with correction from the scattering contribution of the empty cell, and deviations in the pixel efficiency accounted for using the incoherent scattering of a 1 mm pure water sample. Electronic and ambient background was accounted for by the measurement of a cadmium plate. The transmission of water was used to get the instrumental coefficient, assuming the ideal case where non-transmitted neutrons are scattered uniformly over the full solid angle (4 Pi). Finally data were azimuthally averaged, and intensities at different configurations but corresponding to the same sample were merged without the need of a scaling factor. Due to the fact that neutrons interactions with hydrogen and deuterium are widely different, labelling the micro-domains of the micelles with deuterated compounds is possible **[5.17]**. For this reason, different contrast conditions were used: microemulsions were prepared from heavy water, Triton X-100, 1-pentanol, and either hydrogenated or perdeuterated cyclohexane. The former case provide an inner look to the D_2O-based core of the micelles, while in the latter case the hydrogenated interfacial film is probed. Two different methods were used to calculate the hydrodynamic radius, both using the parameters obtained by the Guinier approximation **[5.18]**. The Guinier approximation has the following form:

$$I(q) = I0 \exp\left[-\frac{q^2 Rg^2}{3}\right] \qquad \text{(eq 5.2)}$$

where *I0* is the absolute intensity and *Rg* is the radius of gyration. *Rg* is determined with linear regressions on Guinier plots (ln(*I*) vs. q^2) of the SANS data, and the radius of the corresponding homogeneous spheres is estimated following the form:

$$Rg_{Sph}^2 = \frac{3}{5}R^2 \qquad \text{(eq 5.3)}$$

Small angle neutron scattering theory allows for another basic way of determining the radius of the micelles, namely the coherent macroscopic scattering cross section from an assembly of particles dispersed in a solvent. The macroscopic scattering cross section is represented by the expression given below **[5.17]**:

$$I(q) = \phi \Delta p^2 VpF(q)S(q) \qquad \text{(eq 5.4)}$$

where ϕ is the volume fraction of particles, Vp their volume, Δp the contrast, $F(q)$ is the form factor accounting for the shape and size of particles and $S(q)$ is the structure factor accounting for the spatial correlation between particles.

By considering the micelles to be non-interactive in a dilute solution ($S(q) = 1$) and extrapolating to zero q ($F(q) = 1$), eq 5.4 can be re-arranged and gives:

$$Vp = \frac{I0}{\phi \Delta p^2} \qquad \text{(eq 5.5)}$$

ϕ is calculated with the volume fractions of the polar components:

$$\phi = \phi_{EO10} + \phi_{H2O} + \phi_{D2O} + \left(x_{C5H12O}\phi_{C5H12O}\right) \qquad \text{(eq 5.6)}$$

where ϕ_{EO10}, ϕ_{H2O}, ϕ_{D2O} and ϕ_{C5H12O} are the volume fractions of the polar part of Triton X-100, water attached to the ethoxy chain of the surfactant, deuterium oxide and pentanol, respectively, and x_{C5H12O} is the fraction of pentanol inside the core of the micelles. The contrast is the difference between the scattering length densities (SLD) of the medium composed of cyclohexane-d_{12} and a fraction of pentanol and the mostly hydrogenated particles using the following equation:

$$\Delta p = \frac{\sum SLD_{polar_i}\phi_{polar_i}}{\sum \phi_{polar_i}} - \frac{\sum SLD_{nonpolar_i}\phi_{nonpolar_i}}{\sum \phi_{nonpolar_i}} \qquad \text{(eq 5.7)}$$

The software package *SASfit*, written by Joachim Kohlbrecher (Paul-Scherrer Institute, Switzerland), was used to analyze the SANS spectra.

5.2.7 Conductivity of nonionic microemulsions

A commercially available compact conductivity meter *cond 330i* (WTW, Weilheim, Germany) was used. All conductivity measurements were done at 25 °C.

5.3. Results and discussion

5.3.1 (*p-tert*-Octhylphenoxy)polyethoxyethanol microemulsions

Since Kahlweit presented for the first time the phase prism for ternary water-oil-surfactant systems **[5.19]**, built up from different Gibbs diagrams of the ternary system at different temperatures, studies in this area that dealt with different applications of microemulsions, have mainly used two vertical sections of this prism, as seen in Figure 5.1 (same Figure 2.17), which result in pseudo-binary phase diagrams **[5.20]**. One section with the temperature as ordinate is obtained by keeping the oil-to-water ratio constant (usually at α = 0.5), the other by keeping the amount of surfactant constant. This last diagram shows two biphasic system areas, separated by a horizontal one phase canal. Figure 5.2 shows a part of the one phase canal for two systems: a) [Triton X-100/1-pentanol]/cyclohexane/water and b) Igepal CA-520/cyclohexane/water. Both systems were studied at surfactant concentrations (γ) of 5 and 10 % respectively, showing the typical behaviour for such systems of a wider one phase canal when using higher concentrations of surfactants. 1-Pentanol was added to the Triton X-100 system in order to stabilize the reverse micelles **[5.21]**, as the larger EO group of the Triton X-100 yields a smaller packing parameter that becomes increased by the addition of the pentanol. In addition the presence of pentanol, as it will be shown further, also has an important influence on the DMI hydrogenation catalyzed by the water soluble catalyst complex Rh-TPPTS included in the reverse micelles.

5.3.2 Influence of the water/surfactant ratio (ω) on the hydrogenation of DMI in microemulsions

Using the compositions from Table 5.1 for 100 mL of microemulsion, and hydrogenating 2 g of DMI with 20 mg of $[Rh(cod)Cl]_2$ and 346 mg of TPPTS for each microemulsion, a course of hydrogen consumption rate ($[dV(H_2)\ dt^{-1}]$, mL min^{-1}) versus time (min) is obtained. The maximum hydrogenation rate observed after stabilization of the pressure control system is taken as the initial rate of the hydrogenation ($[dV(H_2)\ dt^{-1}]_o$, mL min^{-1}). Figure 5.3 shows the monitored hydrogen consumption rate when hydrogenating 2 g of DMI in microemulsion *ME 1* containing Triton X-100, the initial hydrogenation rate is 5.9 mL_{H2} min^{-1}.

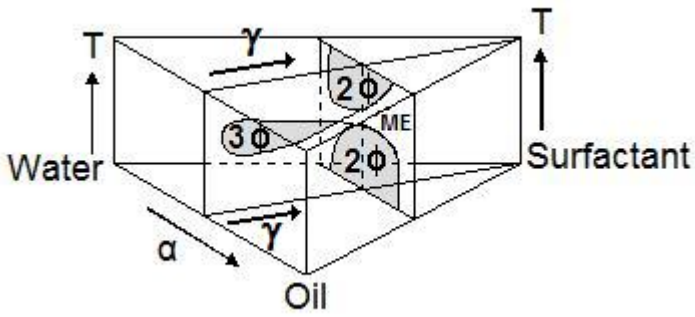

Figure 5.1 Schematic phase prism of a ternary mixture of water–oil–surfactant including two characteristic sections at constant α and constant γ, and whose distinctive regions of one phase microemulsion (ME), biphasic (2ϕ) and three-phase system (3 ϕ) are observed as a function of the temperature (T)

By increasing the amount of water inside the reverse micelles relative to the amount of surfactant (ω) the initial hydrogenation rate of DMI increases. This influence is linearly dependent for all systems as can be seen in the Figure 5.4. For the Igepal CA-520 systems, also an influence of the surfactant concentration is noticeable. As Figure 5.5 shows, there are two different patterns described in this figure. First, by decreasing the concentration of Igepal CA-520 (γ) with a constant ratio cyclohexane-to-water (α = 0.956), the initial hydrogenation rate increases.

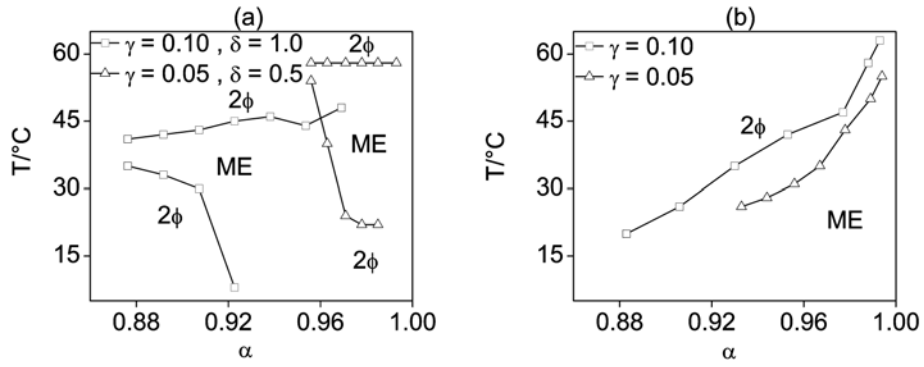

Figure 5.2 Phase prism section (constant γ) with the respective one phase microemulsion (ME) and biphasic system (2ϕ) regions of: (a) the quaternary system [Triton X-100–1-pentanol]–cyclohexane–water with two constant weight fractions of Triton X-100 and 1-pentanol, and (b) the ternary system Igepal CA-520–cyclohexane–water with two constant weight fractions of Igepal CA-520

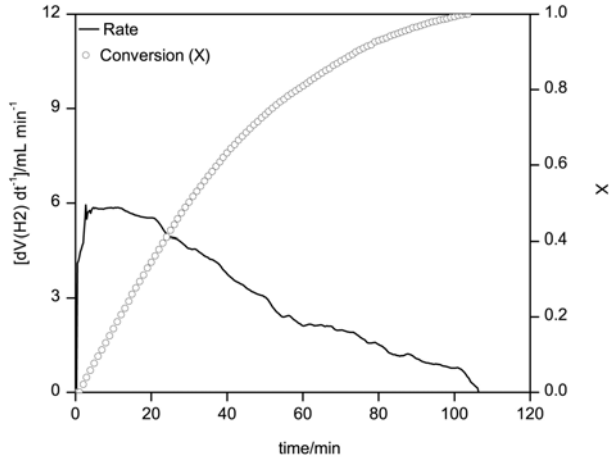

Figure 5.3 Hydrogen flux vs. time and conversion vs. time in the hydrogenation of 2 g of DMI in a microemulsion system constituted by 4.27 g of water, 64.23 g of cyclohexane, 7.61 g of Triton X-100 and 5.71 g of 1-pentanol (ME 1 in Table 5.1), at 25 °C and 1.1 bar, using 20 mg of $[Rh(cod)Cl]_2$ and 357 mg of TPPTS

Second, by keeping the concentration of Igepal CA-520 constant (γ = 0.033) with decreasing ratio cyclohexane-to-water (α), the initial hydrogenation rate also increases. Both patterns are proof of an increase of the initial hydrogenation rate with increase of the molar ratio water to surfactant (ω). Figure 5.5 also shows that by comparing the initial hydrogenation rate of DMI in Igepal microemulsions of equal ω from both patterns, the Igepal microemulsions with lower concentration of surfactant (γ = 0.033) allowed for higher initial hydrogenation rates. By keeping the ratio ω

constant, with higher concentrations of Igepal, we expect an increase in the concentration of micelles of equal size, so the catalyst should distribute itself over more micelle cores. For the Triton X-100 microemulsions, by increasing the amount of cosurfactant in relation to the amount of surfactant (δ), the initial hydrogenation rates for each ω decreases, resulting in a displacement of the linearly dependent curves to smaller initial hydrogenation rates, at constant slope (except for δ = 1). This behaviour indicates a direct proportionality between ω and the initial hydrogenation rate within an even wider ω range than shown in Figure 5.4 (ω = 10-20), where adding pentanol means an additional amount of surfactant is available for stabilizing the reverse micelles. For this reason the pentanol was also taken into account for the correlation of the initial hydrogenation rate of DMI vs ω_T, (Figure 5.6).

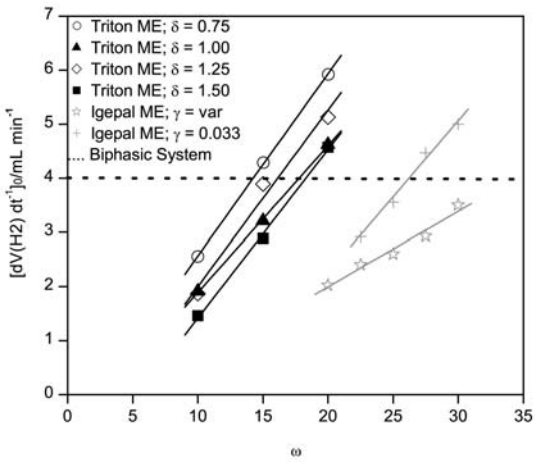

Figure 5.4 Initial hydrogenation rate of the catalytic hydrogenation of DMI (2 g in 100 ml of microemulsion) as a function of o in Triton X-100 microemulsions with different δ, and in Igepal CA-520 microemulsions with γ as a constant and as a variable, at 25 °C and 1.1 bar, using 20 mg of $[Rh(cod)Cl]_2$ and 357 mg of TPPTS

A model of the micelle is represented in the Scheme 5.4. The three domains observed in this scheme should not be well defined in our microemulsions as the polar chains of Triton X-100 and Igepal CA-520 are rather long.

The results from the partitioning study of pentanol between cyclohexane and water, cyclohexane and an aqueous solution of PEG-400, and the same oil and an aqueous solution of PEG-1000 are shown in Table 5.2, and the original data for the partitioning study of pentanol is presented in Tables B1, B2 and B3 of the Appendix B. As we observe in Table 5.2, the percentage of pentanol in the water phase increases when PEG is added and when the ethoxy chain length is increased. This

effect of PEG on the partition of pentanol in cyclohexane/water biphasic systems is a simple representation of the effect of the surfactant in our system. The tendency of the polar part of the surfactant Triton X-100 to introduce pentanol inside the core of the micelles is complex, because it is limited by the solubility of the aliphatic chain of 1-pentanol in the interfacial layer and the continuous phase of the microemulsion. For this reason and in order to simplify our pentanol partition calculations, in the following we assume those values in Table 5.2 (for PEG 400) to represent the amount of pentanol ascribed to the interfacial region, acting as a cosurfactant; the remaining part is therefore diluted in the continuous phase. As we show further in the paper, with this assumption results of micellar volume using the macroscopic scattering cross section are consistent with the micellar volume calculated using the Guinier approximation for ellipsoidal micelles. In Figure 5.6, the curves with $\delta \leq 1$ are overlapped and require higher ratios ω_T, to achieve similar initial hydrogenation rates to the curves with $\delta > 1$, which also are overlapped. By adding less amount of surfactant and controlling the water percentage similar initial hydrogenation rates can be achieved. The two groups of overlapped curves show two different patterns, which could be explained by the size and the geometry of the micelles. The extrapolation of the four curves reach the same point of zero initial hydrogenation rate ($[dV(H_2)\cdot dt^{-1}]_o$ = 0 $mL_{H2}\cdot min^{-1}$) at a ω_T of 1.5. This result was experimentally confirmed by hydrogenations using the four systems with the different δ, which exhibit zero activity.

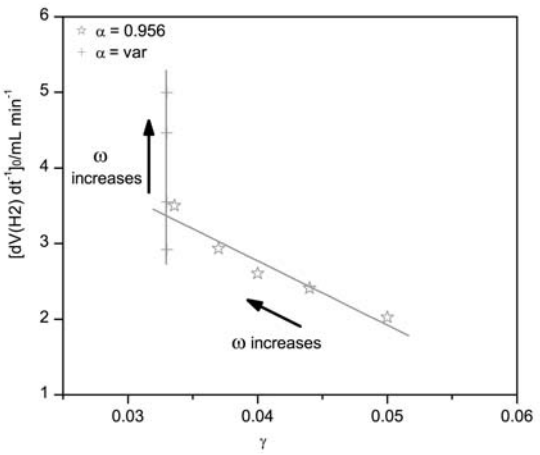

Figure 5.5 Initial hydrogenation rate of the catalytic hydrogenation of DMI (2 g in 100 ml of microemulsion) as a function of g in Igepal CA-520 microemulsions with a as a constant and as a variable, at 25 °C and 1.1 bar, using 20 mg of $[Rh(cod)Cl]_2$ and 357 mg of TPPTS

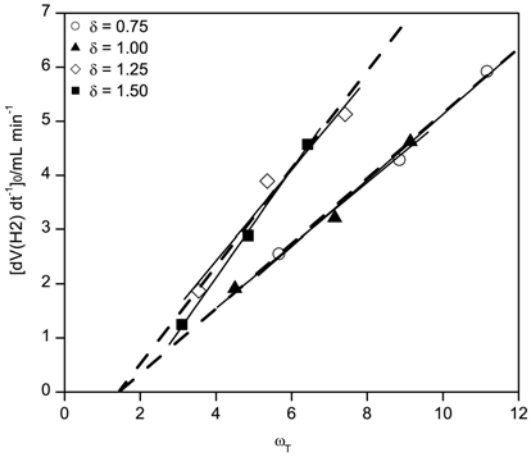

Figure 5.6 Initial hydrogenation rate of the catalytic hydrogenation of DMI (2 g in 100 ml of microemulsion) as a function of ω_T in Triton X-100 microemulsions with different δ, at 25 °C and 1.1 bar, using 20 mg of $[Rh(cod)Cl]_2$ and 357 mg of TPPTS

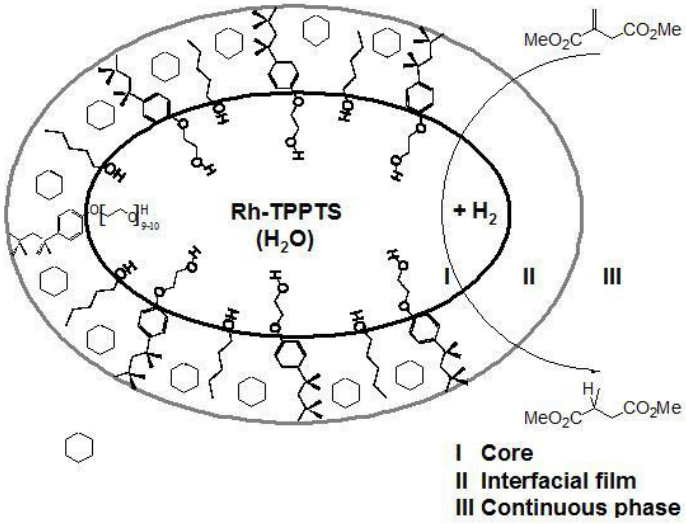

Scheme 5.4 Ellipsoidal micelle model

5.3.3 Igepal CA-520 micelles - structural characterization

DLS measurements of the Igepal CA-520 microemulsions of compositions reported in Table 5.1 could be performed successfully for γ down to 3.36 %. With γ = 3.30 % results were poorly reproducible, and as one observes on the Table 5.3 (*ME 18-21*), the measured radii of the micelles fluctuates without any significant pattern. This behaviour could be explained by the closeness to the cloud point of the system and for this reason they are not taken into account in the following discussion. For higher values of γ the microemulsions are relatively monodisperse. A linear dependence of

the initial hydrogenation rate to the hydrodynamic radius of the micelles was obtained, which can be represented by the following equation of a line:

$$\left[\frac{dV\left(H_2\right)}{dt}\right]_0 = 1.07 + 24.27 \cdot r \qquad \text{(eq 5.8)}$$

where $[dV(H_2)\ dt^{-1}]_0$ is the initial hydrogenation rate in mL min^{-1} and r is the hydrodynamic radius in nm.

Table 5.2 Cosurfactant partitioning: molar percentage (%) of 1-pentanol concentrated in the aqueous phase of a biphasic system PEG400/cyclohexane/water at 25°C, using the compositions from Table 5.1 for Triton X-100 microemulsions with PEG 400 instead of Triton X-100

Sample	$C_5H_{12}O_{without\ PEG}$ [a] (%)	$C_5H_{12}O_{PEG\text{-}400}$ [a] (%)	$C_5H_{12}O_{PEG\text{-}1000}$ [a] (%)
ME 1	11.67	14.62	20.56
ME 2	9.49	12.65	22.85
ME 3	10.65	13.89	28.25
ME 4	13.93	16.43	27.34
ME 5	12.11	15.00	25.08
ME 6	13.39	16.65	27.79
ME 7	14.87	18.75	21.42
ME 8	17.09	19.63	21.10
ME 9	15.25	19.77	29.09
ME 10	18.45	19.42	24.94
ME 11	18.40	19.04	21.76
ME 12	16.49	20.27	30.01

[a] Concentration of pentanol in the aqueous phase.

As observed in Table 5.3, the obtained radii are significantly larger than the length of the fully extended Igepal CA-520 molecule containing 14 C-C bonds, 11 C-O bonds, a benzene ring, and an O-H bond. The radii larger than 12 nm, hence this could mean that a water pool is formed. Another possible explanation is that, because DLS measurements have no means of determining geometrical deformations and it only allows for the determination of an effective hydrodynamic radius, the micelles could be elongated. By doubling the radius from 12 to 24 nm the initial hydrogenation rate of DMI almost doubles as well: from 2 to 3.5 mL_{H2} min^{-1}. Investigations of AOT microemulsions have shown that the properties of the water are modified as the water content in the microemulsion varies, reaching properties similar to bulk water for high values of ω in the microemulsions **[5.22]**. We found earlier that the initial hydrogenation rate of DMI in a biphasic system cyclohexane/water, in which the water properties are those of bulk water, is

approximately 4 mL_{H2} min^{-1} **[5.5]**. Plots of the autocorrelation functions $g^2(\tau)$ are available as Appendix B (Figure B1 & B2).

Table 5.3 Radii of the Triton X-100 micelles, volume of the micelles (V_{Sph}) calculated with the Guinier approximation for homogeneous spheres and (V_{Ellip}) for homogeneous ellipsoids using SANS scattering measurements of the Triton X-100 microemulsions, absolute intensity (I0), volume of the Triton X-100 micelles (V_{I0}) calculated with the coherent macroscopic scattering cross section assuming all the cosurfactant is concentrated in the continuous phase, and radii of the Igepal CA-520 micelles estimated from DLS measurements of the Igepal CA-520 microemulsions at 25 °C

Sample	r_{Rg}/nm	V_{Sph}/nm^3	V_{Ellip}/nm^3	$I0$/cm^{-1}	V_{I0}/nm^3
ME 1	14.4	12588.94	2670.19	138.61	2046.17
ME 2	7.0	1429.35	947.79	37.13	461.91
ME 3	4.3	332.39	323.63	18.42	191.24
ME 4	9.2	3216.55	1437.86	55.10	952.51
ME 4 [a]	13.0	-	-	-	-
ME 4 [b]	7.1	-	-	-	-
ME 5	6.5	1152.32	817.48	28.97	412.88
ME 6	4.2	306.02	289.13	15.15	177.14
ME 7	8.2	2332.92	1035.23	43.25	884.29
ME 8	6.5	1125.36	767.15	25.23	411.91
ME 9	3.5	183.01	170.00	9.45	124.41
ME 10	7.2	1575.70	752.19	34.60	823.00
ME 11	5.7	754.56	588.35	21.76	408.25
ME 12	4.5	383.53	282.86	11.38	168.28
ME 13 [c]	23.5	-	-	-	-
ME 14 [c]	19.0	-	-	-	-
ME 15 [c]	16.3	-	-	-	-
ME 16 [c]	14.3	-	-	-	-
ME 17 [c]	12.0	-	-	-	-
ME 18 [c]	18.9	-	-	-	-
ME 19 [c]	35.5	-	-	-	-
ME 20 [c]	43.0	-	-	-	-
ME 21 [c]	38.9	-	-	-	-

[a] *ME 4 with D_2O and cyclohexane-d_{12}, 0.8 mmol·L^{-1}_{Rh}. using a P/Rh of 7.5.*
[b] *ME 4 with D_2O.*
[c] *Radii were measured using DLS.*

5.3.4 Triton X-100 micelles – structural characterization

As well as for the Igepal CA-520 systems, our first aim for the Triton X-100 systems was to find out if the size of the micelles could be easily correlated to the initial hydrogenation rate of DMI. The SANS measurements were analysed using the Guinier approximation, which generally gives estimates which are accurate to within 5-10% if the analysis is performed using data collected within the range where $qRg \approx 1$, and provided that the particles studied are still so dilute that their interaction can be neglected **[5.13]**.

5.3.4.1 Scattering curves of Triton X-100 microemulsions

Figure 5.7 presents SANS scattering curves for four Triton microemulsions with ω = 20 and different amounts δ of pentanol contained. All the curves show the existence of noninteractive particle systems and by comparing them one could suggest that the change of maximum height that increases with decreasing δ, points to the increasing micellar size. The points of the scattering curves within the marked *q* range were used for the Guinier approximation.

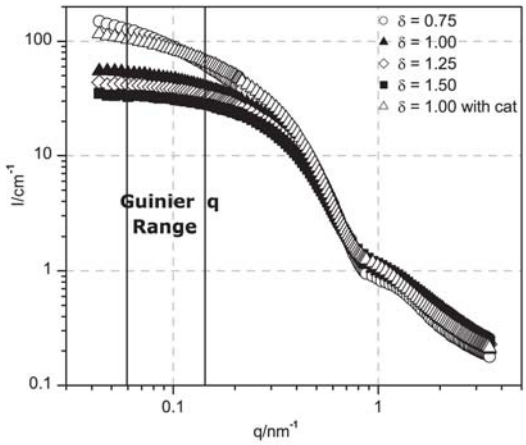

Figure 5.7 SANS spectra of Triton X-100 microemulsions with ω = 20 and different δ, and influence of the water-soluble catalyst complex Rh-TPPTS on the spectra

5.3.4.2 Guinier approximation

Linear regressions on Guinier plots (ln(*I*) *vs.* q^2) of the SANS data give access to the radius of the micelle, as shown on Figure 5.8. The radius of gyration of the micelle was extracted from the eq 5.2 and it is equal to $\sqrt{3m}$, where m is the slope of the curve. The radius of the corresponding homogeneous sphere was obtained by using the eq 5.3. Figure 5.9 summarizes the resulting radii for all the Triton X-100 microemulsions shown in the Table 5.1. In this case the continuous and the internal phase were deuterated, so the sizes determined are the overall radii of gyration of the micelles. The four systems show tendencies which surpass the initial hydrogenation rates obtained with the biphasic system (4 mL_{H2} min^{-1}) **[5.5]**.

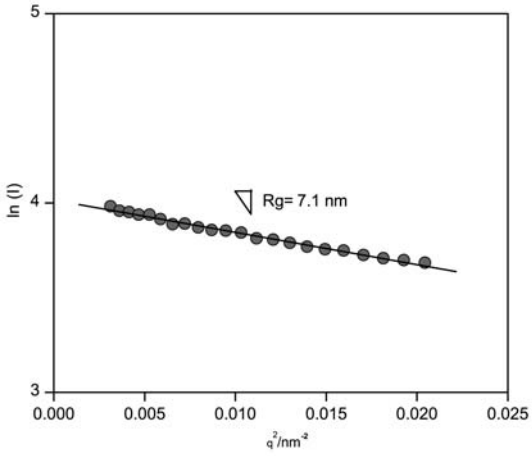

Figure 5.8 Guinier plot of ln(I) vs. q^2 for the Triton X-100 microemulsion constituted by 4.17 g of water, 62.63 g of cyclohexane, 7.43 g of Triton X-100 and 7.43 g of 1-pentanol (ME 4 in Table 5.1), and corresponding fit

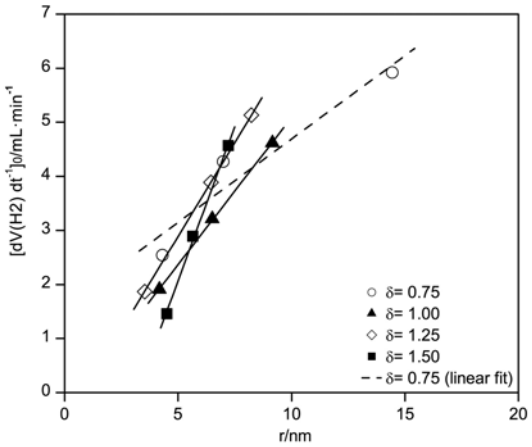

Figure 5.9 Initial hydrogenation rate of the catalytic hydrogenation of DMI (2 g in 100 ml of microemulsion) as a function of the micelle radius of the homogeneous spheres (determined by Guinier approximation of the SANS spectra) in Triton X-100 microemulsions with different δ, at 25 °C and 1.1 bar, using 20 mg of $[Rh(cod)Cl]_2$ and 357 mg of TPPTS

When comparing the four systems with the same ω, the gyration radii of the micelles with different δ have similar tendencies. Only one system (*ME 1* with ω = 20, δ = 0.75) stands out of the standard behaviour, with smaller amount of pentanol but larger amount of deuterium oxide. The comparison of the scattering curves for the four systems with ω = 20, displayed in Figure 5.7, gives a hint. By comparing the scattering curves of the four systems with ω = 20, it is possible to identify the difference of this system, which shows a distinguishable characteristic curve for

ellipsoidal micelles **[5.23]**, in which a smoother decrease of the intensity at mid *q* is observed. This could be caused by the penetration of solvent (cyclohexane or pentanol), originating a Gaussian distribution around the mean value of the radius **[5.24]**. This penetration of solvent is represented in Scheme 5.4 by molecules of cyclohexane in the interface of the micelle.

In order to obtain a preliminary study of the shape of the micelles which could serve as a first step for a deeper analysis of the micelles using specific models, the ratio V_{Sph}/V_{I0} was calculated. The volume of the spherical micelles (V_{Sph}) was calculated with the Guinier approximation and V_{I0} was estimated with the coherent macroscopic scattering cross section (see Tables B4 and B5 in Appendix B). The amount of pentanol inside the micelles increases the contrast and the volume fraction, which decreases the calculated volume of the micelles. For this reason and following the simplifications discussed from the resulting pentanol partitioning study, we assume no pentanol to be introduced inside the core of the micelles. With this assumption the two volumes are more similar. The results are shown in Table 5.3. As Figure 5.10a shows, the volume of the spherical micelles is similar to V_{I0} when ω is smaller. We also calculated the ratio V_{Ellip}/V_{I0}. The volume of the ellipsoidal micelles (V_{Ellip}) was calculated using the following equations for Guinier approximations:

$$Rg^2_{Ellip} = \frac{1}{5}\left(2a^2 + b^2\right) \qquad V_{Ellip} = \frac{4}{3}a^2 b \qquad \text{(eq 5.9)}$$

where *a* and *b* are the short and long cross section of the ellipsoidal micelle.

Guinier approximations are generally used at low *q* to obtain an estimation of the radius of particles. Generally, the decay of the intensity at mid *q* for spherical particles is steeper than the one for ellipsoidal particles. This is because at mid *q* the shorter cross section of the ellipsoidal particles can be looked at. For this reason, a Guinier approximation at mid *q* for ellipsoidal particles allows for an estimation of the smaller radius and it was used to determine *a*. With the eq 5.9, *b* and V_{Ellip} were obtained.

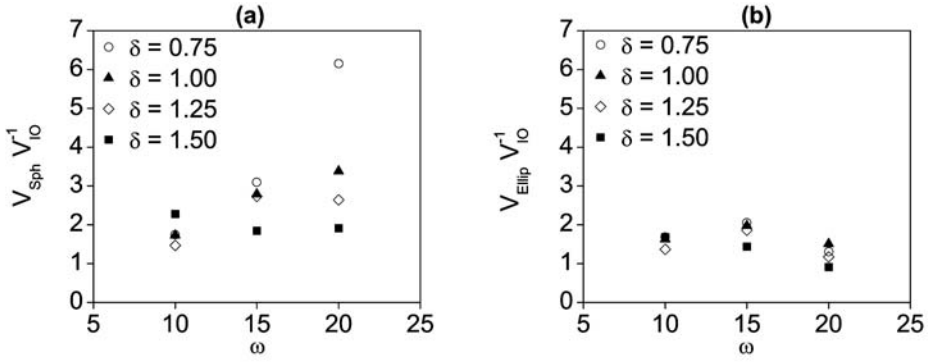

Figure 5.10 Volume ratios of the Triton X-100 micelles with different δ, calculated with Guinier approximation as a function of ω assuming the micelles are: (a) spheres and (b) ellipsoids

As seen in Figure 5.10b complemented with Table B6 of the Appendix B, the volume of the ellipsoidal micelles is similar to V_{IO} when ω is higher so both diagrams in Figure 5.10 corroborate the tendency to form ellipsoids with higher amounts of water. The ellipticity was also calculated, it is the ratio between *b* and *a*. Figure 5.11 shows a very small influence of the cosurfactant on the ellipticity of the micelles. A large ellipticity is observed with small amount of pentanol (δ = 0.75) and large amount of water (ω = 20), which reinforces the idea of solvent penetration.

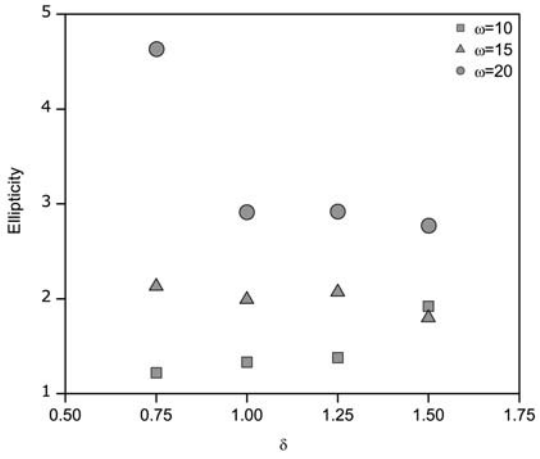

Figure 5.11 Ellipticity of the Triton X-100 micelles as a function of δ

5.3.4.3 Interface

As Table 5.3 shows, the radius obtained for the microemulsion *ME 4* with deuterated core (deuterium oxide) calculated using the slope of the Guinier approximation for this sample, is 7.1 nm. By comparing it to the 9.2 nm radius obtained for the same

microemulsion *ME 4* with deuterated core and cyclohexane-d_{12} as continuous phase, an acceptable interfacial surfactant layer of 2.1 nm thickness is estimated **[5.6]**. Dennis et al. calculated the fully extended length of the octylphenyl group using Corey-Pauling-Koltung models. They obtained a length smaller than 1 nm, so they assumed it to be 1 nm. They also calculated the length of the ethoxy chain, assuming it forms a random coil obtaining a length of 1.6 nm. Adding both parts, results are not so far from ours. The differences can be explained by the solvent penetration, which solvates the aliphatic chain of the surfactant. Because the interface and the continuous phase are diffuse, a defined boundary between interface and continuous phase is difficult to detect.

5.3.4.4 Conductivity of Triton X-100 microemulsions

The difference in geometry was also identified with the conductivity. The conductivity of a microemulsion is influenced by the microstructures of the micelles **[5.25]**. Oil-in-water microemulsions have similar conductivities as bulk water, and in water-in-oil microemulsions, the conductive polar phase is isolated by a continuous oil phase, therefore leading to small conductivities. Bicontinuous microemulsions show high conductivities, which decrease when the water content is lowered **[5.26]**. Water-in-oil microemulsions with small water contents show conductivities which decrease with the decrease of the surfactant concentration **[5.27]**. Independently of what the SANS measurements show, the presence of a maximum conductivity peak of 0.9 μS cm^{-1} on the Figure 5.12 when keeping ω = 20 and changing the pentanol to Triton X-100 ratio (δ), identifies the existence of a different geometry of the microstructure, which could be reaching out, interacting with each other and creating some continuity. The maximum peak is obtained at δ = 0.70. This is in agreement with the SANS data (Figure 5.7) which indicate the presence of elongated micelles at δ = 0.75 and elongated reverse micelles are expected to exhibit a higher conductivity compared to spherical micelles.

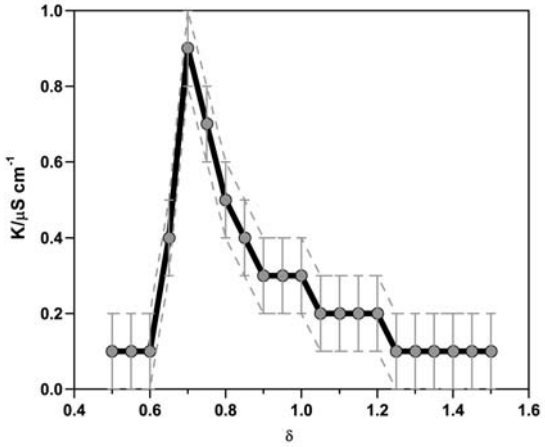

Figure 5.12 Conductivity of 10 % Triton X-100 microemulsions as a function of δ keeping ω = 20 at 25 °C

5.3.4.5 Effect of the catalyst incorporation

When adding the water soluble catalyst complex (Rh-TPPTS) to the microemulsion *ME 4*, the SANS spectrum shows a different size and in similarity to the microemulsion *ME 1*, a steeper decay as *ME 4* at low q is observed (but not so pronounced as observed in Figure 5.7 for *ME 1*). The radius of the catalyst containing micelles (C_{Rh} = 0.8 mmol L^{-1}) determined by Guinier approximation of the SANS spectra is 13.0 nm, which represents almost one and a half times the size of the empty micelles (r = 9.2 nm). This non-proportionate growth of the micelles is an indicator of the deformation of the micelles. The slight elongation of the micelles could be a result of the competition between the polar ethoxylated groups of the Triton X-100 molecules and the water soluble catalyst complex Rh-TPPTS for the water molecules. Other important effects could be: the incorporation of the amphiphilic TPPTS into the interface or the interaction between the trivalent anion TPPTS and the ethoxy head groups. This effect should be stronger when δ is smaller: the 1-pentanol molecules distribute between the interfacial layers where they substitute Triton molecules and the oil rich bulk phase, thereby making the amphiphilic layers effectively more lipophilic, and in turn less interactive with the water molecules **[5.28]**. This behaviour could be the reason of the different tendencies shown in Figure 5.5. A detailed study of the effect of the water soluble catalyst complex on the Triton X-100 reverse micelles is a topic currently under research in our laboratory.

5.4 References

[5.1] Oehme, G., *Micellar systems*, in *Aqueous-Phase Organometallic Catalysis*, B. Cornils and W.A. Herrmann, Editors. 2004, Wiley-VCH: Weinheim. p. 256-271; Langevin, D., *Annu. Rev. Phys. Chem.,* **1992,** *43*, 341-369.

[5.2] Sjöblom, J. and S.E. Friberg, *The Future of Microemulsions*, in *Handbook of Microemulsion Science and Technology*, P. Kumar and K.L. Mittal, Editors. 1999, Marcel Dekker, Inc.: New York. p. 833-842.

[5.3] Schwuger, M.J., K. Stickdorn, and R. Schomäcker, *Chem. Rev.,* **1995,** *95*, (4), 849-864.

[5.4] Dwars, T., E. Paetzold, and G. Oehme, *Angew. Chem. Int. Ed.,* **2005,** *44*, (44), 7174-7199.

[5.5] Milano-Brusco, J.S., M. Schwarze, M. Djennad, H. Nowothnick, and R. Schomäcker, *Ind. Eng. Chem. Res.,* **2008,** *47*, (20), 7586-7592.

[5.6] Robson, R.J. and E.A. Dennis, *J. Phys. Chem.,* **1977,** *81*, (11), 1075-1078.

[5.7] Andrade, S.M. and S.M.B. Costa, *Photochem. Photobiol. Sci.,* **2002,** *1*, (7), 500-506.

[5.8] Wormuth, K., O. Lade, M. Lade, and R. Schomäcker, *Microemulsions*, in *Handbook of Applied Surface and Colloid Chemistry*, K. Holmberg, Editor. 2001, John Wiley & Sons. p. 605-627.

[5.9] Zhu, D.M., K.I. Feng, and Z.A. Schelly, *J. Phys. Chem.,* **1992,** *96*, (5), 2382-2385.

[5.10] Zhu, D.M., X. Wu, and Z.A. Schelly, *Langmuir,* **1992,** *8*, (6), 1538-1540.

[5.11] Dvolaitzky, M., et al., *J. Chem. Phys.,* **1978,** *69*, (7), 3279-3288.

[5.12] Chen, S.H., *Annu. Rev. Phys. Chem.,* **1986,** *37*, 351-399.

[5.13] Freeman, K.S., N.C.B. Tan, S.F. Trevino, S. Kline, L.B. McGown, and D.J. Kiserow, *Langmuir,* **2001,** *17*, (13), 3912-3916.

[5.14] Oberdisse, J., O. Regev, and G. Porte, *J. Phys. Chem. B,* **1998,** *102*, (7), 1102-1108; Verma, G., V.K. Aswal, S.K. Kulshreshtha, P.A. Hassan, and E.W. Kaler, *Langmuir,* **2008,** *24*, (3), 683-687.

[5.15] Caponetti, E., A. Lizzio, R. Triolo, W.L. Griffith, and J.S. Johnson, *Langmuir,* **1992,** *8*, (6), 1554-1562; Garcia-Rio, L. and P. Hervella, *Chem. Eur. J.,* **2006,** *12*, (32), 8284-8295.

[5.16] Provencher, S.W., *Comput. Phys. Commun.,* **1982,** *27*, (3), 213-227.

[5.17] Hammouda, B., *PROBING NANOSCALE STRUCTURES – THE SANS TOOLBOX (http://www.ncnr.nist.gov/staff/hammouda/the_SANS_toolbox.pdf)*.

[5.18] Gradzielski, M., D. Langevin, and B. Farago, *Phys. Rev. E: Stat. Phys., Plasmas, Fluids,* **1996,** *53*, (4), 3900-3919.

[5.19] Kahlweit, M. and R. Strey, *Angew. Chem. Int. Ed.,* **1985,** *24*, (8), 654-668.

[5.20] Schubert, K.V. and E.W. Kaler, *Ber. Bunsen. Ges. Phys. Chem.,* **1996,** *100*, (3), 190-205; Lade, M., H. Mays, J. Schmidt, R. Willumeit, and R. Schomacker, *Colloids Surf., A,* **2000,** *163*, (1), 3-15.

[5.21] Moulik, S.P. and B.K. Paul, *Adv. Colloid Interface Sci.,* **1998,** *78*, (2), 99-195.

[5.22] Garcia-Rio, L., J.C. Mejuto, and M. Perez-Lorenzo, *New J. Chem.,* **2004,** *28*, (8), 988-995; Jain, T.K., M. Varshney, and A. Maitra, *J. Phys. Chem.,* **1989,** *93*, (21), 7409-7416.

[5.23] Glatter, O., *The Inverse Scattering Problem in Small-Angle Scattering*, in *Neutrons, X-rays and Light: Scattering Methods Applied to Soft Matter*, P. Lindner and T. Zemb, Editors. 2002, Elsevier Science B.V.: Amsterdam. p. 73-103; Moitzi, C., N. Freiberger, and O. Glatter, *J. Phys. Chem. B,* **2005,** *109*, (33), 16161-16168.

[5.24] Strey, R., *Colloid. Polym. Sci.,* **1994,** *272*, (8), 1005-1019.

[5.25] Jonströmer, M., B. Jönsson, and B. Lindman, *J. Phys. Chem.,* **1991,** *95*, (8), 3293-3300.

[5.26] Cabaleiro-Lago, C., L. Garcia-Rio, and P. Hervella, *Langmuir,* **2007,** *23*, (19), 9586-9595.

[5.27] Eicke, H.F. and J.C. Shepherd, *Helv. Chim. Acta,* **1974,** *57*, (7), 1951-1963.

[5.28] Kahlweit, M., *J. Phys. Chem.,* **1995,** *99*, (4), 1281-1284; Luo, Z.H., X.L. Zhan, and P.Y. Yu, *Chin. Chem. Lett.,* **2004,** *15*, (9), 1101-1104.

6 Product Isolation and Catalyst Recycling in the Catalytic Hydrogenation of Dimethyl Itaconate using Surfactants

6.1 Introduction

Since decades catalyst recycling in homogeneous catalysis has been one of the most important research topics. Many ideas have been developed in order to overcome the economic problem underlying the expensive prices of the metals that constitute the catalyst, and the even higher costs and environmental problems that have arisen from the catalyst–product processing **[6.1]**: recycling and reusing the catalyst is the most evident solution. Most of these ideas focus on the introduction of an intermediate new phase in the reaction system to immobilize the catalyst, i.e. rhodium catalyst precursors have been anchored on Phosphotungstic acid (PTA) modified alumina and used in enantio- and chemoselective hydrogenation reactions **[6.2]**, and supercritical CO_2 ($scCO_2$) has been used as solvent in hydrogenation reactions catalyzed by such rhodium–PTA–alumina complexes **[6.3]**. Dendrimers as soluble support materials have been shown to overcome the limitations encountered with the use of non–soluble inorganic supports like silica or alumina (mass transport limitation and metal leaching). The tuneable and defined structure of the dendrimers allows for well known architecture of the molecules, and in consequence the number of catalyst attached to the support can be regulated. An important feature of some dendrimers is the solvent–dependent swelling properties of some organic polymer supports, which can have an important influence on the catalytic performance **[6.4]**. Addition of scCO2 to a completed catalytic hydrogenation reaction using ionic liquids (ILs) as reaction media, allows for a very effective isolation process of the product **[6.5]**. Biphasic systems with water soluble catalysts constitutes one of the first approaches in trying to solve the problem of catalyst–product separation **[6.6]**. They have been considered economically viable as solvents for catalytic reactions and in 1984 Ruhrchemie/Rhône-Poulenc (RCH/RP) launched the first 100 000 tons per year plant in Oberhausen (Germany). This plant operates with a water–soluble rhodium complex in a biphasic system **[6.7]**. As shown before in chapter 4, the partitioning behaviour of the substrate between the phases in such systems is crucial for more hydrophobic substrates **[6.8]**. Biphasic systems using ILs with water soluble catalysts have also been studied with important results **[6.9]**. Use of surfactants is an option

among many already mentioned that deals with incompatibility problems between reagents and their partitioning between phases **[6.8, 6.10]**. Micellar systems have been used as solvents for a relatively large number of reactions which include: hydrogenation of amino acid precursors, oxidation of cyclohexene **[6.11]**, hydroformylation of olefins **[6.12]**, C-C coupling reactions **[6.13]**, and others. Because the smaller capacity of micellar systems for dissolving hydrophobic substrates, micellar systems are of limited value for applications as reaction media **[6.10]**. Microemulsions have also been used as reaction media. Their microdomains constituted by aqueous core, interface and continuous organic phase allow for the polar and nonpolar, organic and inorganic substrates to be dissolved and distributed. It is well understood that the effect of micelles on the acceleration of reactions is due to the reactant compartmentalization and accumulation. Additionally, water in the core of reverse micelles using ionic surfactants experience deviating electrophilic and nucleophilic properties in comparison to free “bulk water” because of hydrogen bonds between the head groups of the surfactant and the counterion. For this reason an accelerating effect for hydrolysis reactions is observed when the size of the micelles decreases **[6.14]**. In general, by using microemulsions as reaction media for catalytic reactions, catalyst recycling can be achieved by temperature induced separation of the microemulsion, but as a consequence of the high amount of surfactant in such systems (> 15 wt %), the total separation time is normally extremely long **[6.15]**. By using smaller amounts of surfactant (3-5%), three phase systems are obtained with non-ionic surfactants and ionic surfactants, and in both cases the duration of complete separation is shorter. A three phase system is a thermodynamic equilibrium state in which a microemulsion coexists with excess water and oil phases. The microemulsion is observed as the middle phase and it is characterized on a microscopic scale by presenting three dimensional simply connected surfaces or *“saddle-like”* structures where the midplane of the surfactant film has an average zero mean curvature **[6.16]**.

This chapter deals with the use of microemulsion systems in the catalytic hydrogenation of DMI, using the water soluble catalyst complex Rh–TPPTS, in order to achieve separation of the product and recycling and reusing the catalyst. Different surfactants were used in solutions composed of the same amounts of water and cyclohexane. The surfactants used were the non-ionic surfactant Triton X-100, the ionic surfactant AOT, and the narrow range non-ionic surfactant Lutensol XA 50.

6.2 Experimental

6.2.1 Chemicals

The organic solvent used for the microemulsion systems was cyclohexane (≥ 99.5 %), it was purchased from Roth and it was degassed and purged under nitrogen and used without further purification. The catalyst was prepared from the water–soluble ligand TPPTS (30.7 wt% in water) which was received from Celanese, and the catalyst precursor $[Rh(cod)Cl]_2$ (98 %) from Strem, the chemical formula for both of these substances are shown in Scheme 6.1.

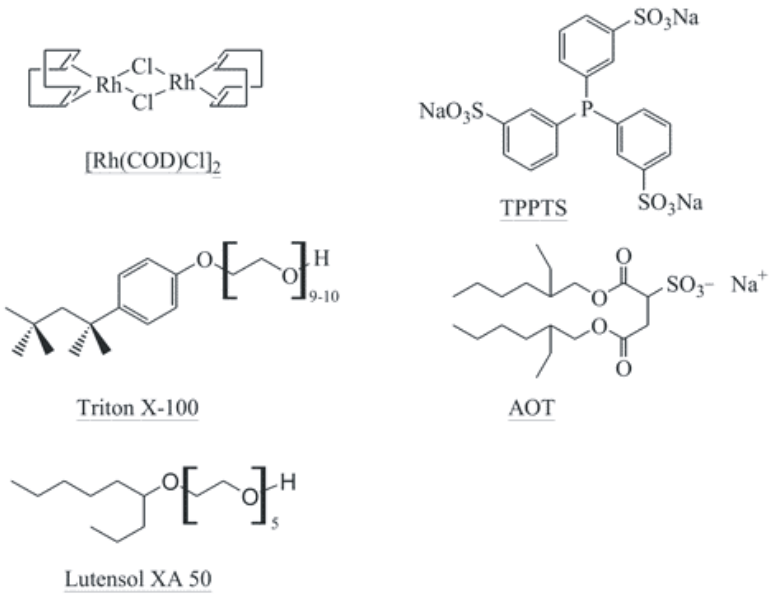

Scheme 6.1 Chemical formula of the Rhodium catalyst precursor, water soluble ligand and the surfactants used in this investigation

The catalyst complex was prepared following the procedure described in chapter 4. The surfactants (*p-tert*-Octylphenoxy) polyethoxyethanol “Triton X-100” (100 %) and dioctyl sulfosuccinate sodium salt “AOT” (98 %) which chemical formula are also shown in Scheme 6.1 were purchased from Sigma–Aldrich and were used as received to prepare the micromulsions. 1-Pentanol (≥ 99 %) was purchased from Merck and used as cosurfactant to stabilize the Triton X-100 microemulsion systems. The narrow range non-ionic surfactant “Lutensol XA 50” (100 %) was received from BASF. The substrate dimethyl itaconate (DMI) was purchased from Fluka (≥ 97%) and used as received.

6.2.2 Phase diagram and reactions

Different microemulsion systems were prepared from water, cyclohexane and different surfactants (Triton X-100, AOT and Lutensol XA 50). Before the hydrogenation of DMI (see Scheme 6.2) was studied, the effect of substrate (DMI), the catalyst complex (Rh-TPPTS) and the product (dimethyl methylsuccinate, DMS) on the phase behaviour of the different microemulsion systems was investigated.

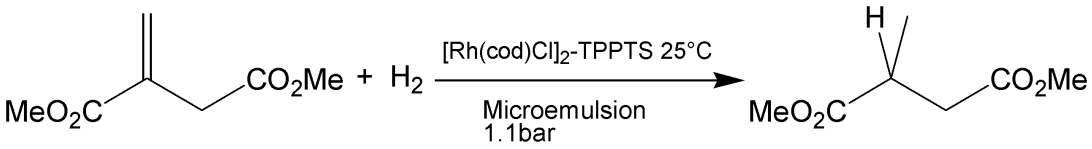

Scheme 6.2 Hydrogenation of dimethyl itaconate formal reaction

The following basic terms were used to describe the composition of the microemulsion systems:

$$\alpha = \frac{m_{\text{oil}}}{m_{\text{oil}} + m_{\text{water}}} \qquad \gamma = \frac{m_{\text{surfactant}}}{m_{\text{oil}} + m_{\text{water}} + m_{\text{surfactant}}}$$

(eq 6.1)

$$\omega = \frac{n_{\text{water}}}{n_{\text{surfactant}}} \qquad \omega_T = \frac{n_{\text{water}}}{n_{\text{surfactant}} + n_{\text{cosurfactant}}} \qquad \delta = \frac{m_{\text{cosurfactant}}}{m_{\text{surfactant}}}$$

these terms simplify when only using three component systems (without cosurfactant).

The phase behaviour study was based on the well known “fish diagram” observed in Figure 6.1, achieved by keeping α = 0.5 constant and varying the surfactant mass fraction γ and temperature.

The phase bounderies show a "fish-like" diagram, where for nonionic surfactants at low temperatures an oil–in–water (o/w) microemulsion coexists with an excess oil phase (2), this system is also denoted as a Winsor I system. At high temperatures a water–in–oil (w/o) microemulsion coexists with an excess water phase ($\bar{2}$ or Winsor II). At temperatures in between, the number of phases depends on the mass fraction of surfactant (γ) in the mixture. At very low γ, the surfactant is completely dissolved in the water and oil in form of monomers, which results in a two-phase system (γ < CMC). By increasing the surfactant mass fraction, a three phase

region is observed, where a surfactant–rich bicontinuous microemulsion phase coexists with a water and oil excess phase (3ϕ or Winsor III). By further increasing γ, the one-phase region is obtained (1ϕ) **[6.10, 6.17]**. For ionic surfactants, the Winsor I and Winsor II systems are inverted in comparison to nonionic surfactants, and the formation of Winsor III systems is normally only achieved with the addition of a cosurfactant (alcohol) and an electrolyte **[6.15, 6.18]**.

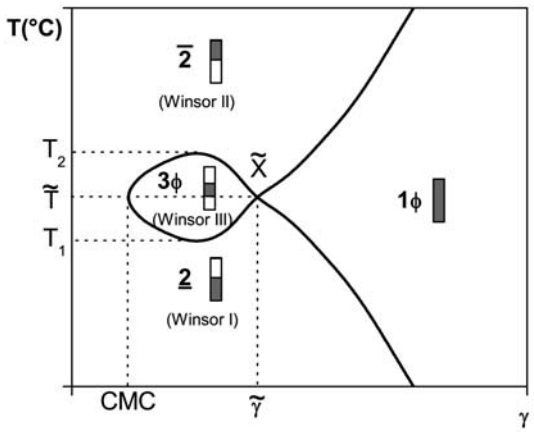

Figure 6.1 Schematic phase diagram also called “fish diagram” of equal amounts of oil and water (α = 0.5) as a function of surfactant concentration (γ) and temperature (T)

The phase behaviour studies for each concentration of surfactant were done before the catalytic hydrogenation of DMI, and both were done subsequently using the same thermostated double wall 200 mL glass reactor equipped with a gas disperser stirrer.

The microemulsion systems were prepared the day before the experiments were done using the compositions shown on the Table 6.1. First, 100 mL of a microemulsion system was filled to the reactor, after evacuating at 150 mbar and refilling with nitrogen 3 times, the phase behaviour of the system was studied after stirring at 600 rpm. The appearance of the microemulsion system at different temperatures was observed. This sequence was repeated changing temperature in 1 °C steps between 5 and 85 °C. When the system had a milky appearance, a Winsor I or Winsor II was identified; if a swirl or “marble-like” colour is observed, a Winsor III is detected; and one phase microemulsions where simply identified by their transparency.

Table 6.1 Composition of the different mixtures for the three microemulsion systems: [Triton X-100/1-pentanol]/cyclohexane/water, AOT/cyclohexane/water and Lutensol XA 50/cyclohexane/water

System	Surfactant [a]	α	γ	ω	ω_T	δ
T1	Triton X-100	0.5	0.03	580	124	0.5
T2		0.5	0.05	340	73	0.5
T3		0.5	0.07	235	50	0.5
T4		0.5	0.10	161	34	0.5
T5		0.5	0.15	102	22	0.5
A1	AOT	0.5	0.03	399	—	—
A2		0.5	0.045	262	—	—
A3		0.5	0.05	234	—	—
A4		0.5	0.07	164	—	—
A5		0.5	0.10	110	—	—
A6		0.5	0.15	70	—	—
L1	Lutensol XA 50	0.5	0.03	395	—	—
L2		0.5	0.05	232	—	—
L3		0.5	0.07	162	—	—
L4		0.5	0.10	109	—	—
L5		0.5	0.15	69	—	—

[a] *For the reactions, all the microemulsions were prepared with cyclohexane and water. For the Triton X-100 system, 1-Pentanol was used as cosurfactant.*

In order to understand the effect of the reaction constituents (substrate and catalyst) on the phase behaviour, the sequence of this study was done after injecting 5 g of DMI, and then after injecting the water soluble catalyst complex Rh–TPPTS (1.2 mL). Finally, after stirring the mixture at 400 rpm at reaction temperature for 30 min, the reaction was started following the sequence described in chapter 4.

6.2.3 Catalyst recycling experiments

The experiments for catalyst recycling were done using the surfactant systems with low concentration of surfactant (3 wt %) which allows for shorter periods of phase separation. After a batch hydrogenation is finished and the temperature induced phase separation is achieved, the oily upper phase is extracted with a peristaltic pump Ismatec ISM597A with Fluran HCA (F-5500-A) flexible tubes (d = 2.06 mm) that are resistant to cyclohexane and allow maximum flows of 15 mL·min^{-1}. While the reaction temperature is re-established, a new surfactant solution is added with the same pump, which is constituted mostly of cyclohexane. Following the injection of fresh amount of substrate, the reaction is restarted.

6.3 Results and discussion

6.3.1 Phase behaviour diagrams of the surfactant systems (*T vs.* γ)

Phase diagrams were determined for the C_6H_{12}/H_20 systems, at α = 0.5 and varying γ from 3 to 15 wt % of surfactant using in one case Triton X-100 as surfactant and 1-pentanol as cosurfactant, as shown in Figure 6.2a; and in another case the ionic surfactant AOT presented in Figure 6.2b. For the Triton X-100 system the three phase system region of the "fish-like" form reaches a maximum surfactant concentration of 8 wt %.

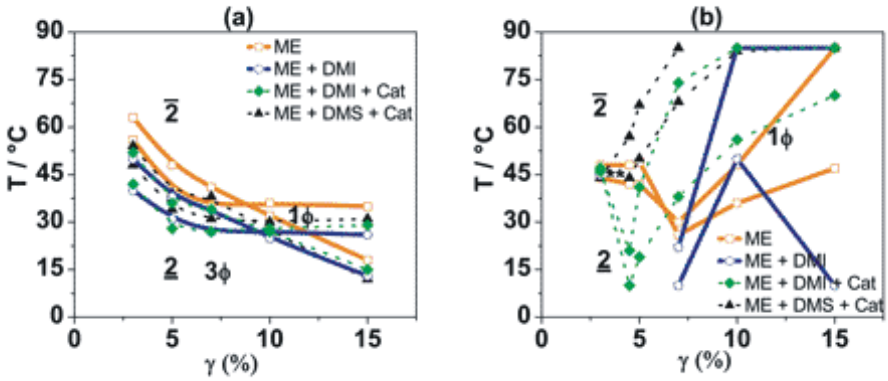

Figure 6.2 "Fish diagram" (α = 0.5) and influence of 5 g of DMI, the water soluble catalyst complex Rh–TPPTS (0.81 mmol·L^{-1} of Rh and 6.09 mmol·L^{-1} of TPPTS) and the product (5 g of DMS) on: a) the quaternary nonionic surfactant system [Triton X-100/1-pentanol]/cyclohexane/water, and b) the ternary ionic surfactant system AOT/cyclohexane/water

Because the surfactant Triton X-100 is polydisperse and also the amount of cosurfactants is large ($m_{pentanol}/m_{Triton}$ = 0.5) the fish diagram is slightly distorted generating an effective "lipophilic" shift of 2–to–3ϕ–to–$\bar{2}$ phase by increasing the Triton X-100 concentration at a constant temperature above $\tilde{T}$ **[6.18]**. As we will see further in this paper, the polydispersity of Triton X-100 plays an important role in the catalyst recycling process. The one phase microemulsion region of the Triton X-100 phase diagram is expanded to temperatures lower than $\tilde{T}$.

The ionic AOT system shows a peculiar phase behaviour between 3 and 5 wt % of surfactant. In this range of AOT concentration, with temperatures in between 42 and 49 °C, a transparent but turbid state is observed. Whereas Winsor III systems

are unlikely to be achieved with ionic surfactants without addition of at least a fourth component, the existence of one phase microemulsions with such small surfactant concentrations is unusual. For this reason this area was marked as unknown with the sign "**". Contrary to the Triton X-100 phase behaviour, the one phase region for the AOT system expands to temperatures higher than $\widetilde{T}$.

6.3.1.1 Substrate influence

As shown in chapter 4, dimethyl itaconate (DMI) in a concentration of 316.1 mmol·L^{-1} has a partition coefficient of 2 in biphasic C_6H_{12}/H_2O systems at 25 °C, but with addition of a surfactant this partition coefficient should decrease. The solubilization of a considerable amount of DMI inside the micelles affects the phase behaviour of both systems (Triton X-100 and AOT) in different ways and intensity. The changes can be attributed to one property, namely the solubility of the surfactant in water. The addition of DMI to the microemulsion systems induces a lipophilic shift of the "fish diagram", meaning that the water solubility of both surfactants decreases. So in order to reach similar solubility of Triton X-100 or AOT in both phases and to achieve the formation of microemulsions, the temperature should be adjusted in the direction where the water solubility of the surfactant increases **[6.19]**: a) to lower temperature for the Triton X-100 system, and (b) to higher temperature for the AOT system (10 wt %). A bigger lipophilic shift is observed with AOT as surfactant. This seems to have an answer in the microstructure of both systems. First, the addition of a high amount of 1-pentanol to the Triton X-100 micelles has increased well enough the lipophilicity of the micelles, so the addition of DMI has a lighter effect. Second, it has been shown that Triton X-100 micelles stabilized by a cosurfactant present a fluid interface. This can be related with a more flexible interface, which allows for the size of the micelles to increase without allowing coalescence of the water. In consequence, if we imagine micelles as balloons made of a flexible material that can be filled up by DMI, this could allow for the system to withstand additions of large amounts of the substrate. In the other hand, AOT micelles have shown interfaces with increased rigidity. Addition of large amounts of DMI, shatter the AOT micelles because of their inability of increasing their size sufficiently. This could explain the complex impact on the phase behaviour for such cases **[6.20]**. The temperatures of phase transition were not

detectable using 3 and 5 wt % of AOT as surfactant; in this case the difference between morphologies (1ϕ, 2 phases or 3ϕ) was not noticeable.

6.3.1.2 Catalyst influence

The addition of the water soluble catalyst complex Rh–TPPTS (0.81 mmol·L^{-1} of Rh and 6.09 mmol·L^{-1} of TPPTS) to Triton X-100 microemulsions has shown to influence the size of the micelles **[6.21]**. It is not quite clear if it is a result of the competition between the polar ethoxylated groups of the Triton X-100 molecules and the water soluble catalyst complex Rh–TPPTS for the water molecules. Other possible explanations could be the incorporation of the amphiphilic TPPTS into the interface or the interaction between the trivalent anion $TPPTS^{3-}$ and the ethoxy head groups. Because the ratio TPPTS/Rh is 7.5, an important excess of TPPTS is present in the systems. As we observe in the Figure 6.2, both systems show a shift of the phase boundaries to higher temperatures. Using Triton X-100 the shift is just perceptible but the AOT system shows a higher sensitivity to the catalyst, which could be an indication of the ionic interaction between TPPTS and the anionic head of the AOT molecules.

6.3.1.3 Product influence

The influence of the product causes again a shift of the phase boundaries to elevated temperatures in the Triton X-100 system. The effect is even more pronounced in the AOT system. The product DMS has a higher partition coefficient between the phases in a biphasic system C_6H_{12}/H_2O than the substrate DMI **[6.6]**, so a step by step sequence can be idealized: (a) DMI is solubilized in the micelles with the catalyst, (b) DMI reacts to DMS when hydrogen is introduced, (c) DMS diffuses to the oily continuous phase, consequently increasing the lipophilicity of the cylohexane, which results in a shift of the phase transitions to higher temperatures. A reason for the weaker sensitivity of the Triton X-100 system to the subsequent additions can be explained by the addition of cosurfactant to nonionic microemulsions. This generally makes the interface more lipophilic, so interactions between the interface and the core of the micelles are milder. Consequently they have less impact on the phase behaviour **[6.22, 6.23]**. This phase behaviour study did not only help to understand

the complex influence of compounds involved in the reaction on the phase behaviour, it also enabled us to find conditions for the selected system used for the recycling of the catalyst.

6.3.2 Catalytic Hydrogenation of DMI in AOT Surfactant Systems

6.3.2.1 Comparison between AOT system and biphasic system (without Surfactant)

As shown already before in chapter 4, in a biphasic system (C_6H_{12}/H_2O, α = 0.5) the hydrogenation of DMI at 25 °C and 1.1 bar follows a typical zero–order reaction profile, as shown also in Figure 6.3a. The reaction rate expressed by the hydrogen consumption flux ($dV_{H2}\cdot dt^{-1}$, $mL_{H2}\cdot min^{-1}$) is almost constant until the end of the hydrogenation. Whereas in a mixture of AOT (α = 0.5, γ = 0.045) with 642.3 $mmol\cdot L^{-1}$ of DMI, the rate of the catalytic reaction increases at the beginning to a maximum flux of hydrogen consumption and then decreases until the substrate is almost completely converted, indicated by the total hydrogen uptake of the reactor in stoichiometric ratio to the substrate.

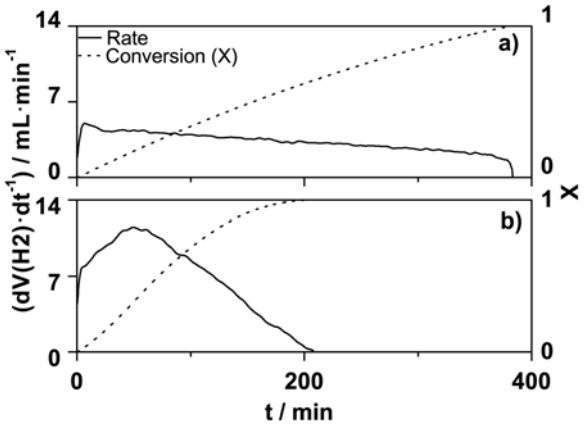

Figure 6.3 Hydrogen flux and conversion as a function of time in the hydrogenation of 10 g of DMI in 100 mL of AOT microemulsion system with the water soluble catalyst complex Rh-TPPTS (0.81 $mmol\cdot L^{-1}$ of Rh and 6.09 $mmol\cdot L^{-1}$ of TPPTS) at 25°C and 1.1 bar in (a) a biphasic cyclohexane/water system (without surfactant), and (b) AOT microemulsion system (α = 0.5, γ = 0.045)

This increase in rate of reaction can be explained by the higher solubility of DMI in the catalyst phase, which at the same time originates a shift of the phase

boundaries. During the hydrogenation of DMI to DMS the system evolves over time. The phase transitions shifts to higher temperatures, so at 25 °C the system (α = 0.5, γ = 0.045) changes from a $\underline{2}$ system, through a 1ϕ, finally to a $\bar{2}$ system, as we can notice in the Figure 6.2b.

We should mention that Figure 6.2b was elaborated using only 316 mmol·L^{-1} of DMI and this comparison (Figure 6.3) is done with double the amount of DMI (632 mmol·L^{-1}) which increases the effect of both components on the phase behaviour, the substrate and the product. This analysis is in line with the change of colour seen during the reaction.

6.3.2.2 Influence of the catalyst concentration on the DMI hydrogenation in AOT systems

Hydrogenation experiments were carried out using the same mixture used in the subsection before (α = 0.5, γ = 0.045) with two different catalyst concentrations: 0.8 mmol·L^{-1} of Rh and 1.6 mmol·L^{-1} of Rh, while maintaining the TPPTS/Rh ratio constant to 7.5. As expected, even though the system is not a homogeneous one phase system, the reaction was much faster with the higher concentration of catalyst.

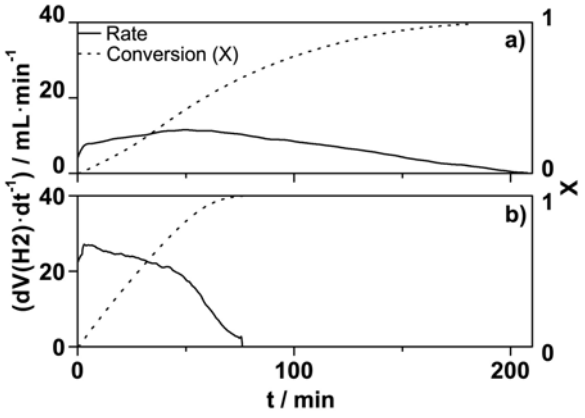

Figure 6.4 Influence of the catalyst concentration on the hydrogenation rate and conversion of the catalytic hydrogenation of 10 g of DMI in 100 mL of AOT microemulsion system (α = 0.5, γ = 0.045) at 25°C and 1.1 bar with (a) 0.81 mmol·L^{-1} of Rh and 6.09 mmol·L^{-1} of TPPTS, (b) 1.62 mmol·L^{-1} of Rh and 12.18 mmol·L^{-1} of TPPTS.

Figure 6.4 allows for a comparison of the hydrogen uptake curves of the catalytic hydrogenation of 10 g of DMI using (a) 0.8 mmol·L^{-1}of [Rh(cod)Cl]$_2$ and (b) 1.6 mmol·L^{-1} of [Rh(cod)Cl]$_2$. With the higher concentration of catalyst an initial

increase of the hydrogen consumption is not noticed, and during the hydrogenation the appearance of the mixture did not show any signs of phase transition. This could be explained by the addition of a bigger amount of catalyst which has a “salting out” effect on the ionic surfactant **[6.22]**, which should be counteracted by higher temperature, for this reason the mixture is already a $\bar{2}$ system. The problem is always the economic disadvantage of the higher amount of catalyst (40 mg in 100 mL), for this reason the recycling of the catalyst is even more important.

6.3.2.3 Influence of the surfactant concentration

The amount of surfactant added to the C_6H_{12}/H_2O solutions affects beneficially the hydrogenation rate of DMI in both cases, but the AOT system is more sensitive to the amount of surfactant, as described in Figure 6.5. Although at 45 °C both systems go through phase transitions, both show a proportional influence of surfactant concentration on the initial hydrogenation rate. The reaction rate seems to be governed by the surfactants solubility in the aqueous phase at the given temperature. As Figure 6.2 shows, at 45 °C with almost all Triton X-100 concentrations used (except 3 wt %), the system is at the beginning of each hydrogenation a $\bar{2}$ system, which allows the reverse micelles to be in a different phase than the water soluble catalyst. This is in line with the appearance of the separated system, where the typical orange colour of the catalyst is only noticed in the lower phase. So the DMI concentrated in the aqueous phase is hydrogenated, and the mixing process allows all the rest of the substrate to react, because it is exchanged between the phases. The same is true for the AOT systems, only the two mixtures with higher concentrations of surfactant (10 and 15 wt %) are $\bar{2}$ systems. When comparing the tendencies of the initial hydrogenation rate against surfactant concentration for both systems (Triton X-100 and AOT) observed in Figure 6.5, AOT has a more effective influence on the acceleration of the hydrogenation. The phenyl ring of the Triton X-100 molecule and the solubility of 1-pentanol in water could be the reasons for an inhibition effect on the catalytic hydrogenation **[6.21, 6.24]**.

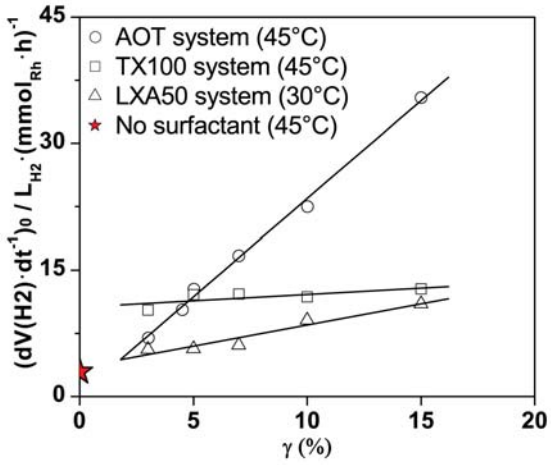

Figure 6.5 Influence of the surfactant concentration on the initial hydrogenation rate of the catalytic hydrogenation of 5 g of DMI in 100 mL of microemulsion system using 0.81 mmol·L^{-1} of Rh and 6.09 mmol·L^{-1} of TPPTS at 25°C and 1.1 bar in three microemulsion systems with the three different surfactants Triton X-100 (circles), AOT (squares), Lutensol XA 50 (triangles) and in a biphasic cyclohexane/water system without surfactant (star)

The hydrogenation was also studied in Lutensol XA 50 systems. The later surfactant does not have a phenyl ring in its molecular structure and no cosurfactant addition was needed. The slope of the initial hydrogenation rate against surfactant concentration for Lutensol XA 50 systems is slightly higher than for Triton X-100 systems, but still smaller than for AOT systems. For this reason the inhibition effects mentioned earlier in this paragraph should not be the only parameters explaining the differences between the AOT and the Triton X-100 systems. The concentration of the rhodium catalyst in the water is the same in both systems and the critical micelle concentration of Triton X-100 and AOT in cyclohexane are similar, 1 mmol·L^{-1} and 0.8-1 mmol·L^{-1} respectively **[6.25]**. As observed in Figure 6.5, by using 15 wt % of surfactant the initial hydrogenation rate is 2.8 times faster using AOT than Triton X-100 as surfactant. When comparing the appearance of both systems (Triton X-100 and AOT systems) with 15 wt % of surfactant at 45 °C and with the complete initial amount of DMI (316.1 mmol·L^{-1}), we observe that the catalyst phase (aqueous lower phase) is three times bigger with Triton X-100. Both are $\bar{2}$ systems. The catalyst phase for the AOT system represents 1/10 of the total volume, whereas the catalyst phase for the Triton X-100 represents 3/10 of the total volume. For this reason the phase where the reaction takes place has a three times higher concentration of catalyst when using AOT as surfactant. Additionally, the concentration of DMI in the

catalyst phase is similar in both systems: 244 mmol·L^{-1} for the Triton X-100 system and 327 mmol·L^{-1} for the AOT system. These two reasons explain the higher initial hydrogenation rate using 15 wt % of AOT. By extrapolating the AOT line to zero concentration, a similar initial hydrogenation rate for the biphasic system without surfactant is obtained. This is not the case for the Triton X-100 system, where the 1-pentanol concentration is not taken into account for the calculated surfactant concentration.

6.3.2.4 Rate comparison

If we compare the hydrogenation rate of DMI in a biphasic system (C_6H_{12}/H_2O, α = 0.5), with the hydrogenation in a microemulsion (Triton X-100/1-Pentanol/C_6H_{12}/H2O, α = 0.5, γ = 0.13, δ = 0.5) and in an emulsion (AOT/C_6H_{12}/H_2O, α = 0.5, γ = 0.045) as function of the concentration of the substrate, we observe that for the biphasic system the velocity is always the same at any concentration of substrate (Figure 6.6) **[6.8]**. This profile indicates different barriers for the reaction and rate limitation by mass transfer between the organic and the aqueous phase. In this case the reaction is mainly limited by solubility of the substrate in the aqueous phase.

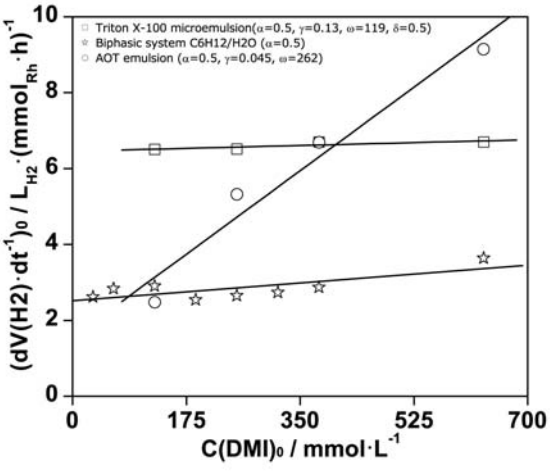

Figure 6.6 Influence of the DMI concentration on the initial hydrogenation rate of the catalytic hydrogenation in a biphasic cyclohexane/water system, and a Triton X-100 microemulsion system (Triton X-100/1-Pentanol/C_6H_{12}/H2O, α = 0.5, γ = 0.13, δ = 0.5) and in an AOT microemulsion system(AOT/C_6H_{12}/H_2O, α = 0.5, γ = 0.045) at 25°C and 1.1 bar, using 0.81 mmol·L^{-1} of Rh and 6.09 mmol·L^{-1} of TPPTS

For the hydrogenation of DMI with the water soluble catalyst complex Rh–TPPTS in microemulsions, the initial hydrogenation rate is higher than in a biphasic cyclohexane/water system. The substrate is embedded inside the micelles with the water soluble catalyst. The higher local concentration of the catalyst facilitates the contact between the substrate and the catalyst. With the Triton X-100 system, an almost unaltered initial hydrogenation rate as a function of the initial DMI concentration is observed. This is an example of the inhibition effect of the phenyl ring on the hydrogenation rate **[6.24]**. This effect is observed when using high concentration of Triton X-100 (γ = 0.13). Otherwise the dependence of the initial rate on the initial concentration of DMI in linear **[6.8]**. For the AOT emulsion, this linear dependence is observed. The initial hydrogenation rate in this system compared to the other systems (biphasic system and Triton microemulsion) shows a substantial increase of the initial hydrogenation rate at initial DMI concentrations higher than 379.4 mmol·L^{-1}.

6.3.3 Catalyst recycling

The microemulsion systems T1 and A1 shown on Table 6.1 were used as reaction media for the catalyst recycling experiments. As we observed in Figure 6.7, using T1 as medium and 5 g of DMI per run, four hydrogenation runs were obtained. During each run 5 g of DMI (316 mmol·L^{-1}) were hydrogenated and after the extraction of the upper phase of the 3ϕ system, 40 ml of a solution consisting of 95.2 wt % cyclohexane, 3.2 wt % Triton X-100 and 1.6 wt % pentanol was introduced into the reactor to fill up the 100 ml of mixture. For all the hydrogenation runs a temperature of 50 °C and 1.1 bar of hydrogen pressure were used, but as Table 6.2 shows, the temperature of the separation steps were different and increasing with the number of runs. This is an indication for a substantial change in the characteristics of the system as a consequence of the oily upper phase extraction, which contain a substantial amount of surfactant. The “salting out” effect caused by the catalyst also helps the extraction of the surfactant from the middle and lower phase to the upper phase. The appearance of our Winsor III system shows a deep orange colour in the lower phase and a light orange colour in the middle phase, but no indications for presence of catalyst in the upper phase are noticed. So by extracting the oily upper phase of our three phase system we extract a significant amount of some of the

lower ethoxilated surfactant molecules, and consequently the introduction of new surfactant with the complete original polidispersity results in a different mixture.

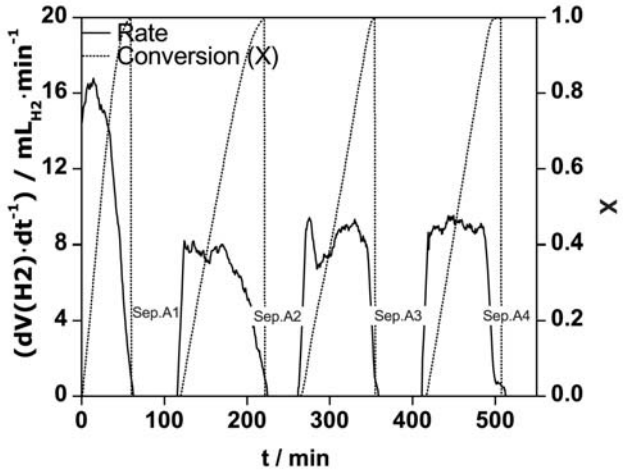

Figure 6.7 Four runs of 5 g DMI hydrogenation in the system A1 Triton X-100 three phase system (α = 0.5, γ = 0.03, δ = 0.5) with recycling of the catalyst at 50°C and 1.1 bar, using 0.81 mmol·L^{-1} of Rh and 6.09 mmol·L^{-1} of TPPTS

This change of composition of the mixture affects the hydrogenation rate as we can observe in Figure 6.7, where the last three runs are similar in initial rate but half as fast as that of the first run.

Table 6.2 Separation temperatures used for achieving the separation processes of the microemulsion systems using 0.81 mmol·L^{-1} of Rh and 6.09 mmol·L^{-1} of TPPTS under 1.1 bar of hydrogen pressure

Separation	T_{Sep} / °C	Surfactant	γ
Sep. A1	50	Triton X-100	0.03
Sep. A2	59		
Sep. A3	63		
Sep. A4	67		
Sep. B1	60	Triton X-100	0.13
Sep. B2	37		
Sep. C1	55	AOT	0.03
Sep. C2	55		
Sep. C3	55		
Sep. D1	39	Lutensol XA 50	0.03
Sep. D2	39		

We also pursued catalyst recycling using a 1ϕ system with 12.3 wt % of Triton X-100, 6.1 wt % of 1-pentanol, 40.8 wt % of cyclohexane and 40.8 wt % of water at 25 °C and 1.1 bar of hydrogen pressure. As Figure 6.8 shows: two runs of 5 g DMI hydrogenation were obtained. The temperatures of the separation steps were even more different (see Table 6.2). After concluding the first run in a 1ϕ system at least

100 min was necessary for the separation. Assuming the surfactant and cosurfactant partitions 1:1 between the phases, a solution consisting of 82.7 wt % cyclohexane, 11.5 wt % Triton X-100 and 5.8 wt % pentanol was introduced into the reactor to fill up the 100 ml of mixture.

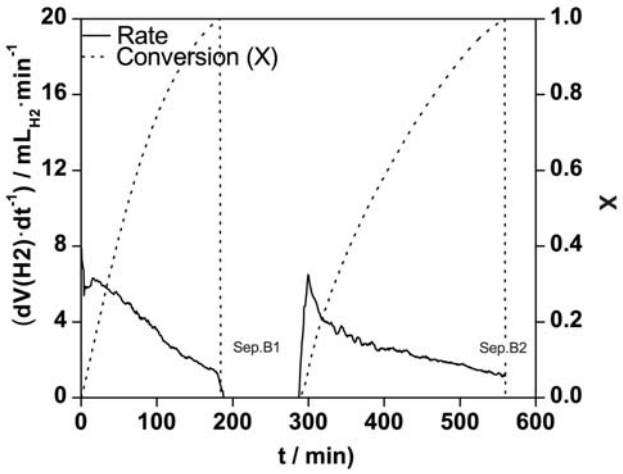

Figure 6.8 Two runs of 5 g DMI hydrogenation in the Triton X-100 microemulsion system (α = 0.5, γ = 0.13, δ = 0.5) with recycling of the catalyst at 25°C and 1.1 bar, using 0.81 mmol·L^{-1} of Rh and 6.09 mmol·L^{-1} of TPPTS

The later composition allowed for the second run to proceed with a smaller rate and the second separation was achieved at a lower temperature in a 3ϕ system, which is a result of the lower concentration of surfactant added.

Figure 6.9 shows that by using the A1 mixture as reaction medium for the hydrogenation runs, three similar hydrogenation runs of 5 g of DMI were achieved at 50 °C and 1.1 bar of hydrogen pressure. In the later only pure cyclohexane was added to fill up the 100 ml of mixture in the reactor, in contrast to the *T1* system. The initial hydrogenation rates in each run are similar, and the separation temperatures are all the same (see Table 6.2) indicating no change on the composition of the mixture.

It is important to mention that the catalyst at the end of each overall process is still not deactivated and more cycles could be achieved. Turn over numbers (TON) of 1530 for the T1 system and 1158 for the A1 system were achieved.

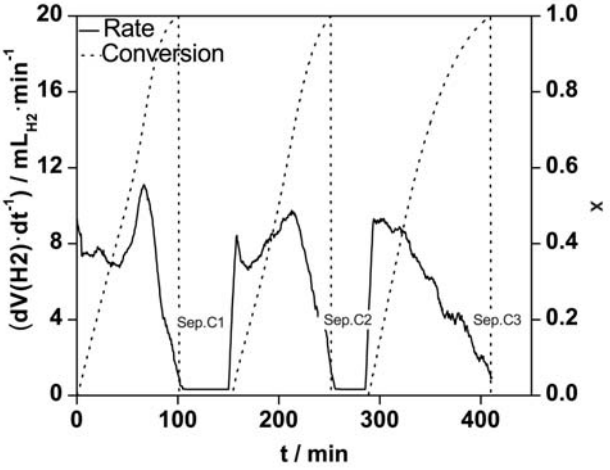

Figure 6.9 Three runs of 5 g DMI hydrogenation in the AOT microemulsion system (α = 0.5, γ = 0.03) with recycling of the catalyst at 50°C and 1.1 bar, using 0.81 mmol·L^{-1} of Rh and 6.09 mmol·L^{-1} of TPPTS

6.3.3.1 Catalyst recycling with narrow range surfactant

Another way for avoiding the problems with catalyst recycling using ethoxilated surfactants, caused by the polidispersity of the surfactant is by using a narrow range surfactant like Lutensol XA 50. As seen in Figure 6.10, the “Fish diagram” in this case is not skewed, and the effects of the substrate (DMI), the catalyst (Rh–TPPTS) and the product (DMS) are similar to that of the Triton X-100 system and as shown in Figure 6.5 by using the systems with the compositions shown in Table 6.1 as reaction medium for the catalytic hydrogenation of DMI under 30 °C and 1.1 bar of hydrogen pressure, a linear dependency of the initial hydrogenation rate on the surfactant concentration is also obtained showing a value of the intercept with the ordinate (γ = 0 wt %) that corresponds to the initial hydrogenation rate using a biphasic system (without surfactant) as solvent.

The system *L1* was used as medium for the catalyst recycling experiments with Lutensol XA 50 and as described in Figure 6.11 two cycles were achieved at 30 °C and 1.1 bar of hydrogen pressure. In this case only pure cyclohexane was added after finishing each 5 g DMI hydrogenation run and extracting the oily upper phase.

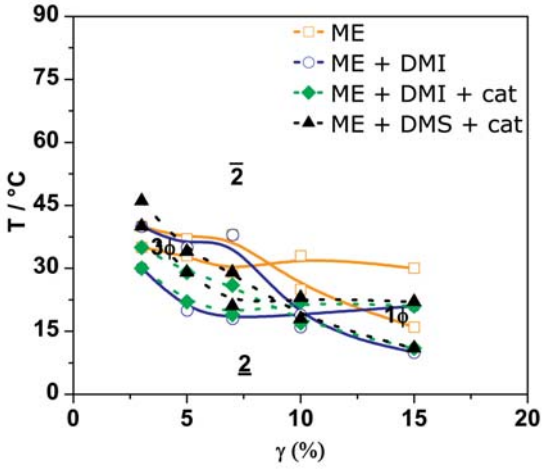

Figure 6.10 "Fish diagram" (α = 0.5) and influence of 5 g of DMI, the water soluble catalyst complex Rh–TPPTS (0.81 mmol·L^{-1} of Rh and 6.09 mmol·L^{-1} of TPPTS) and the product (5 g of DMS) on the ternary nonionic surfactant system Lutensol XA 50/cyclohexane/water

As seen in Table 6.2 the same separation temperatures were used to achieve both separation processes, corroborating the constancy of the mixtures composition during the separation process. In this particular case the differences between the runs are attributed to an unexpected deactivation of the catalyst when using Lutensol XA 50 as surfactant in the mixture, possibly caused by impurities.

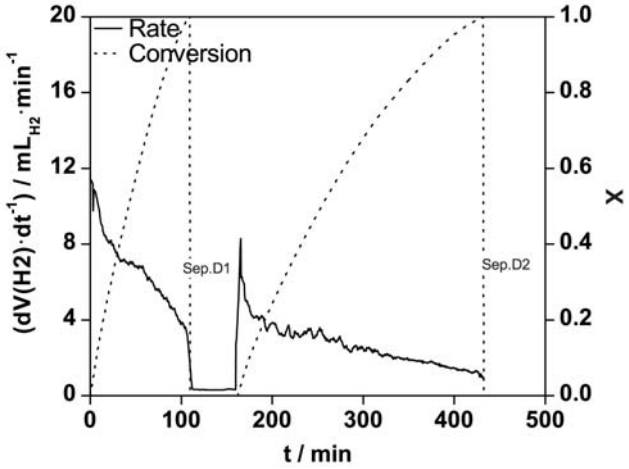

Figure 6.11 Two cycles of 5 g DMI hydrogenation in the Lutensol XA 50 microemulsion system (α = 0.5, γ = 0.03) with recycling of the catalyst at 30°C and 1.1 bar, using 0.81 mmol·L^{-1} of Rh and 6.09 mmol·L^{-1} of TPPTS

6.4 References

[6.1] Baker, R.T. and W. Tumas, *Science,* 1999, *284*, (5419), 1477-1479; Fan, Q.-H., Y.-M. Li, and A.S.C. Chan, *Chem. Rev.,* 2002, *102*, (10), 3385-3466.

[6.2] Brandts, J.A.M. and P.H. Berben, *Org. Process Res. Dev.,* 2003, *7*, (3), 393-398.

[6.3] Seki, T., J.-D. Grunwaldt, and A. Baiker, *Ind. Eng. Chem. Res.,* 2008, *47*, (14), 4561-4585.

[6.4] van Heerbeek, R., P.C.J. Kamer, P.W.N.M. van Leeuwen, and J.N.H. Reek, *Chem. Rev.,* 2002, *102*, (10), 3717-3756.

[6.5] Leitner, W., *Acc. Chem. Res.,* 2002, *35*, (9), 746-756; Liu, F.C., M.B. Abrams, R.T. Baker, and W. Tumas, *Chem. Commun.,* 2001, (5), 433-434.

[6.6] de Bellefon, C., N. Tanchoux, S. Caravieilhes, and D. Schweich, *Catal. Today,* 1999, *48*, (1-4), 211-219.

[6.7] Kuntz, E.G., *(Rhône-Poulenc Ind.). FR Patent 2.230.654, 1983; FR Patent 2.314.910, 1975; FR Patent 2.338.253, 1976; FR Patent 2.349.562, 1976; FR Patent 2.366.237, 1976; FR Patent 2.473.505, 1979; FR Patent 2.478.078, 1980; FR Patent 2.550.202, 1983; FR Patent 2.561.650, 1984.*

[6.8] Milano-Brusco, J.S., M. Schwarze, M. Djennad, H. Nowothnick, and R. Schomäcker, *Ind. Eng. Chem. Res.,* 2008, *47*, (20), 7586-7592.

[6.9] She, J., L. Ye, J. Zhu, and Y. Yuan, *Catal. Lett.,* 2007, *116*, (1-2), 70-75.

[6.10] Hager, M., F. Currie, and K. Holmberg, *Top. Curr. Chem.,* 2003, *227*, 53-74.

[6.11] Dwars, T., E. Paetzold, and G. Oehme, *Angew. Chem. Int. Ed.,* 2005, *44*, (44), 7174-7199.

[6.12] Matsui, Y. and M. Orchin, *J. Organomet. Chem.,* 1983, *244*, (4), 369-373.

[6.13] Beletskaya, I.P., *Pure Appl. Chem.,* 1997, *69*, (3), 471-476.

[6.14] Garcia-Rio, L., J.C. Mejuto, and M. Perez-Lorenzo, *New J. Chem.,* 2004, *28*, (8), 988-995.

[6.15] Nardello-Rataj, V., L. Caron, C. Borde, and J.M. Aubry, *J. Am. Chem. Soc.,* 2008, *130*, (45), 14914-14915.

[6.16] Balogh, J., H. Kaper, U. Olsson, and H. Wennerstrom, *Phys. Rev. E: Stat. Phys., Plasmas, Fluids,* 2006, *73*, (4).

[6.17] Sottmann, T., M. Lade, M. Stolz, and R. Schomacker, *Tenside Surfact. Det.,* 2002, *39*, (1), 20-28.

[6.18] Wormuth, K., O. Lade, M. Lade, and R. Schomäcker, *Microemulsions*, in *Handbook of Applied Surface and Colloid Chemistry*, K. Holmberg, Editor. 2001, John Wiley & Sons. p. 605-627.

[6.19] Kahlweit, M., R. Strey, P. Firman, D. Haase, J. Jen, and R. Schomacker, *Langmuir,* 1988, *4*, (3), 499-511; Kahlweit, M., R. Strey, R. Schomacker, and D. Haase, *Langmuir,* 1989, *5*, (2), 305-315.

[6.20] Andrade, S.M. and S.M.B. Costa, *Photochem. Photobiolo. Sci.,* 2002, *1*, (7), 500-506.

[6.21] Milano-Brusco, J.S., S. Prévost, D. Lugo, M. Gradzielski, and R. Schomäcker, *New J. Chem.,* 2009, DOI: 10.1039/b905063a.

[6.22] Kahlweit, M., *J. Phys. Chem.,* 1995, *99*, (4), 1281-1284.

[6.23] Luo, Z.H., X.L. Zhan, and P.Y. Yu, *Chin. Chem. Lett.,* 2004, *15*, (9), 1101-1104.

[6.24] Schwarze, M., J. Milano-Brusco, V. Strempel, and R. Schomäcker, *Ind. Eng. Chem. Res.*, Submitted.

[6.25] Wong, J.E., T.M. Duchscherer, G. Pietraru, and D.T. Cramb, *Langmuir,* 1999, *15*, (19), 6181-6186; Krishnakumar, S. and P. Somasundaran, *Colloids Surf., A,* 1996, *117*, (3), 227-233.

7 Partial Hydrogenation of Sunflower Oil in Triton X-100 microemulsion Systems

7.1 Introduction

Partial hydrogenation of unsaturated fatty acids is an important process in the food industry because of its widespread application to produce margarines, shortenings, and other food components **[7.1]**. Principal qualities of these natural substances are their ecotoxicity, their great biodegradability, and even more important these resources are renewable and very diverse. In order to improve oxidative stability and change melting point, vegetable oils have been hydrogenated since the beginning of the twentieth century. In general, the degree of hydrogenation which leads to a hardening of the oil depends on the application but it is always desired to reduce the level of polyunsaturated fatty acids like linolenic and linoleic acid (C18:3 and C18:2) because they are very sensitive to oxidation **[7.2, 7.3]**. The oleic acid (*cis* C18:1) has not only the advantage of being more stable under oxygen atmosphere to avoid polymerisation, but moreover it remains liquid at low temperature **[7.4]**. The applications of oleic acid are widespread into many industries: pharmacy, cosmetics, plastics, detergents and lubricants, but these industrial needs require a higher concentration of oleic acid than what traditional sunflower oil provides, which is only between 25 and 30%. Additionally, from the nutritional point of view the concentration of the saturated fatty acids like stearic (C18:0) and palmitic acid (C16:0) in an edible fat should be as low as possible for they have an adverse influence on health. On the other hand a certain consistency and handling characteristics offered by the waxy properties of the saturated acids are required for functionality of the fat. The formation of *trans*-isomers of fatty acids (elaidic acid, *trans* C18:1) is undesired. This fatty acid increases the melting point and is suspected to correlate with cholesterol diseases as well **[7.5]**. The hydrogenation reaction in edible-oil industry is usually carried out in the form of batch processes in slurry reactors, at high temperatures (140-225 °C) over supported Ni catalyst or a nickel aluminium alloy called Raney nickel suspended in the liquid phase **[7.6]**. Studies on the hydrogenation of different oils have been also undertaken on catalysts containing copper **[7.7]** or copper chromites **[7.8]** showing good selectivity though the activities were low even at high reaction temperatures. Selective hydrogenation of sunflower oil has been carried out

using supported monometallic catalysts containing Pd, Pt or Ru showing highest activity for the Pd catalyst **[7.9]**. Actually, Pd has shown to exhibit an activity of 80-100 times that of Ni **[7.10]**. Additionally, the selectivity to oleic acid was achieved by modification of the Pd catalyst by copper and lead, or by addition of amines to the reaction medium, this has been explained as a predominant ligand effect **[7.4]**. Much research has been focused on the effects of diffusion limitations experienced when using supported catalysts on the partial hydrogenation of vegetable oils **[7.6, 7.11]**. Membrane reactors have been designed in order to overcome the already mentioned diffusion limitations **[7.3, 7.12]**. This concept puts the active catalyst at the contact interface between the oil and the H_2, thus reducing diffusion distances for the reactants and reducing transport limitations **[7.6]**. In comparison to slurry reactors, membrane reactors have helped to improve the selectivity to oleic acid. Unfortunately, problems concerning the relation H_2 concentration and oil flow were encountered making difficult the control of the consecutive reaction to stearic acid in the membrane reactor. In order to solve diffusion limitations, propane in supercritical conditions **[7.1, 7.13]** has been used as solvent for the hydrogenation of sunflower oil. An unusual high catalytic activity has been achieved in the first example of partial hydrogenation of polyunsaturated crude methyl esters of linseed and sunflower oils with the water soluble catalyst complex Rh–TPPTS in aqueous/organic biphasic systems **[7.14]**. The use of biphasic systems as reaction media facilitates recovery and recycling of the catalyst and allows the avoidance of organic solvents which cause environmental and economical inconveniences. As shown in chapter 4, the partitioning behaviour of substrates between the phases in such systems is crucial for more hydrophobic substrates, and even more for higher molecular weight starting materials like vegetable oils **[7.15]**. This partitioning behaviour should have an important effect on the selectivity of the catalytic hydrogenation of vegetable oils. The use of surfactants helps overcome these diffusion limitations. In the same reference micellar systems have already been used as reaction media for this reaction and discussed **[7.14]**. The essential characteristics of microemulsion systems as reaction media for partial hydrogenation of vegetable oils are yet to be accounted for.

With the advantage of allowing efficient solubilisation of sunflower oil, Triton X-100 microemulsion systems were used as reaction media for the hydrogenation of the mentioned oil using the water soluble catalyst complex Rh–TPPTS under mild temperature and normal pressure. The ratio *P/Rh* was varied in order to improve the

selectivity for oleic fatty acid (*cis* C18:1) and the influence of the surfactant concentration on the hydrogenation rate was probed.

7.2 Experimental

7.2.1 Chemicals

The solvents cyclohexane (≥ 99.5 %, Roth), and 1-pentanol (≥ 99 %, Merck) were degassed and purged under nitrogen and used without further purification. The water-soluble ligand TPPTS (30.7 wt% in water, Celanese), and the (*p-tert*-Octylphenoxy)polyethoxyethanol surfactant "Triton X-100" (100 %, Sigma-Aldrich) were used as received. The catalyst precursor $[Rh(COD)Cl]_2$ (98 %, Strem) was kept under nitrogen and used as received. Sunflower seed oil (from *Helianthus annuus*) (Sigma-Aldrich) was used as received, and it had the following composition: 65.6% of linoleic acid (C18:2), 25.4% of oleic acid (*cis* C18:1), 6.5% of palmitic acid (C16:0) and 2.5% of stearic acid (C18:0).

7.2.2 Catalytic hydrogenation runs of sunflower oil

For a standard reaction, 25 mg of catalyst precursor (0.101 mmol of Rh) was mixed under nitrogen with 1221 mg of TPPTS 30% solution (375 mg, 0.659 mmol of TPPTS), this represents a ratio *P/Rh* of 6.5. This mixture was stirred under nitrogen at ambient temperature for 24 h before it was used in the hydrogenation reaction. To study the ligand effect on the selectivity of the catalytic sunflower oil hydrogenation, different ratios *P/Rh* were used. A 3 wt% Triton X-100 microemulsion system was used as standard reaction medium. As observed before in chapter 6 **[7.16]** by using a 3 wt% Triton X-100 microemulsion system for catalytic hydrogenations, adequate improvement of the reaction rate is obtained. Additionally, catalyst recycling and product isolation is possible. The composition of the standard reaction medium was: 42.2 g of water, 42.2 g of cyclohexane, 2.6 g of Triton X-100 and 1.3 g of 1-pentanol. To study the influence of the surfactant concentration on the selectivity of the sunflower oil catalytic hydrogenation, different concentrations of Triton X-100 in the range of 3-15 wt% were used.

A thermostated double-wall 200 mL glass reactor equipped with a gas dispersion stirrer was used in this study. Semibatch reactions were performed under a constant pressure of 1.1 bar. The hydrogen flow was monitored for keeping the pressure at a constant level. The microemulsion system was prepared one day before and agitated overnight. The reactor was evacuated to 150 mbar and refilled with nitrogen three times after introducing the solvent and after injection of the catalyst solution (1.2 mL) and the oil (5 g), respectively. The mixture was stirred at 400 rpm at reaction temperature (50 °C). The reaction was initiated after evacuating the reactor to 150 mbar, followed by increasing pressure to 1.1 bar with hydrogen gas and subsequent stirring at 800 rpm. A decreased and finally stopped hydrogen flux indicated the end of the reaction.

7.2.3 Analyses of the polyunsaturated methyl esters

1 mL samples of the reaction mixture were taken in 5 to 10 minute intervals and analyzed by gas chromatography. For GC analysis the reaction product was converted into their methyl esters by transesterification with the following procedure: 1 mL of the sample was mixed with 0.5 mL methanolic potassium hydroxide solution and stirred for 10 minutes. The mixture was left for 10 minutes for phase separation; then 1 mL HCl (1 $mol \cdot L^{-1}$) and one drop of methylorange was added. The samples were slightly agitated and left 10 min to settle for separation into a biphasic system. The upper phase was extracted and centrifuged to ensure complete separation of phases. The organic phase was separated and analysed by gas chromatography (GC) using a Shimadzu 2010 GC (SP-2560 capillary column, approx. 100 m, d = 0.25 mm, with a 0.2 µm film thickness, using 261.5 KPa of N_2 pressure). The oven temperature was initially at 170 °C for 0 min and then increased to 205 °C at a rate of 1 $°C \cdot min^{-1}$, obtaining the following retention times: 19.6 min for methyl palmitate, 24.5 min for methyl stearate, 26.0 min for methyl elaidate, 26.5 min for methyl oleate and 29.7 min for methyl linoleate. The SP-2560 capillary column is one of the columns used in the approved American Oil Chemists' Society (AOCS) official method Ce 1h-05 for the determination of *cis*-, *trans*-, saturated, monounsaturated and polyunsaturated fatty acids in vegetable or non-ruminant animal oils and fats by capillary GLC method **[7.17]**.

7.3 Results and discussion

The reaction network of the hydrogenation of sunflower oil is represented in Scheme 7.1. As observed, linoleic acid (C18:2) is saturated to oleic acid (*cis* C18:1) or to the *trans*- isomer elaidic acid (*trans* C18:1), which are subsequently saturated to stearic acid (C18:0). Parallel reactions are the isomerisation of *cis* C18:2 to *trans* C18:2 and *vice versa*, and the isomerisation of *cis* C18:1 to *trans* C18:1 and *vice versa.* The aim of every hydrogenation process of any type of vegetable oil, within the food industry is the hydrogenation of the polyunsaturated linolenic acid (C18:3) and linoleic acid to oleic acid by suppressing the complete hydrogenation to stearic acid and the *trans* isomerization to elaidic acid.

Scheme 7.1 Reaction mechanism for the hydrogenation of fatty acids in sunflower oil

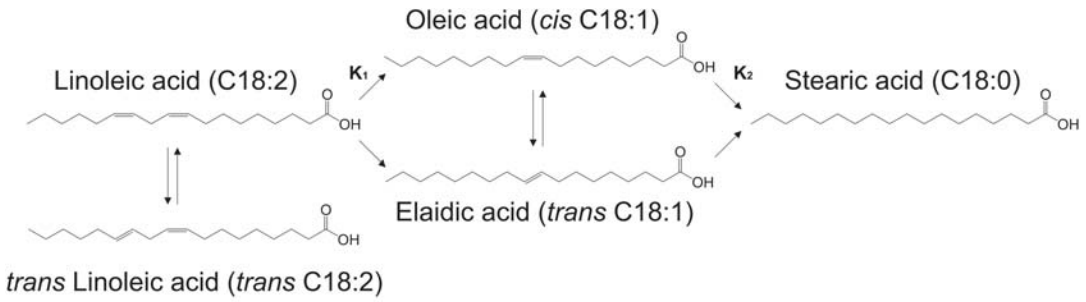

This study is based on the first example of partial hydrogenation of polyunsaturated crude methyl esters of linseed and sunflower oils with the water soluble catalyst complex Rh–TPPTS in aqueous/organic biphasic systems **[7.14]**, which showed unusual results. Furthermore, this approach aims at the control of the selective hydrogenation by adjusting the ligand/metal ratio.

7.3.1 Influence of the ligand/metal ratio

Figure 7.1 shows the monitored change in fatty acid composition during the hydrogenation of 5 g of sunflower oil in 100 mL of 3 wt% Triton X-100 microemulsion system. The hydrogenations were all done at 50 °C and 1.1 bar. All reactions show the same tendencies: as the content of linoleic acid decreases, the content of elaidic acid and stearic acid increases. Whereas the content of oleic acid initially increases, levels off and then decreases.

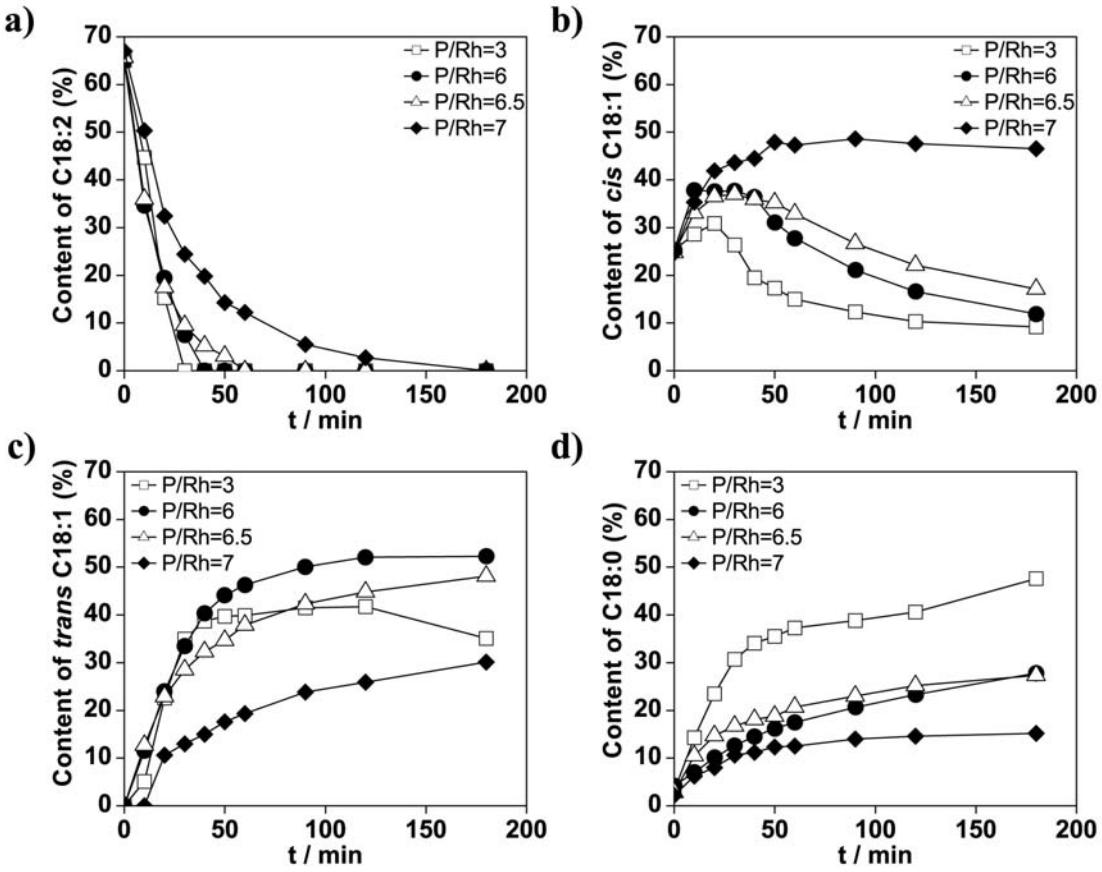

Figure 7.1 Content of fatty acids in sunflower oil during hydrogenation of 5 g sunflower oil in 100 mL of 3 wt % Triton X-100 microemulsion system at 50 °C, 1.1 bar H_2-pressure, with the water soluble catalyst complex Rh–TPPTS (0.81 mmol·L^{-1} of Rh) using different P/Rh ratios

By increasing the ratio *P/Rh*, the hydrogenation reaction becomes slower, in consequence the hydrogenation of C18:2 to *trans* C18:1 and subsequent hydrogenation to C18:0 is better controlled. By using the water-soluble catalyst complex Rh–TPPTS with a *P/Rh* ratio= 3, the total content of linoleic acid is hydrogenated within 30 min, but the composition of elaidic acid continues increasing until 120 min of reaction time as the oleic acid content decreases. This fact is an obvious example of the isomerisation of *cis* C18:1 to *trans* C18:1, which decreases in rate with the increase of the *P/Rh* ratio. After 120 min the *trans* C18:1 content decreases by the subsequent hydrogenation to C18:0. This decrease is only noticed at the *P/Rh* ratio of 3. At this point the isomerisation rate becomes slower as the content of *cis* C18:1 reaches 10%, and the subsequent hydrogenation to C18:0 is supplied by the *trans* C18:1 amount.

Small changes in the *P/Rh* ratio allow for important selectivity improvements in the hydrogenation of sunflower oil. As observed in Figure 7.1a, when changing the *P/Rh* ratio from 3 to 6 and then to 6.5 not much change on the hydrogenation rate of linoleic acid is obtained. But by using a *P/Rh* ratio of 7 the decrease of the content of *cis* C18:1 is much less; levelling at approximately 48% (see Figure 7.1b). Such high composition of oleic acid is not obtained with lower *P/Rh* ratios. Unfortunately, the content of *trans* C18:1 reached a high content of approx. 30%.

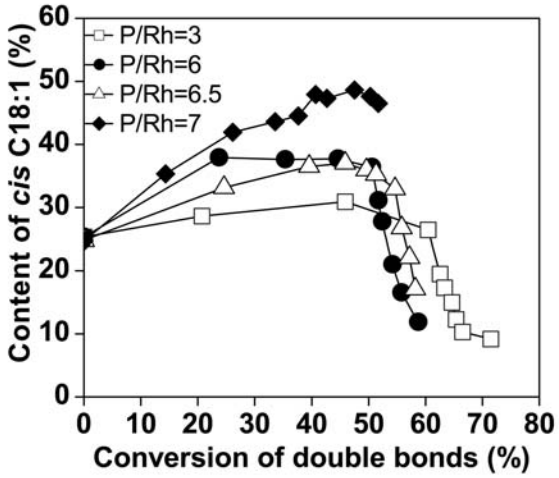

Figure 7.2 Content of oleic acid (cis C18:1) as a function of the conversion of the total amount of double bonds during hydrogenation of 5 g sunflower oil in 100 mL of 3 wt % Triton X-100 microemulsion system at 50 °C, 1.1 bar H_2-pressure, with the water soluble catalyst complex Rh–TPPTS (0.81 mmol·L^{-1} of Rh) using different P/Rh ratios

Figure 7.2 shows the evolution of the oleic acid content as the total amount of double bonds is being hydrogenated. The abscissa axis plots the conversion of double bonds, which is defined as:

$$\text{Conversion of double bonds} = 1 - \frac{x_{\text{MFA}} + 2 \cdot x_{\text{LA}}}{x^0_{\text{MFA}} + 2 \cdot x^0_{\text{LA}}} = 1 - \frac{\text{IV}}{\text{IV}^0} \qquad \text{(eq 7.1)}$$

where x_{MFA} is the liquid molar fractions of monoenic fatty acids (MFA), i.e., *cis* C18:1 and *trans* C18:1, and x_{LA} is the liquid molar fraction of linoleic acid (LA). These fractions are obtained from the gas chromatography measurements. The superscript 0 refers to the initial conditions of the experiment. The iodine value (IV) can also be calculated with this equation and it expresses the degree of unsaturation in the oil. The initial IV of sunflower oil is 133 **[7.18]**.

As observed in Figure 7.2 the content of oleic acid always starts to decrease when approx. 50% of the total amount of double bonds has been hydrogenated, which represents an IV of approx. 65. The higher content of oleic acid (49%) is a result of the higher *P/Rh* ratio. This effect was observed for the hydrogenation of linseed oil in biphasic systems using the same Rh–TPPTS catalyst at a high pressure of 10 bar and it can be explained by the predominant ligand effect **[7.14]**. When the concentration of TPPTS is higher the active metal is mostly protected by the ligand allowing only the most reactive substrate to be attached to the catalyst and consequently be hydrogenated. For this reason linoleic acid is hydrogenated first, and then the less reactive monoenic fatty acids are hydrogenated. As Figure 7.1d shows, an easier hydrogenation of monoenic fatty acids to stearic acid is obtained when the *P/Rh* ratio is lower.

7.3.2 Influence of the surfactant concentration

The use of surfactants in for reaction media is well known to overcome mass transfer limitations and incompatibilities between reactants **[7.19]**. For this reason the effect of the surfactant concentration on the hydrogenation of sunflower oil was studied. It is important to mention that mass transfer is not exclusively influencing the reaction rate to stearic acid. The simultaneous occurrence of consecutive and parallel reactions makes it difficult to separate the effects on the reaction rates.

The monitored composition of linoleic acid during the hydrogenation of sunflower oil using different concentrations of Triton X-100 is seen in Figure 7.3a. As this figure shows, the monitored linoleic acid composition does not suffer any significant change as a consequence of the surfactant concentration. Practically the total content of C18:2 is hydrogenated to monoenic fatty acids within 60 min. But the maximum content of oleic acid is increased by 30% when the surfactant concentration is increased from 3 wt% to 8 wt%, and 40% when the Triton X-100 concentration is changed from 3 wt% to 15 wt%. The contents of elaidic acid and stearic acid are limited to lower values. Though a higher concentration of surfactant is supposed to overcome mass transport limitations, allowing for higher solubility of the oil in the water phase which in consequence allows for a better contact between the water-soluble catalyst complex and the substrate, these results are signs of less

isomerisation of *cis* C18:1 to *trans* C18:1 and less subsequent hydrogenation to C18:0.

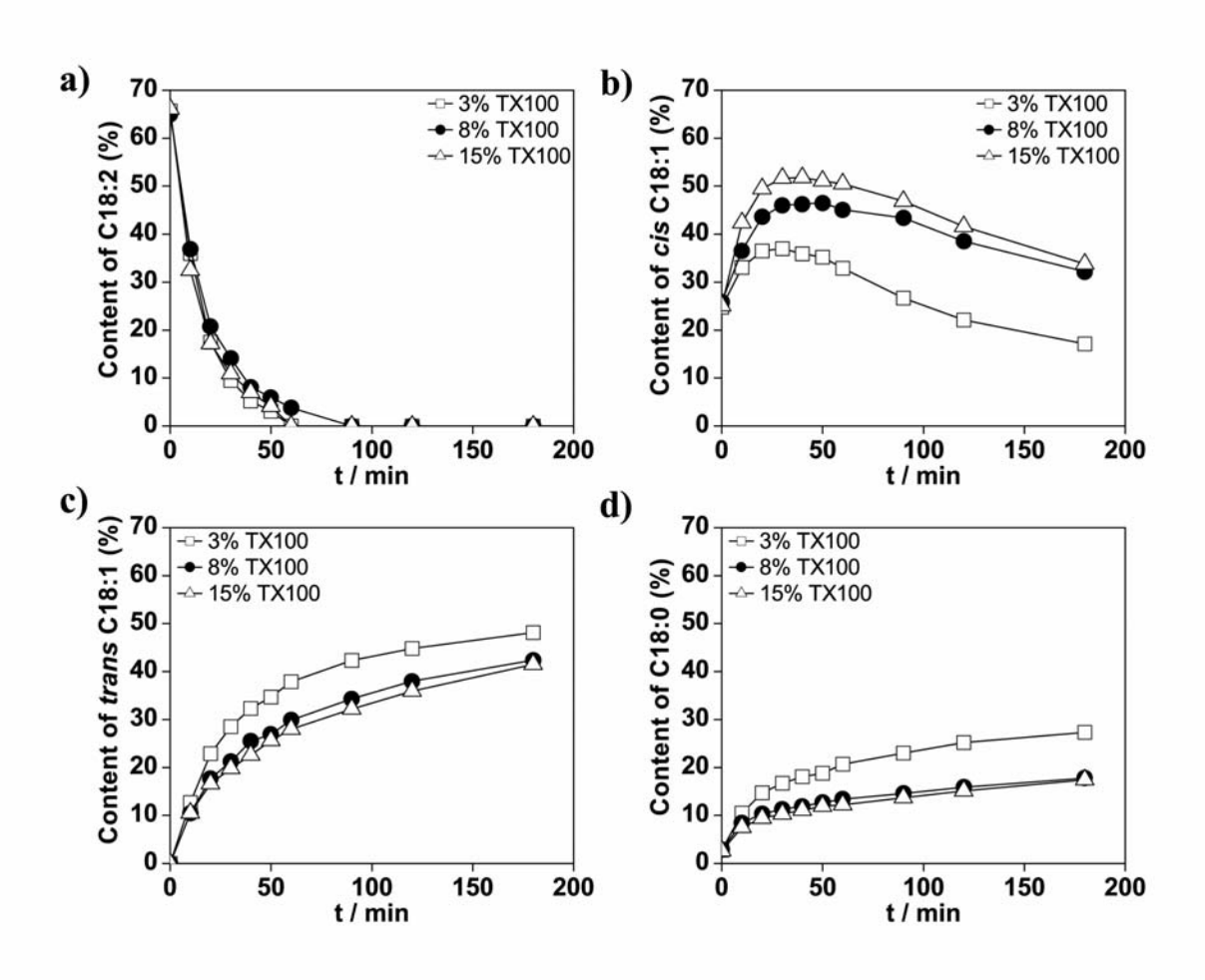

Figure 7.3 Content of fatty acids in sunflower oil during hydrogenation of 5 g sunflower oil in 100 mL of a Triton X-100 microemulsion system at 50 °C, 1.1 bar H_2-pressure, with the water soluble catalyst complex Rh–TPPTS (0.81 mmol·L^{-1} of Rh and 5.27 mmol·L^{-1} of TPPTS) using different Triton X-100 concentrations

Contrary to the effect of the *P/Rh* ratio on the content of oleic acid as the total amount of double bonds is being hydrogenated, the oleic acid content does not start to decrease at a fixed conversion of double bonds when the surfactant concentration is changed. As observed in Figure 7.4, the maximum content of oleic acid is reached at less conversion of double bonds by addition of more Triton X-100 to the microemulsion systems. The hydrogenation of linoleic acid to oleic acid becomes more efficient when the surfactant concentration is higher. With a 3 wt% Triton X-100 microemulsion system, the maximum oleic acid content (37%) is obtained at an IV of 72. This maximum (46.5% of *cis* C18:1) is increased to 73 with 8 wt% Triton X-100

and to 75 (51.8% of *cis* C18:1) with 15 wt%, which means less hydrogen is consumed to achieve these results.

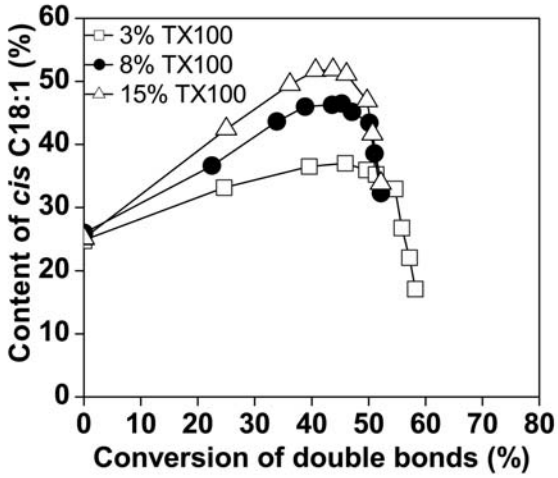

Figure 7.4 Content of oleic acid (cis C18:1) as a function of the conversion of the total amount of double bonds during hydrogenation of 5 g sunflower oil in 100 mL of a Triton X-100 microemulsion system at 50 °C, 1.1 bar H_2-pressure, with the water soluble catalyst complex Rh–TPPTS (0.81 mmol·L^{-1} of Rh and 5.27 mmol·L^{-1} of TPPTS) using different Triton X-100 concentrations

7.3.3 Catalyst recycling

As observed in chapter 6, by using 3 wt% Triton X-100 microemulsion systems as reaction medium for catalytic hydrogenations the catalyst can be recycled by the extraction of the oil-phase of the three-phase system **[7.16]**. Figure 7.5 shows four hydrogenation runs of sunflower oil (5 g of sunflower oil each run) in a 3 wt% Triton X-100 three-phase microemulsion system with the water-soluble catalyst complex Rh–TPPTS (*P/Rh* ratio= 7). Each run had a standard duration of 30 min. As observed in Figure 7.5, the catalyst goes through an activity decrease process until near deactivation. The first reaction produces a higher content of oleic acid (43.6%) with an IV of 88. Although the activity of the catalyst increases in the second reaction, less content of oleic acid is produced (38%) with a lower IV of 81. Isomerisation, hydrogenation of C18:2 to *trans* C18:1, and subsequent hydrogenation of monoenic fatty acids to C18:0 are the reasons for such lower content of *cis* C18:1. The third and fourth reactions show a continuous decrease of activity of the catalyst, in which *cis* C18:1 contents of 35.4 and 31.3% with IV's of 100 and 107, respectively, are obtained. The fast deactivation process of the water-soluble catalyst complex Rh–TPPTS is contradictory to other results shown in chapter 6, where 4

hydrogenation runs of dimethyl itaconate are obtained without deactivation of the Rh–TPPTS catalyst using the same 3 wt% Triton X-100 microemulsion system. This contradiction can be explained by the fact that in the present chapter the *P/Rh* ratio is lower (*P/Rh* ratio=7) than the ratio used in the hydrogenation of dimethyl itaconate (*P/Rh* ratio=7.5) and as observed in this contribution, small changes in the *P/Rh* ratio make an important difference in the results obtained for the partial hydrogenation of sunflower oil.

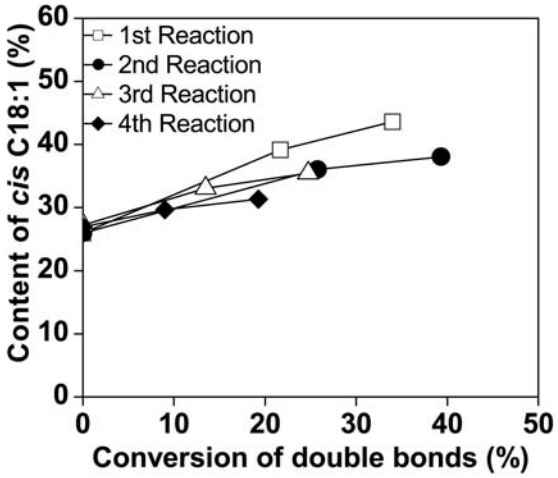

Figure 7.5 Content of oleic acid (cis C18:1) as a function of the conversion of the total amount of double bonds during different hydrogenation runs of 5 g sunflower oil each run in 100 mL of a 3 wt % Triton X-100 microemulsion system at 50 °C, 1.1 bar H_2-pressure, with the water soluble catalyst complex Rh–TPPTS (0.81 mmol·L^{-1} of Rh and 5.67 mmol·L^{-1} of TPPTS)

7.4 References

[7.1] Ramírez, E., F. Recasens, M. Fernández, and M.A. Larrayoz, *AIChE J.,* **2004,** *50*, (7), 1545-1555.

[7.2] O'Brien, R.D., *Fats and Oils: Formulating and processing for applications*. 2nd ed. 2004, Boca Raton: CRC Press LLC. p. 92-98.

[7.3] Schmidt, A. and R. Schomäcker, *J. Mol. Catal. A: Chem.,* **2007,** *271*, (1-2), 192-199.

[7.4] Nohair, B., C. Especel, P. Marecot, C. Montassier, L.C. Hoang, and J. Barbier, *C. R. Chimie,* **2004,** *7*, (2), 113-118.

[7.5] Ascherio, A. and W. Willet, *Am. J. Clin. Nutr.,* **1997,** *66*, 1006S-1010S; Oomen, C., M. Ocké, E. Feskens, M. van Erp-Baart, F. Kok, and D. Kromhout, *Lancet,* **2001,** *357*, (9258), 746-751.

[7.6] Veldsink, J., *J. Am. Oil Chem. Soc.,* **2001,** *78*, (5), 443-446.

[7.7] Ravasio, N., et al., *Appl. Catal., A,* **2002,** *233*, 1.

[7.8] Fragale, C., M. Gargano, N. Ravasio, M. Rossi, and I. Santo, *Inorg. Chim. Acta,* **1984,** *82*, (2), 157-160.

[7.9] Cecchio, J., E. Castano, and E. Uccieni, *Rev. Fr. Corps Gras,* **1979,** *26*, 391.

[7.10] Gray, J. and L. Russell, *J. Am. Oil Chem. Soc.,* **1979,** *56*, (1), 36-44; Ray, J., *J. Am. Oil Chem. Soc.,* **1985,** *62*, (8), 1213-1217.

[7.11] Colen, C., G. van Duijn, and H. van Oosten, *Appl. Catal.,* **1988,** *43*, (2), 339-350; Cordova, W. and P. Harriott, *Chem. Eng. Sci.,* **1975,** *30*, (10), 1201-1206; Schmidt, S., *Eur. J. Lipid Sci. Technol.,* **2000,** *102*, (10), 646-648; Jonker, G.H., J.W. Veldsink, and A.A.C.M. Beenackers, *Ind. Eng. Chem. Res.,* **1998,** *37*, (12), 4646-4656.

[7.12] Fritsch, D. and G. Bengtson, *Catal. Today,* **2006,** *118*, (1-2), 121-127; Ilinitch, O., P. Simonov, and F. Cuperus, *Stud. Surf. Sci. Catal.,* **1998,** *118*, 56-61.

[7.13] Ramírez, E., M.A. Larrayoz, and F. Recasens, *AIChE J.,* **2006,** *42*, (4), 1539-1553.

[7.14] Bouriazos, A., K. Mouratidis, N. Psaroudakis, and G. Papadogianakis, *Catal. Lett.,* **2008,** *121*, (1-2), 158-164.

[7.15] Milano-Brusco, J.S., M. Schwarze, M. Djennad, H. Nowothnick, and R. Schomäcker, *Ind. Eng. Chem. Res.,* **2008,** *47*, (20), 7586-7592.

[7.16] Milano-Brusco, J.S., J. Touitou, V. Strempel, and R. Schomäcker, **2009**, In preparation.

[7.17] Ratnayake, W., S. Hanse, and M. Kennedy, *J. Am. Oil Chem. Soc.,* **2006,** *83*, (6), 475-488.

[7.18] Pocklington, W., *Pure Appl. Chem.,* **1990,** *62*, (12), 2339-2343.

[7.19] Hager, M., F. Currie, and K. Holmberg, *Top. Curr. Chem.,* **2003,** *227*, 53-74.

8 Conclusion and Outlook

The aim of this thesis was to have an overall insight of catalytic hydrogenations in microemulsion systems using a water soluble catalyst complex. Hydrogenation of the valuable substrate itaconic acid (IA) and its derivates has been used as reference reaction for catalyst testing for their selectivity and activity in many studies. In order to minimize diffusion limitations and overcome incompatibilities between substrates, our work has focused on the effect of surfactants on catalyzed reactions, among them the hydrogenation of IA and derivates in micellar systems. Many investigations have revealed the fact that microemulsions have higher capacity than micellar systems for dissolving indifferently any type of substrate. Since microemulsions on the microscopic level form different micro-domains: core, interface and continuous phase, they have a higher versatility for dissolving and compartmentalizing any polar and nonpolar, organic and inorganic substrates than micellar systems. On the macroscopic level, the ability of forming different multiphase systems as a function of the temperature allows for the excess phases to act as exchangeable reservoirs for substrates and products, which at the same time enables an easy and fast catalyst recyclability and product isolation.

A kinetic study of the hydrogenation of dimethyl itaconate (DMI) with the water soluble catalyst complex Rh–TPPTS allowed for the reaction to be kinetically compared between using a biphasic system cyclohexane/water and using a [Triton X-100/1-pentanol]/cyclohexane/water microemulsion as reaction medium. Since the hydrogenation rate showed a strong dependence on the substrate concentration when the reaction took place in a microemulsion, the Osborn-Wilkinson model was used. This model combines the hydrogen insertion and the attack of the uncomplexed substrate at the dihydrido complex in one step, the latter is responsible for the dependence of the rate on the substrate concentration. Though the equilibrium constant of the dihydrido complex formation and the rate constant are the same in both systems, the effective activation energy for the biphasic system was approx. 5 times lower as the activation energy of the elemental reaction. This difference demonstrates the existence of mass transport limitation in the biphasic system, which is not the case in a microemulsion. Additionally, the hydrogenation of DMI in a biphasic system was demonstrated to be governed by the partition coefficient of the substrate between the two phases. In the same study, the effect of

the surfactant amount (Triton X-100 + 1-pentanol) in biphasic cyclohexane/water systems on the initial hydrogenation rate of DMI at mild conditions (1.1 bar and 25 °C) was demonstrated and can be doubled by adding 7 wt% of the surfactant with an additional 7 wt% of pentanol.

The formulation of the microemulsions has an important effect on the rate of the hydrogenation of DMI using the water soluble catalyst complex Rh–TPPTS. Two commercial *t*-octylphenoxypolyethoxyethanol surfactants (Triton X-100 and Igepal CA-520) where used to demonstrate this influence. The last one has approx. half the ethoxylated group number as the first. With both systems, by increasing the amount of water inside the reverse micelles relative to the amount of surfactant (ω) the initial hydrogenation rate of DMI increased. This influence was linearly dependent on the concentration of water for all systems. For the Triton X-100 microemulsions, by increasing the amount of cosurfactant in relation to the amount of surfactant (δ), the initial hydrogenation rates for each ω decreased. As a result, the linearly dependent curves were displaced to smaller initial hydrogenation rates. The cosurfactant content of the Triton X-100 microemulsions was also demonstrated to have a complex influence on the hydrogenation, and a partitioning study of the pentanol in biphasic systems helped to estimate the real amount of cosurfactant helping to form the micelles. Two different patterns were found when the initial hydrogenation rate of DMI was represented graphically as a function of the amount of water inside the reverse micelles relative to the amount of surfactant plus cosurfactant (ω_T). Because all these formulation influences have an impact on the size of the micelles, the size of the micelles was measured with the help of Small Angle Neutron Scattering (SANS) and Dynamic Light Scattering (DLS). The hydrogenation rate of DMI was strongly influenced by radius of the octylphenyl based micelles. The SANS measurements allowed the determination of the ellipsoidal shape of the micelles and they indicated a complex influence of the water soluble catalyst complex Rh-TPPTS on the shape and size of the Triton X-100 micelles, which induces an elongation of the aggregates. The elongation is a result of the competition between the polar head group of the surfactant and the water-soluble catalyst complex Rh–TPPTS for the water molecules.

Three different microemulsion systems with three different surfactants were used to study the recycling of the water soluble catalyst complex Rh–TPPTS and the isolation of the product dimethyl methylsuccinate (DMS). The three surfactants used

were: the non-ionic Triton X-100, the ionic dioctyl sulfosuccinate sodium salt (AOT) and the narrow range non-ionic ethoxylated Guerbet alcohol “Lutensol XA 50”. The initial hydrogenation rate of DMI catalyzed by Rh–TPPTS was proportional to the surfactant concentration. This effect was more pronounced for AOT systems, resulting in an almost 3 times higher initial hydrogenation rate of DMI than with Triton X-100 when using 15 wt % of surfactant. The appearance of both systems (Triton X-100 and AOT systems) with 15 wt % of surfactant at 45 °C and the initial amount of DMI (316.1 $mmol \cdot L^{-1}$) showed that the catalyst phase (aqueous lower phase) is three times bigger with Triton X-100. Both were $\bar{2}$ systems and the catalyst phase for the AOT system was only a 1/3 of the Triton X-100 system. For this reason the phase where the reaction took place had 3 times higher concentration of catalyst when using AOT as surfactant. Additionally, the concentration of DMI in the catalyst phase was similar in both systems. These two reasons explain the higher initial hydrogenation rate using 15 wt % of AOT. The catalyst could be recycled 3 times using Triton X-100, 2 times using AOT and only once using Lutensol XA 50 obtaining turn over numbers of 1500, 1200 and 800 for the surfactants Triton X-100, AOT and Lutensol XA 50, respectively. The recycling process of the water soluble catalyst complex Rh–TPPTS using 3 wt% surfactant systems, with non-polydisperse surfactants like AOT and Lutensol XA 50, was achieved without the necessity of additional amount of surfactant per run. This difference can be explained by the polidispersity of the surfactant Triton X-100.

In order to extend the use of microemulsion systems for other hydrogenation reactions than the hydrogenation of DMI, the catalytic hydrogenation of sunflower oil was studied using Triton X-100 microemulsion systems. These studies under mild conditions with 50 °C and 1.1 bar of H_2 pressure in Triton X-100 microemulsion systems using the water-soluble catalyst complex Rh–TPPTS has improved the understanding of the relation between the *P/Rh* ratio and the hydrogenation of linoleic acid to oleic acid. A small increment of the *P/Rh* ratio from 6.5 to 7 allowed for a high oleic acid content of 49% and for the contents of elaidic acid and stearic acid to be levelled at 30 and 15%, respectively. These results are lower values than the ones obtained when using a lower *P/Rh* ratio. The retarding effect of the ligand TPPTS on the hydrogenation of linoleic acid and less production of stearic acid was observed and should be explained by a more protected catalyst, at which only the more active substrates can be hydrogenated. A higher concentration of Triton X-100

allowed for an unusual lowering of the contents of elaidic acid and stearic acid reaffirming that the hydrogenation of sunflower oil is not only an issue of mass diffusion, it is comprised of a complex network of consecutive and parallel reactions. The addition of Triton X-100 to the reaction mediam promoted a more efficient hydrogenation of linoleic acid to oleic acid. With the higher concentration of 15% of Triton X-100, a content of oleic acid as high as 51.8% is obtained with less hydrogen consumed. The water-soluble catalyst complex Rh–TPPTS was recycled three times after 30 min of hydrogenation of 5 g of sunflower oil in 100 mL of a 3 wt% Triton X-100 microemulsion system. The catalyst decreased its activity and became less selective to oleic acid with the number of reactions, but a high oleic acid content of 43.6% with an IV of 88 was still obtained.

9 Appendix A

Program 1

{Worksheet for the estimation of the kinetic parameters using the Osborn-Wilkinson model for microemulsions as reaction media}

METHOD RK2	{numerial analysis method Runge-Kutta}
init CDMI=252.9	{Initial concentration of DMI, [mmol·L^{-1}]}
d/dt(CDMI)=-(K*K1*(CH2)*CRh*CDMI)/(1+(K1*(CH2))+(K2*CDMI))	{Osborn-Wilkinson model equation}
CRh=0.872	{Rhodium concentration, [mmol·L^{-1}]}
CH2=0.8249	{H_2 concentration in the aqueous core of the micelles, [mmol·L^{-1}]}
K=0.0629633	{Rate constant of the hydrogen insertion and the attack of the uncomplexed substrate at the dihydrido complex, [L·(mmol·min)$^{-1}$]}
K1=1.85105	{Equilibrium constant of the reversible dihydrido complex formation, [mmol·L^{-1}]}
K2=0.0166149	{Equilibrium constant of the reversible attack of uncomplexed hydrogen on the substrate-complex, [mmol·L^{-1}]}
STARTTIME = 0	
STOPTIME=180	
DT = 5	

Program 2

{Worksheet for the estimation of the kinetic parameters using the Osborn-Wilkinson model for biphasic systems as reaction media}

METHOD RK2	{numerial analysis method Runge-Kutta}
init CDMI=184.95	{Initial concentration of DMI in the aqueous-phase calculated with eq. 3.6 for a total concentration of DMI of 252.9 mmol·L^{-1}, [mmol·L^{-1}]}
d/dt(CDMI)=-(K*K1*(CH2)*CRh*CDMI)/(1+(K1*(CH2))+(K2*CDMI))	{Osborn-Wilkinson model equation}
CRh=0.872	{Rhodium concentration, [mmol·L^{-1}]}
CH2=0.8249	{Hydrogen concentration in the aqueous phase, [mmol·L^{-1}]}
K=0.07	{Rate constant of the hydrogen insertion and the attack of the uncomplexed substrate at the dihydrido complex, [L·(mmol·min)$^{-1}$]}
K1=1.4	{Equilibrium constant of the reversible dihydrido complex formation, [mmol·L^{-1}]}
K2=0.138	{Equilibrium constant of the reversible attack of uncomplexed hydrogen on the substrate-complex, [mmol·L^{-1}]}
STARTTIME = 0 STOPTIME=160 DT = 5	

10 Appendix B

Table B1 Original data of the cosurfactant partitioning study: molar percentage (%) of 1-pentanol concentrated in the aqueous phase of a biphasic system PEG 400/cyclohexane/water at 25°C

Sample	m_{H2O} /g	m_{C6H12} /g	m_{PEG400} /g	m_{C5H12O} /g	Peak area	n_{C5H12O}C6H12 /mmol	n_{C5H12O}H2O /mmol	$\%_{C5H12O}$H2O
ME 1	0.43	6.42	0.47	0.57	14061112.9	5.53	0.95	14.62
ME 2	0.32	6.52	0.47	0.57	14152069.2	5.64	0.81	12.65
ME 3	0.21	6.61	0.47	0.57	13696833.8	5.56	0.90	13.89
ME 4	0.42	6.27	0.46	0.74	18677920.0	7.04	1.38	16.43
ME 5	0.31	6.37	0.46	0.74	18678078.8	7.16	1.26	15.00
ME 6	0.21	6.46	0.46	0.74	17986361.8	7.00	1.40	16.65
ME 7	0.41	6.14	0.45	0.91	22927464.7	8.38	1.93	18.75
ME 8	0.30	6.23	0.45	0.91	22271529.3	8.27	2.02	19.63
ME 9	0.20	6.30	0.45	0.90	21859081.2	8.22	2.03	19.77
ME 10	0.40	6.00	0.44	1.07	27487785.3	9.75	2.35	19.42
ME 11	0.30	6.09	0.44	1.06	27145658.0	9.77	2.30	19.03
ME 12	0.20	6.18	0.44	1.06	26272920.4	9.61	2.44	20.27

Table B2 Original data of the cosurfactant partitioning study: molar percentage (%) of 1-pentanol concentrated in the aqueous phase of a biphasic system cyclohexane/water at 25°C

Sample	m_{H2O} /g	m_{C6H12} /g	m_{C5H12O} /g	Peak area	n_{C5H12O}C6H12 /mmol	n_{C5H12O}H2O /mmol	$\%_{C5H12O}$H2O
ME 1	**0.43**	**6.42**	0.57	14584854.0	5.72	0.76	11.67
ME 2	**0.32**	**6.52**	0.57	14703252.0	5.85	0.61	9.49
ME 3	**0.21**	**6.61**	0.57	14251234.0	5.76	0.69	10.65
ME 4	**0.42**	**6.27**	0.74	19266890.0	7.25	1.17	13.93
ME 5	**0.31**	**6.37**	0.74	19351388.0	7.41	1.02	12.11
ME 6	**0.21**	**6.46**	0.74	18731613.0	7.27	1.12	13.39
ME 7	**0.41**	**6.14**	0.91	24072494.0	8.78	1.53	14.87
ME 8	**0.30**	**6.23**	0.91	23008840.0	8.54	1.75	17.09
ME 9	**0.20**	**6.30**	0.90	23151346.0	8.68	1.56	15.25
ME 10	**0.40**	**6.00**	1.07	27833765.0	9.87	2.23	18.45
ME 11	**0.30**	**6.09**	1.06	27367684.0	9.85	2.22	18.40
ME 12	**0.20**	**6.17**	1.06	27567972.0	10.06	1.99	16.49

Table B3 Original data of the cosurfactant partitioning study: molar percentage (%) of 1-pentanol concentrated in the aqueous phase of a biphasic system PEG 1000/cyclohexane/water at 25°C

Sample	m_{H2O} /g	m_{C6H12} /g	m_{PEG400} /g	m_{C5H12O} /g	Peak area	n_{C5H12O}C6H12 /mmol	n_{C5H12O}H2O/ mmol	$\%_{C5H12O}$H2O
ME 1	0.43	6.42	1.18	0.57	13008825.4	5.14	1.33	20.56
ME 2	0.32	6.52	1.17	0.57	12374776.9	4.99	1.48	22.85
ME 3	0.21	6.61	1.17	0.57	11234869.8	4.63	1.82	28.25
ME 4	0.42	6.27	1.15	0.74	16099999.6	6.12	2.30	27.34
ME 5	0.31	6.37	1.15	0.74	16336232.7	6.31	2.11	25.08
ME 6	0.21	6.46	1.14	0.74	15439785.9	6.06	2.33	27.79
ME 7	0.41	6.14	1.12	0.91	22140432.2	8.10	2.21	21.42
ME 8	0.30	6.23	1.12	0.91	21843548.8	8.12	2.17	21.10
ME 9	0.20	6.30	1.12	0.90	19194788.2	7.26	2.98	29.09
ME 10	0.40	6.00	1.10	1.07	25533580.8	9.08	3.02	24.94
ME 11	0.30	6.09	1.10	1.06	26195294.1	9.44	2.63	21.76
ME 12	0.20	6.18	1.09	1.06	22933571.5	8.43	3.62	30.01

Table B4 Absolute intensity of the SANS measurements from the Triton X-100 microemulsions, volume fraction of the polar components, contrast factor and volume of the Triton X-100 micelles calculated using the macroscopic scattering cross section, considering the limits of no and full penetration of pentanol in the core of the micelles

Sample	ω	δ	$I0$ /cm^{-1}	ϕ_0	ϕ_1	Δp_0 /cm^{-2}	Δp_1 /cm^{-2}	V_{I0_0} /nm^{-3}	V_{I0_1} /nm^{-3}
ME 1	20	0.75	138.61	0.09	0.17	-2.69E+10	-4.87E+10	2046.17	341.16
ME 2	15	0.75	37.14	0.08	0.16	-3.13E+10	-5.20E+10	461.91	85.86
ME 3	10	0.75	18.42	0.07	0.15	-3.67E+10	-5.57E+10	191.24	39.93
ME 4	20	1.00	55.11	0.09	0.19	-2.52E+10	-5.12E+10	952.51	109.19
ME 5	15	1.00	28.97	0.08	0.18	-2.96E+10	-5.42E+10	412.88	54.41
ME 6	10	1.00	15.15	0.07	0.17	-3.50E+10	-5.75E+10	177.14	26.94
ME 7	20	1.25	43.26	0.09	0.21	-2.35E+10	-5.32E+10	884.29	72.22
ME 8	15	1.25	25.24	0.08	0.20	-2.80E+10	-5.59E+10	411.91	40.12
ME 9	10	1.25	9.45	0.07	0.19	-3.34E+10	-5.88E+10	124.41	14.33
ME 10	20	1.50	34.60	0.09	0.23	-2.20E+10	-5.47E+10	823.00	50.05
ME 11	15	1.50	21.77	0.08	0.22	-2.64E+10	-5.72E+10	408.25	30.18
ME 12	10	1.50	11.38	0.07	0.21	-3.19E+10	-5.99E+10	168.28	15.13

Table B5 Radius of gyration, radius of the micelles, volume of the corresponding homogeneous micelles with the assumption of spherical shape and volume ratio considering no penetration of pentanol in the core of the micelles

Sample	Rg_1 /nm	R_1 /nm	V_{Sph} /nm^3	V_{Sph}/V_{I0_1}
ME 1	11.18	14.43	12588.94	6.15
ME 2	5.41	6.99	1429.35	3.09
ME 3	3.33	4.30	332.39	1.74
ME 4	7.09	9.16	3216.55	3.38
ME 5	5.04	6.50	1152.32	2.79
ME 6	3.24	4.18	306.02	1.73
ME 7	6.37	8.23	2332.92	2.64
ME 8	5.00	6.45	1125.36	2.73
ME 9	2.73	3.52	183.01	1.47
ME 10	5.59	7.22	1575.70	1.91
ME 11	4.37	5.65	754.56	1.85
ME 12	3.49	4.51	383.53	2.28

Table B6 Radius of gyration, radius of the micelles, volume of the corresponding homogeneous micelles with the assumption of ellipsoidal shape and volume ratio considering no penetration of pentanol in the core of the micelles

Sample	Rg_2 /nm	a /nm	b /nm	V_{Ellip} /nm^3	V_{Ellip}/V_{I0_1}	*Ellipticity*
ME 1	4.00	5.16	23.90	2670.19	1.30	4.63
ME 2	3.67	4.74	10.08	947.79	2.05	2.13
ME 3	3.09	3.99	4.86	323.63	1.69	1.22
ME 4	3.80	4.91	14.26	1437.86	1.51	2.91
ME 5	3.57	4.61	9.19	817.48	1.98	1.99
ME 6	2.89	3.73	4.96	289.13	1.63	1.33
ME 7	3.40	4.39	12.83	1035.23	1.17	2.92
ME 8	3.45	4.45	9.23	767.15	1.86	2.07
ME 9	2.39	3.09	4.26	170.00	1.37	1.38
ME 10	3.11	4.01	11.14	752.19	0.91	2.77
ME 11	3.31	4.27	7.69	588.35	1.44	1.80
ME 12	2.54	3.28	6.28	282.86	1.68	1.92

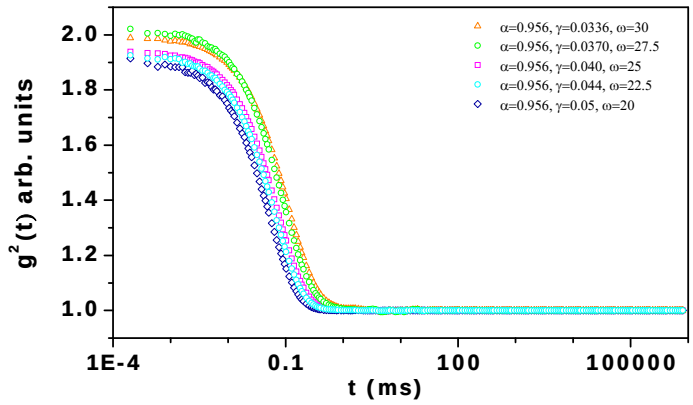

Figure B1 Autocorrelation functions $g^2(\tau)$ of the DLS measurements of Igepal microemulsions with different concentrations of Igepal CA-520 (γ) and constant cyclohexane-to-water ratios (α = 0.956) at 25°C

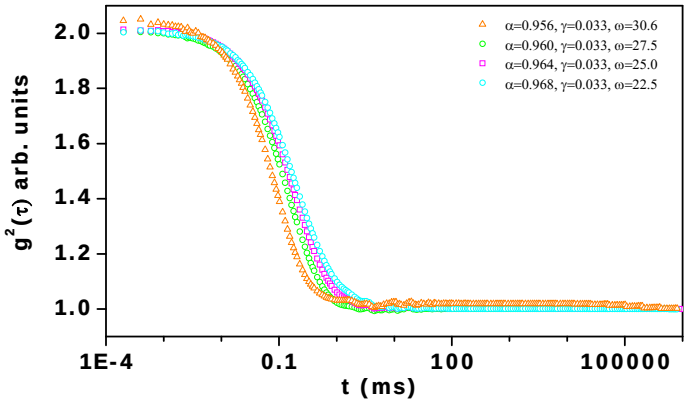

Figure B2 Autocorrelation functions $g^2(\tau)$ of the DLS measurements of Igepal microemulsions with different cyclohexane-to-water ratios (α) and constant concentration of Igepal CA-520 (γ = 0.033) at 25°C

Dipl.-Ing Juan Sebastian Milano Brusco

Curriculum Vitae (4 Pages)

Personal Details

Born in Cumaná – Venezuela, 24.03.1977

Single and no children

Present Affiliation

Technical University of Berlin, Institute of Chemistry, Sec TC 8, Straße des 17. Juni 124, 10623 Berlin, Germany

Contact

Email: juan.milano@chem.tu-berlin.de

Phone: +49 30 31426006, Fax: +49 30 31421695

Research Interest

- Homogeneous Catalytic Hydrogenation
- Water soluble catalysts
- Small Angle Neutron Scattering (SANS) and Dynamic Light Scattering (DLS)
- Microemulsions

Professional and Teaching Experience

- SANS study of microemulsions at the National Institute of Standards and Technology (NIST) in Gaithersburg USA. (18.09.2009 – 20.09.2009)
- Supervision of Lab courses at TU-Berlin: *Technical Chemistry I* and *Reaction Engineering*. (2007-2008)
- Assistance in the application for third-party funds in the framework of the AiF project N°14832 supported by the German Federation of Industrial Research Associations.
- Supervision of a Master Student at TU-Berlin. (07.04.2008 – 31.07.2008)
- Instructor Professor in the Universidad de Oriente (Venezuela) of the basic subjects: Physical Chemistry I. Physical Chemistry II. Physical Chemistry Laboratory. Unitary Operations Laboratory. Gas Technology. (01.10.2002 – 15.03.2005)
- Supervision of two Chemical Engineering Thesis Students at Universidad de Oriente (Venezuela). (2004-2005)
- Maintenance Supervisor: Venelin, C.A. (24.09.2001 – 11.03.2002)
- Supervision of Lab courses at Universidad de Oriente: Transport Phenomena. (1999)

Education

2009	o PhD Thesis *Homogeneously Catalyzed Hydrogenation Reactions in Inverse Micelles with Recycling of the Catalyst* at the TU Berlin. (Supervisor: Prof. Dr. Schomäcker). Grade: "Sehr Gut"
04/2001	o Diploma Thesis *Microparticle Brownian Movement in Ducts with Large Diameters* at the Universidad de Oriente. Grade: with Distinction (Supervisors: Dr. J. Murgich and Dr. S. Marfisi)
04/2000 – 12/2000	o Research Internship at Instituto Venezolano de Investigaciones Cientificas (IVIC)
10/1995 – 07/2001	o Engineering Chemistry Studies at the Universidad de Oriente. Grade: 7.11/10
10/1992 – 07/1994	o Diversified Secondary Education at Liceo Antonio José de Sucre, Cumaná – Venezuela
10/1985 – 07/1992	o Primary and Secondary Education at Unidad Educativa Instituto Privado "Santa Ines" Cumaná – Venezuela
04/1982 – 07/1985	o Primary Education at Portswood primary school, Southampton – United Kingdom

Languages and Software Skills

- Spanish (mother tongue), English (fluent) (5 years in Southampton, UK) *& 247 (TOEFL-CBT),* and German (fluent) (4 years in Berlin, Germany)
- MS Office, Maple, Origin, Berkeley Madonna

Awards and Scholarships

- Poster prize at the 7th World Surfactant Congress (Cesio 2008)
- DAAD Scholarship (2005 – 2009)
- Fundayacucho Scholarship (1998-2000)

Hobbies

Soccer, Pool, Snooker, Beach Volleyball,

Publications

- Milano-Brusco, J. S.; Touitou, J.; Strempel, V.; Schomäcker, R., "Catalytic Hydrogenations in Microemulsion Systems with Rh–TPPTS: Product Isolation and Catalyst Recycling in the Hydrogenation of Dimethyl Itaconate". **2009**, *in preparation*
- Schwarze, M.; Milano-Brusco, J. S.; Strempel, V.; Hamerla, T.; Wille, S.; Fischer, C.; Baumanm, W.; Arlt, W.; Schomäcker, R., "Rhodium catalyzed reactions in micellar systems" **2009**, *in preparation*

(5) Milano-Brusco, J. S.; Schomäcker, R., "Catalytic Hydrogenations in Microemulsion Systems with Rh–TPPTS: Partial Hydrogenation of Sunflower Oil". *Catal. Lett.* **2009**. DOI: 10.1007/s10562-009-0187-5

(4) Milano-Brusco, J. S.; Nowothnick, H.; Schwarze, M.; Schomäcker, R., "Catalytic Reactions in Surfactant Systems: Product Isolation and Catalyst Recycling". *Ind. Eng. Chem. Res.* **2009**. *Article ASAP*. DOI: 10.1021/ie900753t

(3) Milano-Brusco, J.; Prévost, S.; Lugo, D.; Gradzielski, M.; Schomäcker, R., "Catalytic Hydrogenation of Dimethyl Itaconate in Nonionic Microemulsions: Influence of the Size of Micelle". *New J. Chem.* **2009**, 33, 1726-1735

(2) Milano-Brusco, J. S.; Schwarze, M.; Djennad, M.; Nowothnick, H.; Schomacker, R., *"Catalytic Hydrogenation of Dimethyl Itaconate in a Water-Cyclohexane-Triton X-100 Microemulsion in Comparison to a Biphasic System". Ind. Eng. Chem. Res.* **2008,** 47, (20), 7586-7592

(1) R. Schomäcker, M. Schwarze, J. Milano, S. Jost. *"Asymmetrische Hydrierungen von C-C-Doppelbindungen in mizellaren Lösungen und Mikroemulsionen". Chemie Ingenieur Technik,* **2007**, *79, No.9,* V1.08

Conference Contributions

(12) Milano-Brusco, J. S.; Schwarze, M.; Schomäcker, R., *"Homogeneously catalyzed hydrogenation in inverse micelles with recycling of the catalyst"*. ***Poster*** presented at the ***3rd Workshop on Industry-Academia partnership in Catalysis.*** Berlin, Germany. 26-27 October 2009

(11) Milano-Brusco, J. S.; Nowothnick, H.; Schwarze, M.; Schomäcker, R., *"Catalytic Reactions in Surfactant Systems: Product Isolation and Catalyst Recycling"*. ***Oral presentation*** presented at the ***8th World Congress of Chemical Engineering.*** Montreal, Canada. 23-27 August 2009

(10) Seifert, K.; Milano-Brusco, J. S.; Nowothnick, H.; Schwarze, M.; Schomäcker, R.,

"Product isolation and catalyst recycling in catalytic reactions using surfactant systems as solvents". ***Poster*** presented at the ***Jahrestreffen Reaktionstechnik.*** Würzburg, Germany. 8-10 June 2009

(9) Schwarze, M.; Milano, J., and Schomäcker, R., *"Asymmetrische Hydrierung in Mizellaren Lösungen: Reaktionstechnische Untersuchungen zur Katalysatorrückführung durch MEUF"*. ***Poster*** presented at the ***42. Jahrestreffen Deutsche Katalytiker***. Weimar. Germany. 11-13 March. 2009

(8) Schwarze, M; Milano, J. and Schomäcker, R. *"Kontinuierliche Hydrierung in wässrig-mizellarer Lösung"*. ***Poster*** presented at the ***ProcessNet-Jahrestagung.*** Karlsruhe, Germany. 7-9 October 2008

(7) Milano-Brusco, J. S.; Schwarze, M and Schomäcker, R. *"Non-ionic surfactants applied in catalytic hydrogenations"*. ***Poster*** presented at the ***ProcessNet-Jahrestagung.*** Karlsruhe, Germany. 7-9 October 2008

(6) Milano-Brusco, J. S.; Schwarze, M and Schomäcker, R. *"Catalytic Hydrogenations in Nonionic Surfactant Systems: a way of recycling the catalyst"*. ***Poster*** presented at the ***International Symposium on Homogeneous Catalysis (ISHC XVI).*** Florence, Italy. 6-11 July 2008

(5) Milano-Brusco, J. S.; Prèvost, S.; Gradzielski, M and Schomäcker, R., *"Non-ionic W/O Microemulsions as Mediums for Catalytic Hydrogenations"*. ***Poster*** presented at the ***7th World Surfactant Congress (CESIO).*** Paris, France. 22-26 June 2008. ***"Won the Poster Prize"***

(4) Milano-Brusco, J. S.; Schwarze, M.; Schomäcker, R., "Catalytic Hydrogenations in Non-ionic Microemulsions". ***Oral presentation*** presented at the ***Jahrestreffen Reaktionstechnik.*** Würzburg, Germany. 18-20 May 2008

(3) J. S. Milano, R. Schomäcker. *"Katalysierte Hydrierung von Itaconsäuredimethylester in nicht-ionischen W/O Mikroemulsionen"*. ***Poster*** presented at the ***41. Jahrestreffen Deutsche Katalytiker.*** Weimar, Germany. 27-29 Februar 2008

(2) R. Schomäcker, M. Schwarze, J. Milano, S. Jost. *"Asymmetrische Hydrierungen von C-C-Doppelbindungen in mizellaren Lösungen und Mikroemulsionen"*. ***Oral presentation*** presented at the ***ProcessNet-Jahrestagung.*** Aachen, Germany. 16-18 October 2007

(1) J. S. Milano, R. Schomäcker. *"Katalysierte Hydrierung von Itaconsäuredimethylester in einer Cyclohexan-Triton X-100 Mikroemulsion"*. ***Poster*** presented at the ***40. Jahrestreffen Deutsche Katalytiker.*** Weimar, Germany. 14-16 March 2007